NUCLEAR INSTRUMENTS

A JOURNAL ON ACCELERATORS, INSTRUMENTATION
AND TECHNIQUES IN NUCLEAR PHYSICS

EDITOR K. SIEGBAHN - UPPSALA

VOLUME 2

JANUARY - MAY 1958

NORTH-HOLLAND PUBLISHING COMPANY — AMSTERDAM

NUCLEAR INSTRUMENTS

EDITORIAL BOARD:

J. B. ADAMS (CERN)
E. AMALDI (Rome)
H. L. ANDERSON (Chicago)
K. T. BAINBRIDGE (Cambridge, Mass.)
C. J. BAKKER (CERN)
P. R. BELL (Oak Ridge)
R. E. BELL (Montreal)
A. BERTHELOT (Saclay)
H. BRINKMAN (Groningen)
S. DE BENEDETTI (Pittsburgh)
M. DE HEMPTINNE (Louvain)
A. DE-SHALIT (Rehovoth)
M. DEUTSCH (Cambridge, Mass.)
S. DU TOIT (Pretoria)
B. S. DŽELEPOV (Leningrad)
W. GENTNER (CERN)
P. C. GUGELOT (Amsterdam)
H. HALBAN (Paris)
O. HAXEL (Heidelberg)
P. HUBER (Basel)
D. J. HUGHES (Brookhaven)
S. KIKUCHI (Tokyo)
J. KOCH (Copenhagen)
M. S. KOZODAEV (Moscow)
S. LIVINGSTON (Cambridge, Mass.)
E. M. MCMILLAN (Berkeley)
M. G. MEŠČERJAKOV (Moscow)
P. B. MOON (Birmingham)
M. L. OLIPHANT (Canberra)
W. PAUL (Bonn)
A. S. RAO (Bombay)
G. SALVINI (Rome)
P. SAVIĆ (Belgrade)
P. SCHERRER (Zürich)
CH. SCHMELZER (CERN)
H. W. B. SKINNER (Liverpool)
R. TANGEN (Blindern)
V. I. VEKSLER (Moscow)
O. WERNHOLM (Stockholm)
D. TAYLOR (Harwell)
G. VON DARDEL (CERN)
R. R. WILSON (Cornell)
S. D. WINTER (Saclay)

JANUARY 1958 VOLUME 2 (1958) No. 1

GREGG M. SINCLAIR LIBRARY
UNIVERSITY OF HAWAII
8-7-63

NUCLEAR INSTRUMENTS

A JOURNAL ON ACCELERATORS, INSTRUMENTATION AND TECHNIQUES IN NUCLEAR PHYSICS

EDITOR K. SIEGBAHN - UPPSALA

CONTENTS

P. A. TOVE, Automatic single-channel pulse-height analyser 1
R. I. WELLER, Ionization chamber radioisotope comparator 5
S. MAYO, C. A. HERAS and J. ROSENBLATT, Regenerative beam extraction on the Buenos Aires synchrocyclotron 9
A. TANARRO, Small gas compressor for accelerator ion sources (Letter to the Editor) 13
K. O. NIELSEN and O. SKILBREID, The electromagnetic isotope separator in Copenhagen . . . 15
J. KOCH, Study of some characteristics of the GM-discharge. 34
P. G. HANSEN and R. K. SHELINE, Chemical techniques used in connection with β-spectroscopic work on rare earth elements 39
C. F. COLEMAN, Gain-scanned single channel kicksorter using precision cascade attenuators . 44
M. A. POMERANTZ and A. E. SMITH, Automatic counting-rate recorder 49
J. F. VERVIER, Correction de diffusion lors des mesures de sections efficaces totales pour neutrons rapides 53
B. JOHANSSON, 25-channel time analyzer for the mμs-range and a simple time to pulse height converter 61

NORTH-HOLLAND PUBLISHING COMPANY - AMSTERDAM

NUCLEAR INSTRUMENTS

A journal on accelerators, instrumentation and techniques in nuclear physics

EDITOR: K. SIEGBAHN, UPPSALA

EDITORIAL BOARD:

J. B. ADAMS (CERN)
E. AMALDI (Rome)
H. L. ANDERSON (Chicago)
K. T. BAINBRIDGE (Cambridge, Mass.)
C. J. BAKKER (CERN)
P. R. BELL (Oak Ridge)
R. E. BELL (Montreal)
A. BERTHELOT (Saclay)
H. BRINKMAN (Groningen)
S. DE BENEDETTI (Pittsburgh)
M. DE HEMPTINNE (Louvain)
A. DE-SHALIT (Rehovoth)
M. DEUTSCH (Cambridge, Mass.)
S. DU TOIT (Pretoria)
B. S. DŽELEPOV (Leningrad)
W. GENTNER (CERN)
P. C. GUGELOT (Amsterdam)
H. HALBAN (Paris)
O. HAXEL (Heidelberg)
P. HUBER (Basel)
D. J. HUGHES (Brookhaven)
S. KIKUCHI (Tokyo)
J. KOCH (Copenhagen)
M. S. KOZODAEV (Moscow)
S. LIVINGSTON (Cambridge, Mass.)
E. M. MCMILLAN (Berkeley)
M. G. MEŠČERJAKOV (Moscow)
P. B. MOON (Birmingham)
M. L. OLIPHANT (Canberra)
W. PAUL (Bonn)
A. S. RAO (Bombay)
G. SALVINI (Rome)
P. SAVIĆ (Belgrade)
P. SCHERRER (Zürich)
CH. SCHMELZER (CERN)
H. W. B. SKINNER (Liverpool)
R. TANGEN (Blindern)
V. I. VEKSLER (Moscow)
O. WERNHOLM (Stockholm)
D. TAYLOR (Harwell)
G. VON DARDEL (CERN)
R. R. WILSON (Cornell)
S. D. WINTER (Saclay)

Contributions may be sent to the Editor, Professor K. Siegbahn, Institute of Physics, the University of Uppsala, either directly or through the intermediary of one of the members of the Editorial Board of the country or region in which the author is working. Contributions may be written in English, French or German, with an abstract in English.

Books for review should be sent to Professor Siegbahn.

Nuclear Instruments is published in bi-monthly issues. The subscription price of a volume of 360 pages is $ 17.00 (130 s), postage free.

Subscriptions should be sent to the publishers, North-Holland Publishing Company, P.O.Box 103, Amsterdam or to any subscription-agent. Subscriptions for U.S.A. are to be sent exclusively to Interscience Publishers, Inc., 250 Fifth Avenue, New York, 1 N.Y.

No part of this issue may be reproduced in any form, by print, photoprint, microfilm or any other means without written permission from the publisher. Reprints, photoprints or microfilms are obtainable at cost from the publisher.

NUCLEAR INSTRUMENTS 2 (1958) 1–4; NORTH-HOLLAND PUBLISHING CO. – AMSTERDAM

AUTOMATIC SINGLE-CHANNEL PULSE-HEIGHT ANALYSER

P. A. TOVE

The Gustaf Werner Institute for Nuclear Chemistry, University of Uppsala, Uppsala

Received 8 November 1957

An automatic single-channel pulse-height analyser is described. It works with a variable step attenuator to give 300 channel positions and has constant relative channel width.

1. Introduction

The single-channel pulse-height analyser has long been used for the determination of energy spectra from nuclear radiation detectors, particularly scintillation detectors. Compared with the multichannel analyser, it has the inherent disadvantage of only accepting a small energy band at a time, making the measurement time much longer. On the other hand, it has the advantage of being much cheaper and simpler in design than a multichannel analyser of comparable accuracy and stability. The circuitry is more complex in the modern multichannel analyser, making servicing more difficult, and the number of components apt to fail is rather great.

The disadvantage of the single-channel analyser can sometimes be overcome by making it automatic. Normally the channel position is then continuously varied and the counting rate is registered with a rate-meter and a recorder.

With a constant channel width, a disadvantage often found in γ-scintillation spectrometer work is that peaks of low energy appear considerably larger than those of high energy even if the corresponding transitions have equal probability. This is caused by increased detector efficiency with decreasing energy and by the fact that detector resolution is approximately proportional to the square root of the energy, meaning that the channel covers a proportionately larger part of the line at low energies. To overcome this, Åström introduced an ingenious discriminator system giving constant relative channel width[1]).

This paper describes a different method of obtaining a similar result, together with a wide energy range, and good stability and energy reading accuracy over the whole range. The principle is to use a stepwise variable attenuator in the amplifier preceding the single-channel discriminators, which are set at constant levels. The ratemeter is replaced by a pulse counter working on the predetermined count method, giving better and constant statistical accuracy. After each count the attenuator is forced one step automatically.

2. Description of the Analyser

The single-channel analyser consists of a linear amplifier followed by two discriminators the outputs of which are fed to a simple anticoincidence circuit. As is conventional, the linear amplifier is constituted of two series-coupled subamplifiers with negative feedback. Between these is inserted a coarse attenuator in series with a fine attenuator, both variable in steps, one step of the coarse attenuator corresponding to ten steps of the fine attenuator. As fig. 1 shows, the attenuator design is chosen so that the coarse attenuator represents constant load impedance to the first subamplifier, while the requirement of negligible load (the integration condenser disregarded) on the fine attenuator output is fulfilled by the high input impedance of the second subamplifier. Also the coarse and fine attenuators match each other

[1]) B. Åström, Nuclear Instruments 1 (1957) 143.

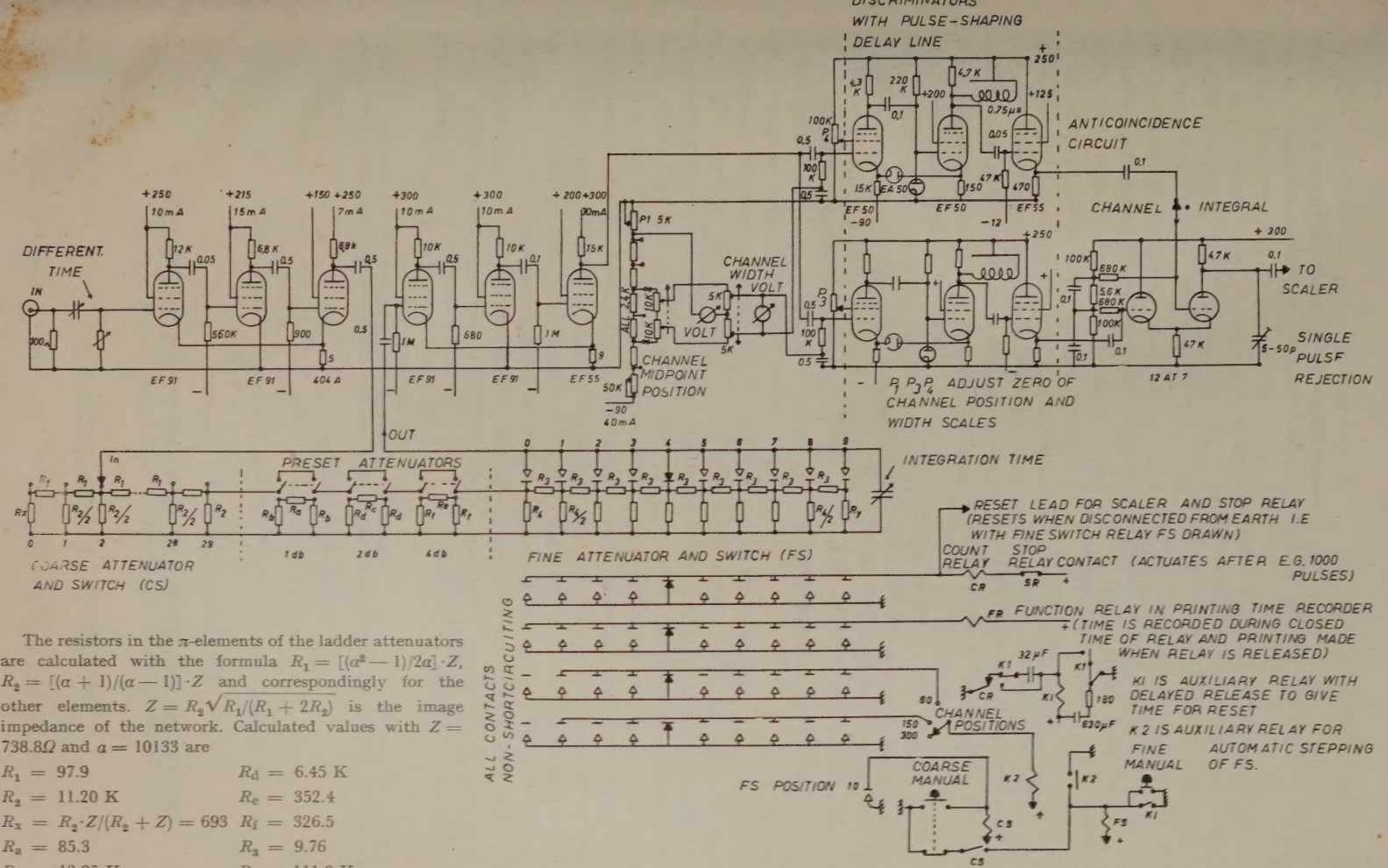

The resistors in the π-elements of the ladder attenuators are calculated with the formula $R_1 = [(\alpha^2 - 1)/2\alpha] \cdot Z$, $R_2 = [(\alpha + 1)/(\alpha - 1)] \cdot Z$ and correspondingly for the other elements. $Z = R_2\sqrt{R_1/(R_1 + 2R_2)}$ is the image impedance of the network. Calculated values with $Z = 738.8\Omega$ and $\alpha = 10133$ are

$R_1 = 97.9$	$R_d = 6.45$ K
$R_2 = 11.20$ K	$R_e = 352.4$
$R_x = R_2 \cdot Z/(R_2 + Z) = 693$	$R_f = 326.5$
$R_a = 85.3$	$R_3 = 9.76$
$R_b = 12.85$ K	$R_4 = 111.8$ K
$R_c = 171.6$	$R_y = R_y \cdot Z/(R_y + Z) = 735$

High-stability resistors were used, measured to better than $\frac{1}{2}\%$.

Fig. 1. Simplified diagram for the automatic single-channel pulse-height analyser. The system involves a feedback amplifier (modified A.E.R.E. 201 with twobuilt-in discriminators), two attenuators with switches and automatic stepping relays and a scaler working on the predetermined count method. The count time is registered by a printing register (Simplex Time Recorder SC-5A) in units of 0.1 sec. FS is a spiral switch (Swedish Telegraph Service No. E16861) and CS a L M Ericsson RVF 1216 switch. The single-channel pulse-height analyser can also be used in the conventional way, in which the setting of the discriminators is varied.

as well as the intermediate preset attenuation stages. The resistance values are low enough that no detrimental effect is produced because of stray capacitances when short amplifier time constants are used.

The switching of the attenuators is done by two switches coupled together so that on every tenth step of the fine attenuator the coarse attenuator is moved one step. Counting with the predetermined-count method is done for every setting of the fine attenuator. After the counting time has been registered by a printing time recorder the fine attenuator is stepped one stage. This is done automatically, giving 300 channel settings for a complete run through both attenuators. After that the measurement is started from the beginning again, as the attenuator switches are of the rotating type. This makes it easy to follow the decay of different peaks over long times. The levels of the discriminators are constant during the run but are set to suit the detector resolution and at a relatively high level to decrease the influence of discriminator drift. In this respect a back-bias amplifier would be better as it allows a higher absolute difference between the discriminator settings but the present arrangement is sufficiently good for normal purposes.

The attenuation factor per stage was chosen starting from the consideration that with a photopeak of 7% resolution, which is normal for a NaI γ-crystal around 1 MeV, about 6 count points were desired above the half-height level, in order to determine the position of the peak sufficiently well. If the attenuation per step is α this gives $\alpha^5 \approx 1.07$, leading to $\alpha = 1.0136$. For the attenuator in fig. 1 $\alpha = 1.0133$ was chosen. This gives an energy range of 53:1 with 300 steps, enough to cover the range from the highest energy to X-rays for many γ emitters. For a worse peak resolution the number of points in the peak increases, the number varying approximately inversely with the root of the energy. If desired the switches can be set to operate two steps at a time, or five, before counting (fig. 1). This is of value in quick checks of the spectra. If fewer points at low energies are desired, the coarse switch could control this changing-over automatically.

As usual, the channel width, i.e. the difference between the settings of the discriminators determines how well the spectrum is reproduced by the count points.

In the present arrangement the counting time for each point is registered by a printing recorder. The times are plotted on logarithmic paper versus step number. If the paper is turned around the curve appears in the normal way as if the counting rate had been plotted on a logarithmic scale. If the peak heights are wanted a transparent logarithmic scale is placed inversely to that of the paper (i.e. with 1 against 10 and 10 against 1), and the points read off this scale.

The energies corresponding to the step-number scale are easily calculated by exponential-slide-rule calculation or read from a straight calibration line in fig. 2, with the energy on the vertical logarithmic scale. The accuracy in reading off is independent of the energy, in contrast to the ordinary linear scale. Any faults normally caused by the discriminator scale not passing through zero are ruled out. Assuming the first subamplifier, favourably working on rather low level, is linear, the accuracy is only dependent on the attenuator, which can be checked by d.c. measurements, e.g. by a potentiometer.

An automatic plotting system is planned, which works with a synchronous motor, the revolutions of which give the time, and a logarithmic cam to give a direct mechanical deviation of $\log T_c = \text{const.} - \log N$ (T_c is count time, N count rate) on a recorder drum which is on the same axis as the fine attenuator switch.

3. Discussion of the Method

Assume the number of pulses per sec with amplitude v, and within the small interval dv at the input of the amplifier is $N = f(v)dv$. This should be a reproduction of the desired curve of pulse rate versus energy. If the amplifications in the subamplifiers are called A_1 and A_2; and the attenuation with n steps is α^n, then we

have for the output voltage to the discriminator $V = v A_1 \alpha^{-n} A_2 = v A \alpha^{-n}$, where $A = A_1 A_2$.

The count rate is $N(n) = f(v)\mathrm{d}v \approx f(V\alpha^n/A)\,\alpha^n \mathrm{d}V/A$ with the channel width $\mathrm{d}V$. $f(v) \approx A\, N(n)\, \alpha^{-n}/\mathrm{d}V = \text{const.}\ N(n)\, \alpha^{-n}$. The function $f(v)$ thus is obtained by multiplying the N values with α^{-n}. The displacement of the peak position in the $N(n)$ curve relative to the $f(v)$ curve is usually quite negligible. If desired the $f(v)$ curve is easily constructed for the few points around the top. The width $\mathrm{d}V$ determines how well the function is reproduced.

For intensity comparisons between two peaks $\int f(v)\ \mathrm{d}v$ is wanted

$$\int f(v)\ \mathrm{d}v = \int cN(n)\alpha^n \frac{V}{A} \ln\alpha \mathrm{d}n = c_1 \int N \mathrm{d}n$$

where c and c_1 are constants. Thus the intensity of a line is proportional to the area under the photopeak count rate plotted on linear paper versus attenuation step number. For comparison of peak heights, the intensity is also approximately proportional to $N(n)\, w \sim \alpha^{-n/2}\, N(n)$ at the peak, where w is the relative half-width.

4. Acknowledgements

The author wishes to thank Prof. The Svedberg for his generous support, and Mr. S. Sundell and P. Isacsson for skilful technical help. He is indebted to Dr. P. Hillman for correcting the language of the paper.

This work was supported by the Swedish Atomic Energy Commission.

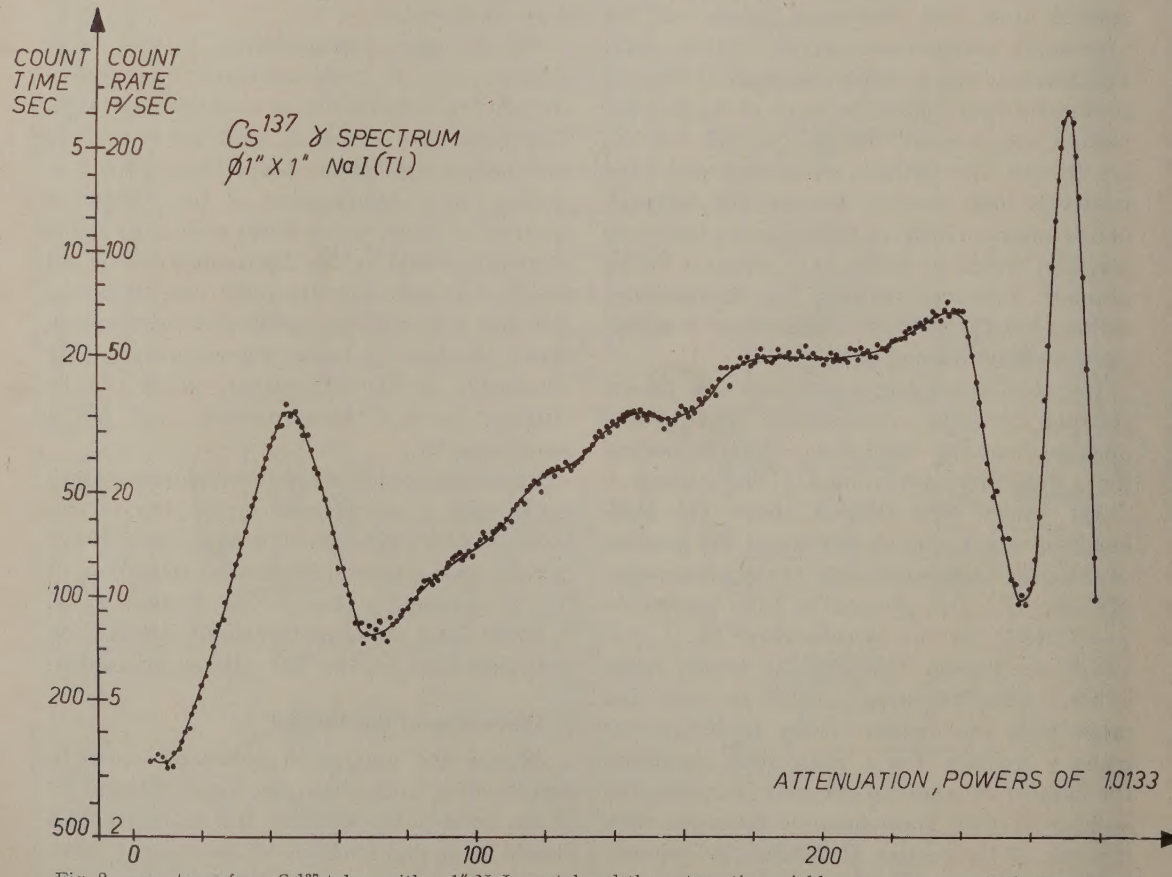

Fig. 2. γ-spectrum from Cs^{137} taken with a 1″ NaI crystal and the automatic variable attenuator method. The energy scale is in factors of 1.0133. This makes the Ba X-ray peak appear wider than the 0.66 MeVγ, as it has worse resolution. On the vertical scale the count time for a predetermined count number was plotted on a log scale. Channel width was approximately 3%.

NUCLEAR INSTRUMENTS 2 (1958) 5–8; NORTH-HOLLAND PUBLISHING CO. – AMSTERDAM

IONIZATION CHAMBER RADIOISOTOPE COMPARATOR

RICHARD I. WELLER†

Brookhaven National Laboratory, Upton, N.Y.

Received 15 September 1957

A precision instrument for the routine measurement of liquid beta-emitting radioisotopes was developed by modifying a portable Chang and Eng fast neutron detector. The battery-powered unit is rugged and dependable, and assays can be made rapidly. The minimum radioactivity measurable is of the order of 0.1 microcurie per milliliter and extends upward by a factor of 10^5. The inherent accuracy of the comparator is within $\pm$ 2% and the over-all absolute accuracy is estimated as $\pm$ 5%.

1. Introduction

A precision instrument was needed for the routine measurement of liquid samples of primarily beta-ray-emitting radioisotopes of relatively high activity (essentially carrier-free). The use of an ionization chamber, in which the sample to be assayed would be placed, was considered. A Chang and Eng portable instrument[1, 2]) formerly used for the detection of fast neutrons in the presence of gamma radiation was obtained. This was a small unit for health physics surveying and was designed to be compact and rugged. It consisted of two ionization chambers connected in a bridge circuit, with a Lindemann-Ryerson electrometer to measure the difference in the ionization currents in the two chambers. Fig. 1 is a simplified schematic diagram of the circuit.

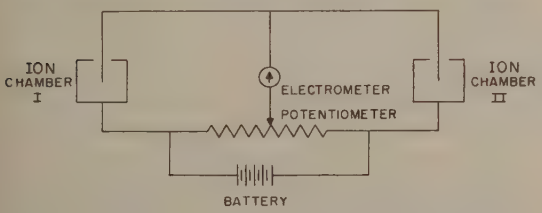

Fig. 1. Simplified schematic diagram of Chang and Eng fast neutron detector.

[1]) P. W. Reinhardt, Chang and Eng, a portable instrument for the detection of fast neutrons in the presence of gamma radiation, MDDC-819 (March 5, 1947).

[2]) W. H. Ray, Chang and Eng in Use, AECD-2357 (December 1, 1947).

[3]) L. S. Taylor, Accurate measurement of small electric charges by a null method, Radiology **17** (1931) 294.

The Chang and Eng instrument appeared to be readily adaptable for use in the secondary standardization of isotopes against absolutely measured samples and standards secured from other sources. A rate-of-charge null system of measurement could be set up based on the Townsend balance principle[3]), whereby the electrometer merely indicates that the charge collected by one of the ion chambers is balanced with the charge placed on a capacitor which replaces the second ion chamber of the Chang and Eng pair. The electrometer, viewing microscope, light source, collecting electrode interconnections, frictionless grounding switch, and housing could be used without modification. The two ion chambers could be modified to serve as the assay chamber and compensating capacitor connector.

2. Instrument Development

The end of one ion chamber was cut off so that the cylindrical walls were at the same height as the existing central collector electrode. The ion chamber was now 3 in. in diameter and 4 in. long. The other end of the chamber containing the insulators and guard ring assembly was left intact. A hemispherical volume was formed from a brass cylinder to fit the open end of the ion chamber, with the inner diameter matching the chamber diameter (see fig. 2). This furnished a symmetrical electric field distribution within

†Now at Franklin and Marshall college, Lancaster, Penna.

the chamber. It was determined that a collecting potential of 600 V insured saturation current.

The brass base was enclosed in Lucite to provide insulation against the high voltage applied to the chamber wall. The upper portion of the

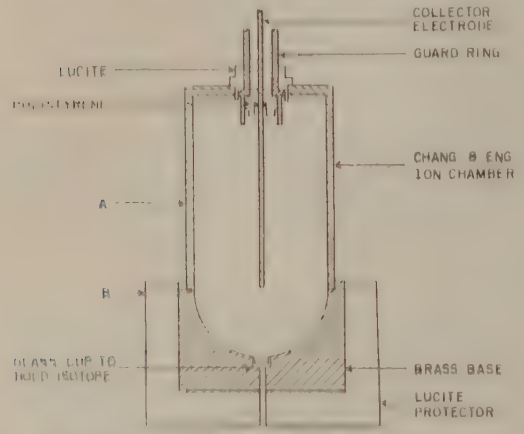

Fig. 2. Ionization chamber with isotope holder.

ion chamber, A, not so protected, was sprayed with an insulating coating. In the newly formed brass base, B, a cylindrical recess was provided to support a small glass beaker containing the liquid isotope. Accurate machining prevented source displacement from the centre and yet allowed the glass beaker to be smoothly inserted and withdrawn. A small hole continuing down through the bottom of the base facilitated the removal of the glass beaker after use.

Glass beakers were made of precision bore tubing with an inner diameter of 19 mm. The inner depths were made 5 mm and 15 mm to accommodate the range of isotopes used. The precise depth is not important, as long as the "infinite depth" is exceeded, i.e., the maximum range of the most energetic particles in solution is less than the total depth (see table 1). In this case the concentration is measured rather than the total quantity. In order to assure a constant distance between the sample surface and the collecting volume, precise amounts of the isotopes were always measured, 1.50 ml for the 5-mm beaker and 4.30 ml for the 15-mm beaker. The radioactive area presented to the collecting volume is critical, and its constancy was insured

TABLE 1

Isotope	Maximum energy[4]) MeV	Maximum range in water[5]) mm	Half-life[4])
S^{35}	0.167	0.3	87.1 days
Tl^{204}	0.765	3	3.5 years
P^{32}	1.70	8	14.3 days

[4]) J. M. Hollander, I. Perlman and G. T. Seaborg, Table of isotopes, Revs. Mod. Phys. 25 (1953) 469.

[5]) A. T. Nelms, Energy loss and range of electrons and positrons, Natl. Bur. Standards (U.S.), Circ. 577 (July 26, 1956).

by the use of precision materials and methods of fabrication, as verified by tests (see below). Coating the edge of the beaker with a hydrophobic agent was tested, but this treatment was found to be unnecessary, since the active solutions lacked the tendency to creep over the edge of the cell.

A commercially available variable air capacitor† was utilized for the instrument standard. This capacitor was inexpensive, rugged, and stable, with adequate insulation and three-terminal construction adaptable to the guard ring assembly of the ionization chamber. It was totally enclosed in an aluminum case and rigidly attached to the electrometer housing. The base of the second Chang and Eng chamber was utilized as the guarded electrode connector between the shielded capacitor and the electrometer. A micrometer dial and gear reduction mechanism†† was attached to the shaft of the capacitor, to allow direct readings to one part in 500; it furnished smooth, precise control and high reset accuracy, with no noticeable backlash.

After the variable capacitor was installed on the electrometer, it was calibrated with a precision bridge. The results were verified by measurements over the entire range with two different sets of accurately standardized fixed capacitors†††.

† General Radio Company, Type 1428-A.

†† National Company, Type PW-O.

††† One set of fixed capacitors had been standardized at the National Bureau of Standards; the other set, at the Columbia University Radiological Research Laboratory, courtesy of William Gross.

The range of the variable capacitor was from 7.197 to 592.2 $\mu\mu$F, with an estimated accuracy of $\pm$ 0.3%.

The electrometer housing with the attached capacitor was suspended by a simple framework which permitted the unit to be easily raised and lowered for insertion in the ion chamber of the beaker containing liquid isotope, and for its removal.

Fig. 3 presents the circuit diagram of the entire instrument. Dry batteries were used exclusively for the power supply; hence there were no problems of regulation. All critical leads were thoroughly shielded and grounded, and switches were of the rotary ceramic type. Polarity reversing connections on the switches permitted the measurement of both positive and negative currents to eliminate the effect of the direct contribution of the beta-particles from the source. The voltmeters were precision multirange instruments of high resistance (10 000 ohm/V), a factor of importance, since these instruments present the only sizable load on the critical circuit batteries. Ten-turn variable resistors provided fine control in the electrometer circuit.

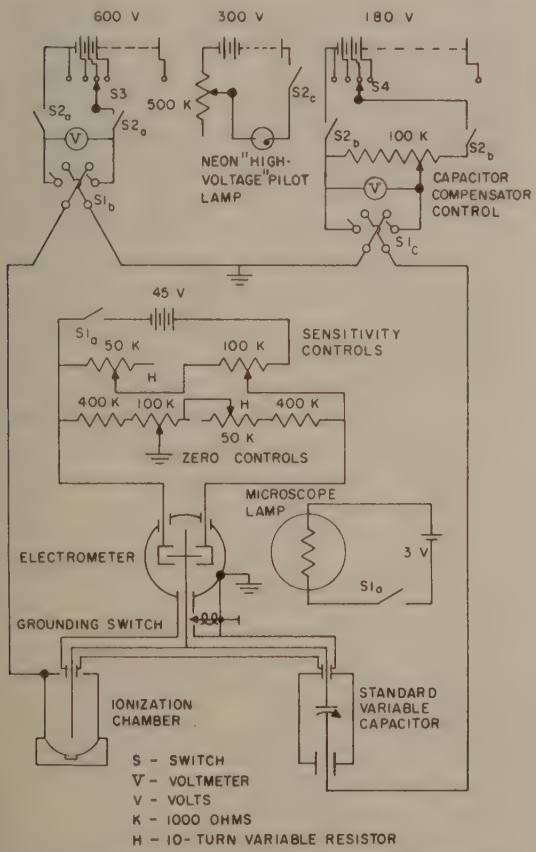

Fig. 3. Circuit diagram of radioisotope comparator.

The batteries were placed in a metal cabinet 21 $\times$ 10.5 $\times$ 13.5 in., with all the controls mounted on the front panel. The structure supporting the electrometer housing, capacitor, and ionization chamber had over-all dimensions of 20 $\times$ 24 $\times$ 18 in. The two units were connected by cables which could be easily disconnected.

3. Tests and Calibration

For convenience the instrument was placed in a low-radiation-level dilution laboratory so that the samples could be readily diluted if necessary and then measured nearby. The average background current measured here was 5×10^{-15} A, which represents the order of magnitude of the minimum measurable current. The lower limit was fixed by the minimum attainable capacitance of the variable air capacitor.

Three radioisotopes were primarily used in the development of the instrument: sulfur-35, thallium-204, and phosphorus-32 (see table 1). These covered the energy range of immediate interest and were readily available.

After early exploratory determinations, the instrument was standardized with absolutely determined samples of the three isotopes. The primary absolute standardization was performed by 4π beta counting†. Table 2 presents the

TABLE 2

Isotope	Calibration factor, $\frac{\mu\mu A}{\mu C/ml}$	Concentration measurable, μC/ml	
		Minimum	Maximum
S^{35}	0.124	0.414	48 400
Tl^{204}	0.472	0.109	12 700
P^{32}	1.98	0.0260	3 030

† Courtesy of Mary T. Kinsley, Nuclear Engineering Department.

calibration constants of the instrument together with the maximum and minimum concentrations which can be determined. This range of measurement, approximately 10^5, could be extended in either direction by use of other capacitors. As a measure of the sensitivity of such a chamber, Seliger and Schwebel[6]) suggest the term "background equivalent activity" (BEA), defined as the activity of a radionuclide that produces an ionization current equivalent to the background. This chamber furnishes a BEA of 0.002 μC/ml for phosphorus-32, which compares well with the value of 0.001 reported for the precision chamber at the National Bureau of Standards.

The null method of measurement requires the observation of three variables: capacitance, change in voltage, and elapsed time. Then the ionization current measured is computed as: current ($\mu\mu$A) = capacitance ($\mu\mu$F) $\times$ voltage (v) $\div$ time (sec).

The accuracy of the measurement depends upon the precision of the absolutely determined standard isotope and the reproducibility or internal consistency of the instrument. The absolute disintegration rates of the standardized sources were determined within $\pm$ 3%. The individual standard deviations in a set of readings were usually less than 0.5%. The instrument itself, account being taken of the errors of the three quantities mentioned above and of the errors discussed below (including those of volumetric techniques), was found to furnish reproducible readings within $\pm$ 2%. Thus, the over-all estimated accuracy of the measured samples was $\pm$ 5%, which was adequate.

The personal error involved in the correlation of visual observations of the electrometer fiber image and manual operation of the stopwatch was found to be negligible. Since stopwatch readings were always greater than 60 sec, the 0.1-sec stopwatch had a maximum probable error of $\pm$ 0.17%.

Potential sources of error were eliminated by the rigid mechanical construction and reproducible fixed geometry of the ionization chamber and source. Studies were made of the effects of using different glass beakers and different pipettes; no measurable differences in current resulted. Variation of the quantity of isotope (i.e., depth in glass beaker) with measured current, as long as the "infinite depth" was exceeded, caused only slight inaccuracies. In an extreme case a variation of $\pm$ 0.01 ml caused a difference of $\pm$ 0.5% in measured current.

The error caused by the variation of temperature (and to a lesser extent of barometric pressure) could amount to several percent if the temperature excursions were extensieve. However, since the apparatus was kept in a temperature-regulated room, error from this source was small. For example, a temperature variation of $\pm$ 4°C over the mean room temperature of 26°C caused a current variation of $\pm$ 0.75%. Correction for this type of error can be made by empirical methods[7,8]), but it was not deemed necessary in this work.

4. Summary

A convenient and satisfactory instrument suitable for the assay of beta-emitters in solution was developed. The apparatus is portable, compact, rugged, and stable; its circuitry is relatively simple. The unit is independent of external power lines, can be stored indefinitely without deterioration, and will function accurately and dependably when needed, with only normal attention required for the dry batteries. The measurement geometry is accurately and rapidly reproducible and the entire assay may be performed quickly. The minimum amount of radioactivity measurable is about 0.4 μC/ml for sulfur-35, 0.1 μC/ml for thallium-204, and 0.03 μC/ml for phosphorus-32. The range of measurement is about 10^5 times the minimum values. The response is linear throughout the range and the relative accuracy is within $\pm$ 2%. The over-all absolute accuracy is estimated as $\pm$ 5%.

[6]) H. H. Seliger and A. Schwebel, Standardization of beta-emitting nuclides, Nucleonics **12**, No. 7 (1954) 54.

[7]) N. A. Baily, The Measurement of Low Energy Beta Emitters—Ionization Chamber Techniques, AECU-650 (CUF-4) (November 15, 1949).

[8]) W. Gross, S. Deutsch and G. Failla, Isotopes and Beta-Rays, Annual Report of Research Project, Section C, NYO-4582 (April 1, 1954).

NUCLEAR INSTRUMENTS 2 (1958) 9–12; NORTH-HOLLAND PUBLISHING CO. – AMSTERDAM

REGENERATIVE BEAM EXTRACTION ON THE BUENOS AIRES SYNCHROCYCLOTRON

SANTOS MAYO, CARLOS A. HERAS and JORGE ROSENBLATT

Comisión Nacional de Energía Atómica, Buenos Aires

Received 15 September 1957

The nonlinear regenerative theory was applied to the extraction of the deuteron beam of the Buenos Aires 30 MeV synchrocyclotron. The theory of LeCouteur proved successful even though the approximation of the $n(r)$curve with two straight lines gives an n-value for the extraction radius very different from the actual one for that radius. A regenerator field of the form $T = 0.05\,\rho + 0.11\,\rho^2$ produced a radial gain up to 1.5 cm. An electrostatic channel extended over a 30° arc with a 80 kV/cm field deflected the beam 3 cm out. A magnetic channel following the electrostatic one brought the beam out from the cyclotron vacuum chamber. A fraction of 2–3% of the internal beam could be removed by such an arrangement.

1. Introduction

From previous work at Liverpool[1]) and Chicago[2]) it would appear possible to remove a considerable fraction of the circulating beam from the synchrocyclotron in this Commission and make it available for experimental purposes in the form of a well collimated beam. The nonlinear regenerative theory[3]) was applied to this particular machine giving a regenerative field

$$T = 0.05\rho + 0.11\rho^2 \qquad (\rho \text{ positive and measured in cm})$$

where

$$T = \frac{r}{H}\int_0^{2\pi} \Delta H \, \mathrm{d}\theta .$$

This was the best regenerator compatible with the magnetic and geometrical machine data, fig. 1. However it was felt that this field would not give the necessary regenerative action, based as it was on an approximate n-value rather different from the actual one. It would be more reasonable to take an average n-value determined by considering the radial amplitudes of the particle motion on the inside of the starting radius for the regenerative action. Two reasonable possibilities were $n = 0.06$ and $n = 0.1$, and with these the corresponding regenerator fields were calculated, namely $T = 0.25\rho + 0.03\rho^2$ and $T = 0.35\rho + 0.04\rho^2$. These regenerators were built and tested but no evidence of regenerative action was observed. So it was decided to take the theory exactly as it is and

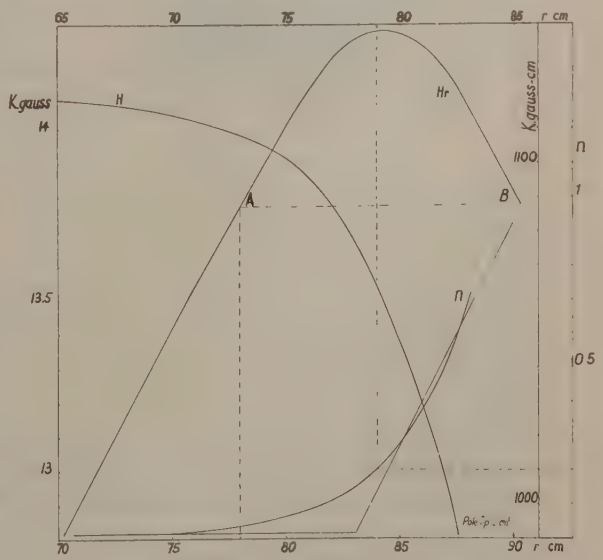

Fig. 1. Cyclotron magnetic data. The upper scale is for n; the lower one is for H and Hr.

[1]) A. V. Crewe and J. W. G. Gregory, Proc. Roy. Soc. A **232** (1955) 242.

[2]) A. V. Crewe and U. E. Kruse, Rev. Sci. Inst. **27** (1956) 5.

[3]) K. J. LeCouteur and S. Lipton, Phil. Mag. **46** (1955) 1265.

the abovementioned field was adopted; a radial gain up to 1.5 cm was measured at 40° phase from the regenerator.

In order to improve the extraction efficiency an electrostatic channel was installed as a first stage for a magnetic one thus getting a 2–3% fraction of the circulating beam out of the machine.

2. Construction of the Regenerator

The regenerator was built with Armco iron sheets 8.75 mm thick piled up forming blocks

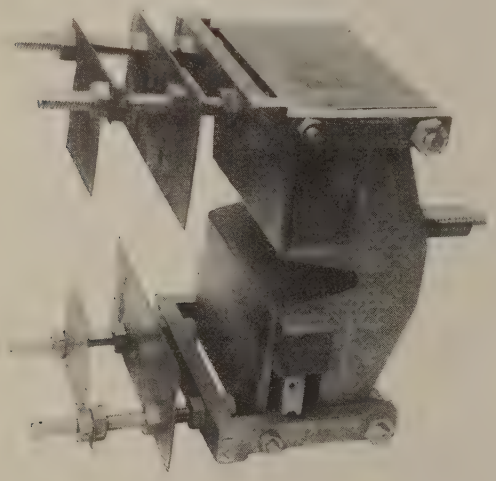

Fig. 2. Regenerator assembly.

35 mm thick, 40 mm wide and 190 mm long held in a brass frame. The system could be moved from the outside by means of a screw. A pair of shims attached to the brass support was enough to correct the field just in front of the blocks. Fig. 2 is a view of the regenerator assembly.

The measuring equipment for the magnetic field was an electronic fluxmeter and a search coil which could be moved with uniform motion both radially and azimuthally. Fig. 3 is a block diagram of the fluxmeter: A is a dc Liston Mod. 10 linear amplifier with variable gain; I is an integrator of conventional design and R is a Philips PR 2000M/00 graphical recorder.

The magnetic field of the cyclotron was measured with a Varian nuclear fluxmeter with an accuracy of 1:10 000[4]) in order to provide a standard field to calibrate the electronic fluxmeter. This was done by moving the search coil

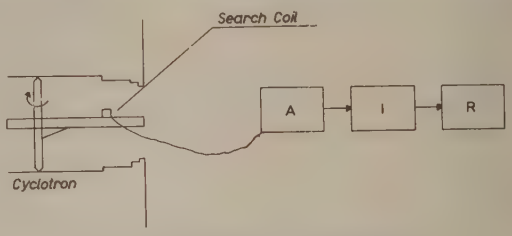

Fig. 3. Block diagram of the fluxmeter.

radially and comparing the deflection on the pen recorder with nuclear fluxmeter data. A sensibility was thus obtained of 4 gauss per mm on the recording paper.

A synchronous motor produced the azimuthal movement at a constant angular speed of 1 rad/min. The search coil was thus made to sweep

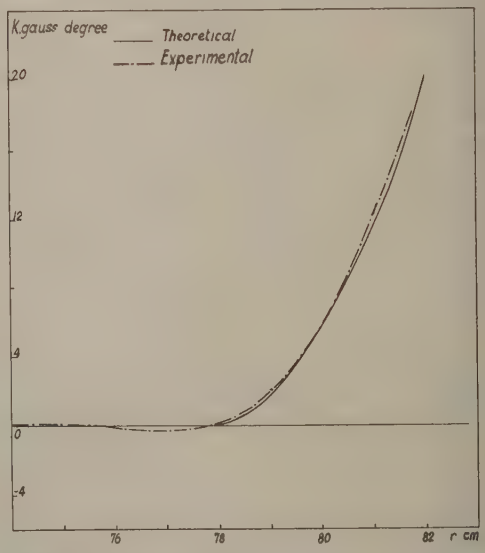

Fig. 4. Regenerator field as a function of radius.

the median plane of the magnet over an angle of 90° at different radii in steps of 1 cm. The value of the field defect $\int \Delta H \mathrm{d}\theta$ as a function

[4]) This was done up to a 100 gauss/cm gradient, but the whole cyclotron magnet was measured with the electronic fluxmeter.

of radius in the machine was obtained by a step-wise integration. The shims were designed according to the shape of the perturbation desired.

Fig. 4 shows the final regenerator field obtained and the theoretically desired one. The differences are within 200–300 gauss-degrees, which is the limit of the measuring apparatus.

3. Test of Regenerative Action

The regenerator action was studied by means of a special target showed in fig. 5. It consists

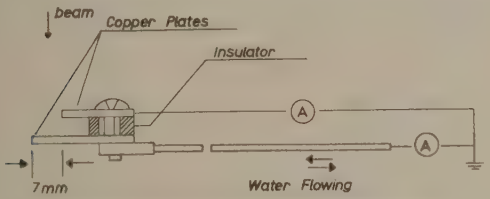

Fig. 5. Probe used to test regenerative action.

of two insulated copper plates, a collector and a detector, used to measure radial gain and relative intensity of the deflected beam fraction.

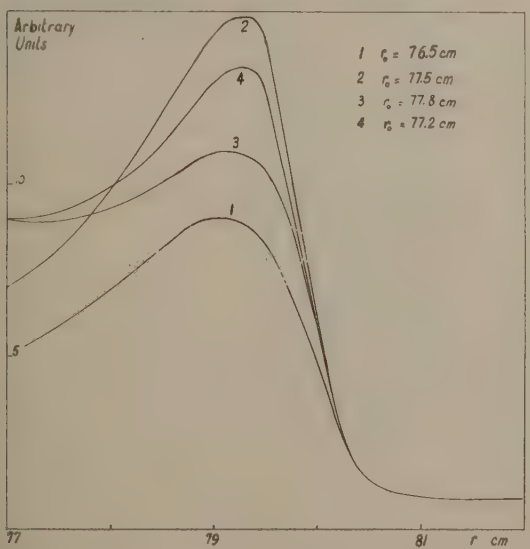

Fig. 6. Detector current versus radius for different radial position of the regenerator.

Fig. 6 is a plot of the detector current as a function of radius when the regenerator is at different radial positions. It is seen that a 10–20% fraction of the beam can be expected to enter the channel mouth, since the distance between the edges of the collector and detector in the target is 7 mm. It appears that the regenerative action starts between 77 and 77.5 cm, whereas the $n = 0.2$ point is at 79 cm radius. The autoradiographic method showed a radial gain up to 1.5 cm.

The conclusion was that a reasonable extraction efficiency can be expected under a 40° phase, with the field $T = 0.05\rho + 0.11\rho^2$ (ρ measured in cm). Considering fig. 1 it is quite astonishing that LeCouteur two straight lines approximation is the one that works for this machine. It seems that it is the best to represent the asymptotic behaviour; or may be the errors thus introduced provide a compensation to some others inherent to the theory.

4. The Electrostatic Channel

From LeCouteur approximation it was seen that the maximum radial gain obtainable in this particular machine would be of the order of 1 cm; so it was impossible to introduce a magnetic wall due to the 1 cm wide region near the wall in which the field perturbation cannot be corrected. It was decided then to use as a first section of the channel an electrostatic one which would deflect the beam over 3 cm, this distance being considered the minimum in order to continue the channel with magnetic sections, far more simple to handle.

Actually, two curved parallel plates were built with an electrostatic field of 80 kV/cm between them, equivalent to a magnetic channel with a field defect of 1.5 kG. The inner (grounded) wall is a 1 mm thick molybdenum plate held in position by a water-cooled copper frame; the outer one is a 10 mm thick oil-cooled copper plate.

The electrostatic channel was mounted on a base plate which could be moved from the outside of the accelerating chamber so that the best position could be adjusted with the circulating beam without destroying the vacuum.

5. The Magnetic Channel

The magnetic channel was installed following the electrostatic one; it consisted of three straight vertical sections made of Armco iron, the dimensions of which are given in table 1.

TABLE 1

Magnetic channel dimensions

Section	Wall thickness	Wall height	Channel width	Length	Wall material
1	10 mm	80 mm	10 mm	100 mm	Armco iron
2	17 mm	80 mm	15 mm	100 mm	Armco iron
3	17 mm	80 mm	15 mm	170 mm	Armco iron

They were aligned by the wire technique adjusting the tension and current in the wire to simulate 30 MeV deuterons.

The shims were designed by installing first each channel section independently normal to a radius of the cyclotron magnet and measuring the field reduction. When the channel sections

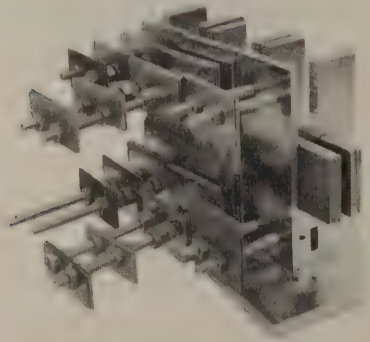

Fig. 7. Magnetic channel.

were set in their correct position a new field correction was needed since they were far from being normal to a radius. Fig. 7 shows a view of the magnetic channel with shims.

6. Assembly of the whole Extraction System and Final Tests

Once the shimming was finished, the orbit centers were determined by floating a wire loop at different radii up to 77 cm. It was found that magnetic centres were enclosed in a 4 cm diameter circle around the geometrical magnet center. This was considered good enough and the whole system was tested with the beam. An insulated copper target was installed at the end of the magnetic channel and a current of deuterons about 2–3 % of the internal current[5]) was measured with a microammeter. The energy of the beam was estimated from magnetic data as being 29 MeV.

The beam was let out of the vacuum chamber through the airlock for the ion source. Since in this region the disperse magnetic field is 9 kG, the beam is bended over an angle of about 15°, just the amount needed in order to reduce direct cyclotron radiations on the experimental room.

Photographs of the external beam were taken inside the ion source airlock by exposing photographic paper wrapped in aluminium foil. It appears that the beam is well focussed horizontally but has a rather large vertical size.

Focussing of the external beam will be made by quadrupole lenses in order to have a good spot 7 m away from the machine at the experimental room.

We would like to express here our thanks to Dr. A. V. Crewe for his invaluable help during his visit to our Institute for a six-week period. We wish to thank also the cyclotron crew, particularly Eng. C. Paganini, Mr. J. Garanzini and Mr. V. S. Tejero for their kind assistance.

[5]) The maximum internal current attained was 30 μA.

NUCLEAR INSTRUMENTS 2 (1958) 13–14; NORTH-HOLLAND PUBLISHING CO. – AMSTERDAM

LETTER TO THE EDITOR:

SMALL GAS COMPRESSOR FOR ACCELERATOR ION SOURCES

ANTONIO TANARRO

Junta de Energía Nuclear. Madrid

Received 28 September 1957

A simple, small-sized compressor designed to fill with deuterium the storage tank of the ion source in a pressurized Van de Graaff accelerator up to a pressure of five atmospheres is described.

To increase the useful working time of a pressurized accelerator it is necessary to have, near the ion source, a small tank with a large enough amount of gas to be ionized, so that the machine can run as much time as possible without opening the pressurized tank.

source. But very often, deuterons are to be accelerated, and then the deuterium is obtained in the laboratory at atmospheric pressure either by electrolysis or by a reduction process of heavy water. It is then neccesary to compress the gas in order to fill the small volume of the

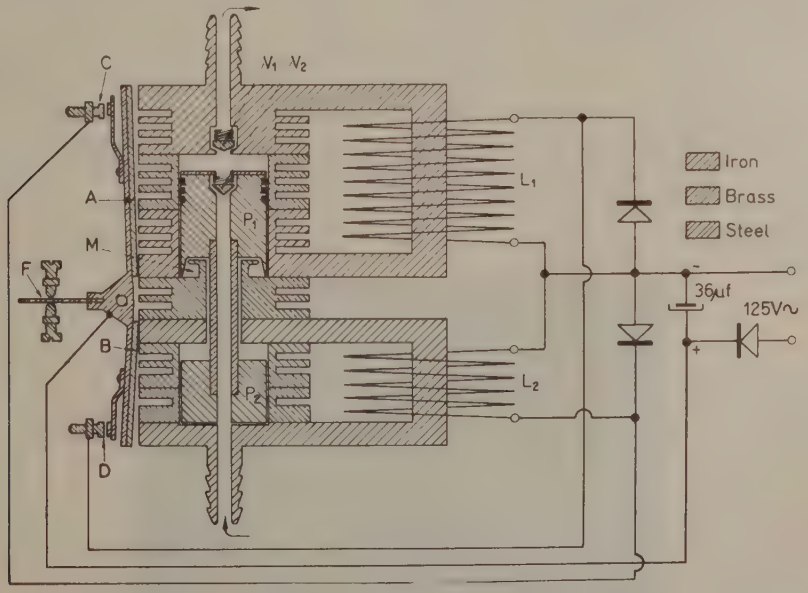

Fig. 1

When we deal with gases comercially available in pressurized bottles (i.e. hydrogen to accelerate protons) we have no difficulty in filling at the desired pressure the storage tank of the ion storage tank with a sufficient amount of gas.

To perform such operation we have devised and constructed a simple compressor of small size which does not need driving motor, suitable

to compress deuterium up to a pressure of five atmospheres without practically any loss of such a gas.

In fig. 1 a schematic of the instrument is given. It works in the following way.

Two independent magnetic circuits excited by one of the two coils L_1, L_2 are so disposed that when piston P_1 is at its upper position it closes the ferromagnetic circuit of the coil L_1, whereas in the lower position such as ferromagnetic circuit is opened by a free space surrounded by a non ferromagnetic material (brass). The opposite hapens with the ferromagnetic circuit of the coil L_2 and piston P_2. Both pistons move together, fixed to the same axis.

When both pistons are in down position, an electric current in L_1 draws P_1 upward, to close its ferromagnetic circuit. For the same reason, an electric current in L_2 when both pistons are in up position draws P_2 down.

Hence, by switching the current between L_1 and L_2, piston P_1 goes up and down, and the pair of values V_1V_2 forces the gas from the input to be compressed in the tank connected to the output.

The switching of the current between L_1 and L_2 is performed automatically by a special switch (at left of fig. 1) drawn by the same magnetic effect which pulls P_1 and P_2 up and down. In down position, the iron sheet A is attracted to the body of the cilinder and contacts D close; the current flows through L_1 and pistons are drawn up. When the up position is reached, the iron sheet B is attracted, contacts D open, contacts C close, current flows through L_2 and both pistons are pulled down.

The elasticity of the steel sheet F contributes to the reliable operation of the switch.

The main characteristics are: Piston diameter 36 mm; piston strokes 5 mm; cubic capacity 5 cc. Coil L_1 with 5350 turns of 0.5 mm wire and 80 ohms total resistance. Coil L_2 with the same number of turns, 0.3 mm wire and 240 ohms resistance.

Piston P_1 is fitted with three compression rubber rings ("quad rings", from Minnessota Rubber and Gasket Company). The volume M under P_1 is filled once or twice a year with the oil used in vacuum difussion pumps, through a hole closed with a screw. This way, suitable lubrication is achieved.

Fig. 2 shows a photograph of the instrument.

The compressor has been used for a year to fill, when necessary, the storage tank of the ion source of a two-million volt pressurized Van de Graaff accelerator. This tank has about 1000 cc capacity, and filled with deuterium up to a pressure of five atmospheres allows the normal operation of the machine during more than 700 hours.

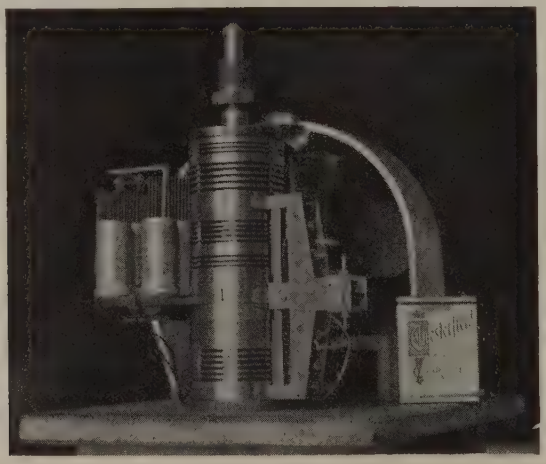

Fig. 2.

NUCLEAR INSTRUMENTS 2 (1958) 15–33; NORTH-HOLLAND PUBLISHING CO. – AMSTERDAM

THE ELECTROMAGNETIC ISOTOPE SEPARATOR IN COPENHAGEN

K. O. NIELSEN AND O. SKILBREID

Institute for Theoretical Physics, University of Copenhagen

Received 14 October 1957

An electromagnetic isotope separator of a 90° sector type with 800 mm radius and 50 kV accelerating voltage is described. The focusing properties and the possibility of concentrating the beam on a small area at the collector are discussed. Direct deposition and a sputtering method for collecting the isotopes are used. In both cases, separated samples for direct utilization in various apparatus for nuclear physics investigations can be obtained. A few applications are briefly described.

1. Introduction

The electromagnetic isotope separator was designed and constructed by J. Koch and put into operation in 1943. A description of the instrument at that stage is given by J. Koch and B. Bendt-Nielsen[1]).

In 1951, the isotope separator was moved into a new laboratory building and several technical improvements were introduced. At that time the apparatus was used almost exclusively for noble gases. A description of the apparatus and a survey of the experiments carried out with separated isotopes of noble gases until 1951 are given by J. Koch[2]).

Since then various improvements have been introduced, and it is the purpose of this paper to bring the description of the apparatus up to date. These improvements have been made mainly in order to serve the needs for separated samples of the different nuclear research groups at the Institute.

The improvements fall into four categories: (1) development of ion sources for solids for the purpose of separating isotopes of most elements with high efficiency; (2) development of a scanning device which permits control of the beam focusing during the separating process; (3) development of a two-directional focusing system which makes it possible to concentrate the beam on a small area of the collector; (4) development of mechanical and electronic devices which make possible stable runs over a long period of operation.

The ion sources and the scanning devices are described in separate publications by O. Almén and K. O. Nielsen[3]), K. O. Nielsen[4]), and K. O. Nielsen and O. Skilbreid[5]). The subject covered by these publications will be mentioned only briefly in this paper.

Parallel to the development of the isotope separator, production of separated samples for nuclear investigations has been carried out. A short description of some of the separations is given at the end of this paper, while the results of the investigations carried out on the separated samples will be published elsewhere.

2. Basic Description

The design of the isotope separator is shown in fig. 1, and a simplified block diagram demonstrating the operation is given in fig. 3. The ion source is at a high potential, 50 kV to 70 kV. All connecting wires to the ion source and the rubber tubings for cooling water are assembled

[1]) J. Koch and B. Bendt-Nielsen, Mat. Fys. Medd. Dan. Vid. Selsk. 21 (1944) no. 8.

[2]) J. Koch, Circ. US. Nat. Bur. Stand. No. 522, (Washington, 1953) p. 165.

[3]) O. Almén and K. O. Nielsen, Nuclear Instruments I (1957) 302.

[4]) K. O. Nielsen, Nuclear Instruments I (1957) 289.

[5]) K. O. Nielsen and O. Skilbreid, Nuclear Instruments I (1957) 159.

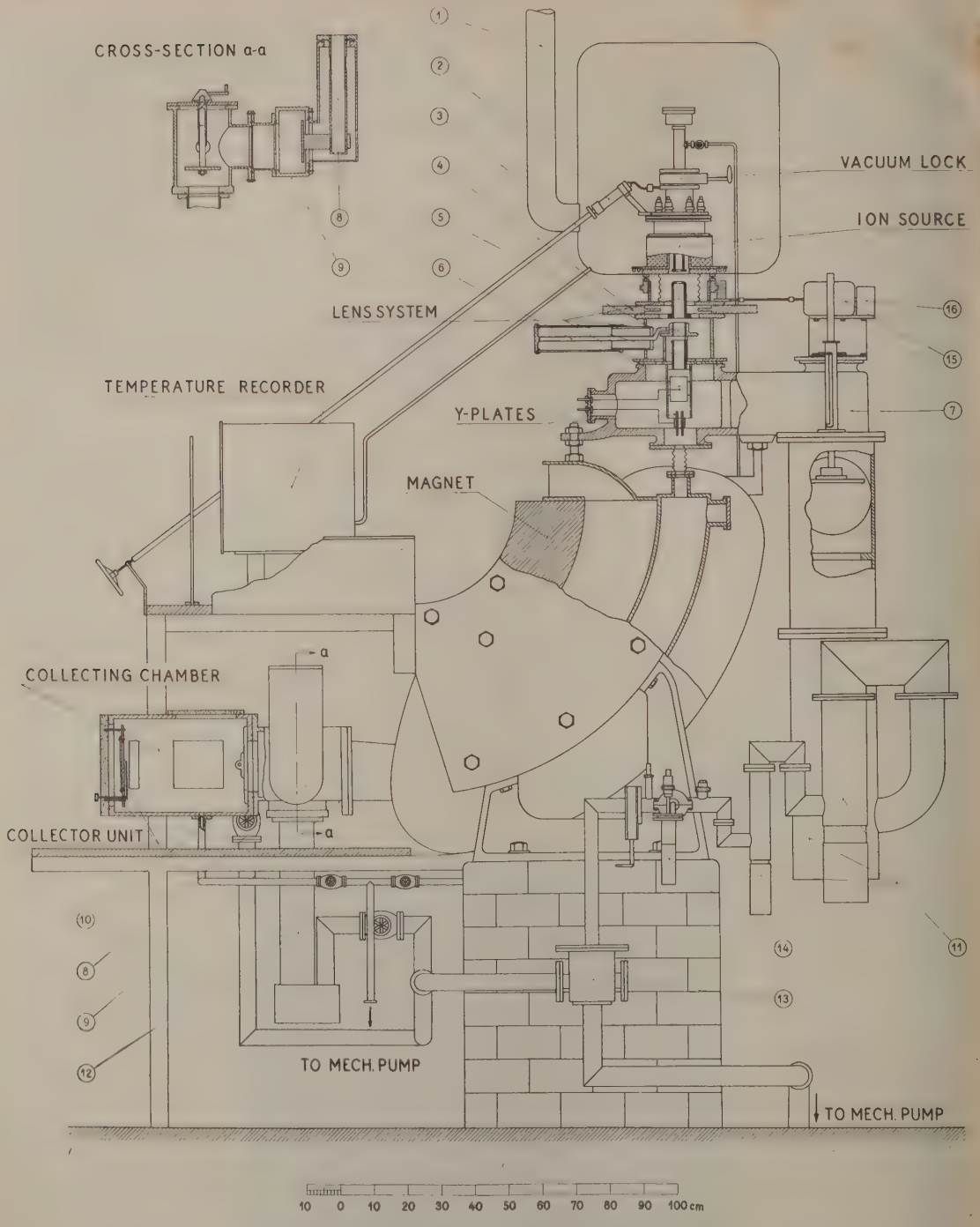

Fig. 1. Constructional details of the isotope separator.

in the aluminium tube (1). Two needle valves (2) serve for the adjustment of the gas inlet to the ion source. Both valves can be adjusted from the control desk by means of the insulating rods (3). The ion source is provided with a vacuum lock so that the furnace with the charging material can be introduced without breaking the main vacuum. The high tension insulator (4) is made of a 20 mm thick perspex plate.

The electrostatic focusing system is mounted in chamber (5) and consists of a set of three cylindrical electrodes of equal diameter and of a set of plane plates, the x-plates, parallel to the pole surfaces of the analyzing magnet. Another set of plane plates, the y-plates, is mounted above the magnet perpendicular to the pole surfaces.

The deflection magnet is of the 90° sector type with a radius of 80 cm, and a gap width of 6 cm[1]). The magnet field can be raised to approximately 8 000 gauss.

The collecting chamber is equipped with a valve (10) which makes it possible to change the collector arrangement without breaking the main vacuum.

2.1. VACUUM SYSTEM

A low pressure in the separator is very important since scattering from the residual gas atoms is the factor limiting the enrichment (see section 11).

The volume of the vacuum system is about 100 liters. In order to limit the pressure rise from the ion source to as short a portion of the beam path length as possible, the tube connecting chamber (7) to the deflecting chamber is made rather narrow and differential pumping is performed by the two sets of oil diffusion pumps (11) and (12). At a pressure of 10^{-4} mm Hg the pumping speeds are $\approx$ 1 000 liters/sec and $\approx$ 200 liters/sec, respectively.

Two liquid air traps are used. One is connected to chamber (7) in order to remove the condensable vapour originating from the ion source. The other trap (8) is attached to (9) opposite the pump (12) (see fig. 1, cross-section a–a). The main purpose of this trap is to limit the carbon layer on the collector.

A mechanical pump (pumping speed 10 m^3/h) is connected to the diffusion pumps via the manifold (13) which contains P_2O_5.

The pressure during operation is about 5×10^{-6} mm Hg and is measured by means of a Penning ionization gauge. The region above 10^{-3} mm Hg is measured by means of Pirani gauges.

In order to protect the insulators of the Penning gauge against deposition, this unit is mounted in a separate chamber connected by means of a bafled tube to chamber (7). A leak detector (14) is also connected to the vacuum system.

3. Remote Control of Ion Source Position

A systematic investigation of the magnetic ion source has shown the importance of being able to change the distance d between the ion source outlet and the first lens electrode in order to obtain the best working conditions[3]).

By means of the unit shown in fig. 4, d can easily be changed from the control desk during the separation.

4. Power Supply

Most of the power needed by the separator is delivered by an assembly consisting of a synchronous motor, a DC generator, and an AC generator (see fig. 3).

4.1. DC UNIT

The DC generator supplies the deflecting magnet. By means of a feed-back system the current delivered by the generator is kept constant within 1 part in 5 000. The principle of the feed-back system is shown in fig. 3. The zero drift of the DC coupled amplifier used is approximately 1 mV with respect to the input terminals. Therefore, in order to stay within the stated limits of constancy, the reference voltage has to be at least 5 volts. The reference voltage can be set from the control desk to any desired value corresponding to the range between zero and maximum current through the deflecting magnet coils. A detailed description of the

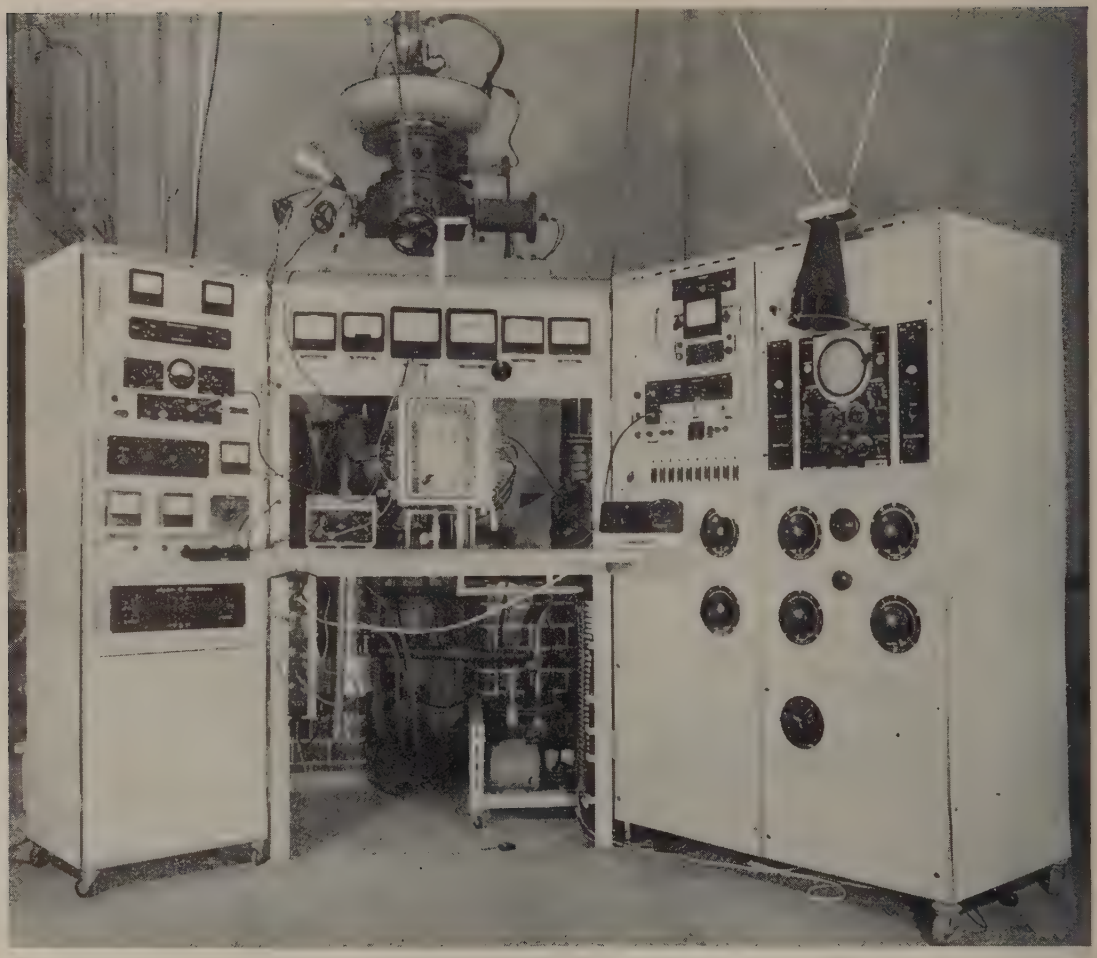

Fig. 2. The isotope separator.

current regulator is given by J. R. Jensen and K. O. Nielsen[6]).

4.2. AC UNIT

In order to obtain the degree of constancy required for the AC supply at the separator, it was found necessary to regulate the voltage from the AC generator. Since the high voltage supply is not separately regulated, peak-voltage regulating was preferred.

The generator and the regulator are shown schematically in fig. 3. The difference between a highly constant reference voltage and the peak voltage from the generator is amplified and controls the excitation current to the generator. The feedback thus introduced keeps the peak-voltage from the generator constant within 1 part in 1 000, between no-load and full-load conditions. The root-mean-square voltage increases by about 2%, while the mean voltage decreases by about 2%, when the load is increased from zero to its maximum value. This effect occurs since the content of higher harmonics depends on the load conditions.

[6]) J. R. Jensen and K. O. Nielsen, Ingeniøren No. **23** (1952)

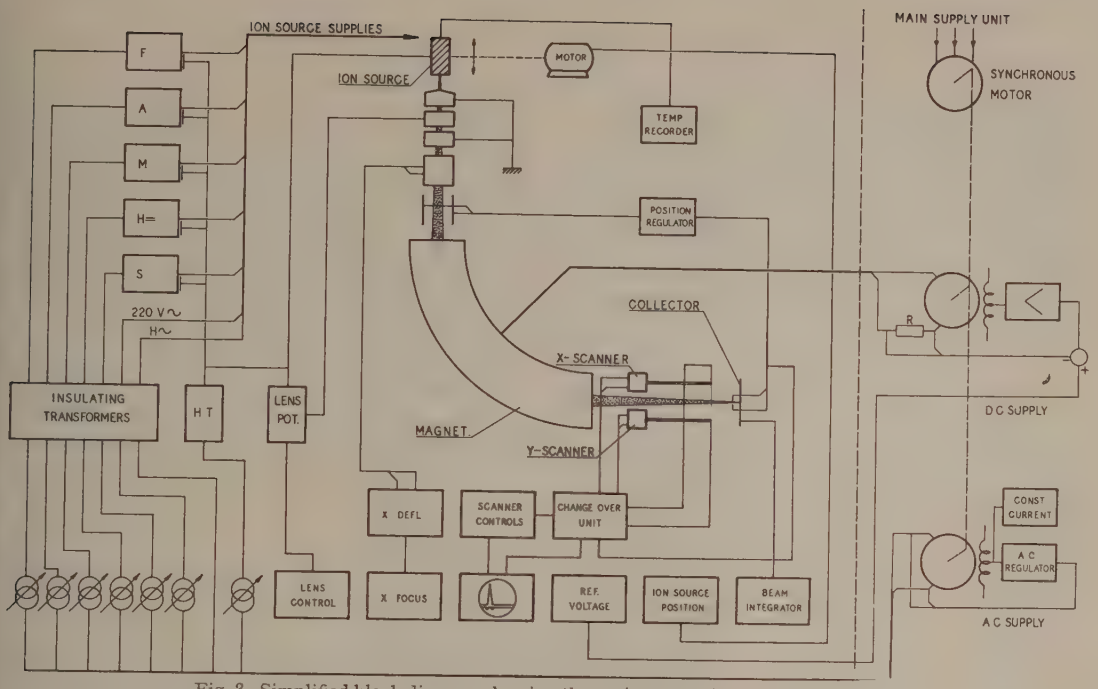

Fig. 3. Simplified block diagram showing the various supply and control units.

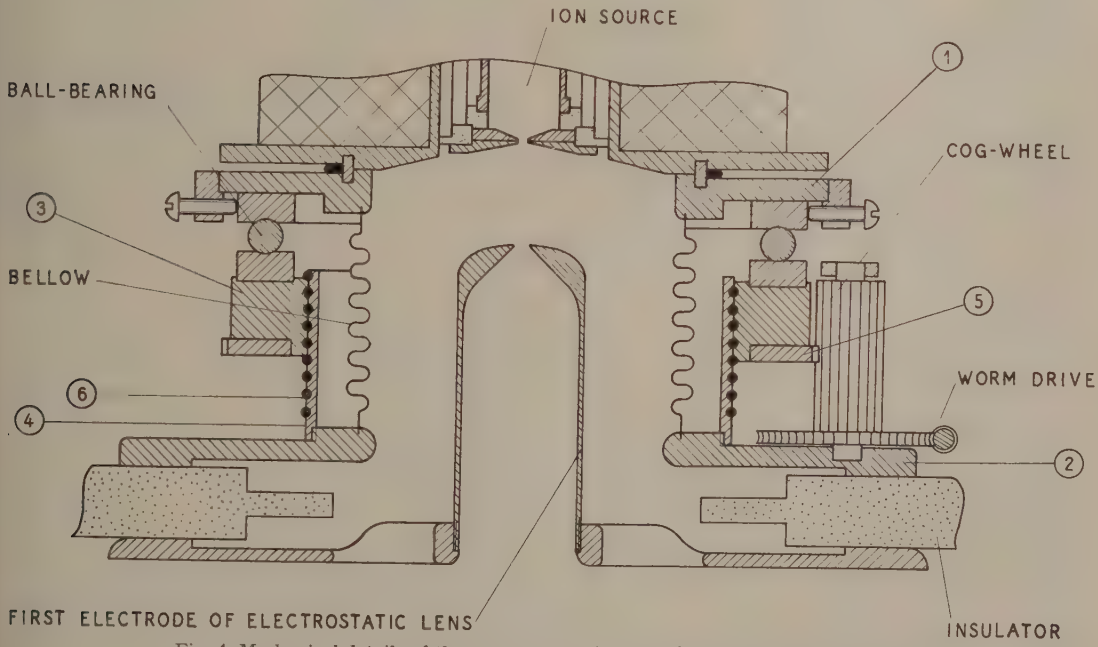

Fig. 4. Mechanical details of the remote control system for the ion source position.

The ion source is mounted on flanges (1). Flange (1) and flange (2) are connected by means of tombak bellows. The distance between the two flanges is determined by a cylindrical screw consisting of two cylinders (3) and (4). Cylinder (4) slides in cylinder (3), and both are provided with a semicircular groove in which a steel wire (6) is placed. Cylinder (3) is provided with a ring gear. To avoid torsion of the bellows, a ball bearing is inserted between flange (1) and cylinder (3). The ring gear (5) is meshed with a long cog wheel which is driven by means of a motor ((15) in fig. 1) at ground potential via an insulating rod and a worm gear. The change in position obtainable is 40 mm, and is carried out at a rate of 1.5 mm/sec. A potentiometer and two switches are also operated by the motor through a suitable gear system. The switches stop the motor when the ion source reaches the extreme positions. A voltmeter, which is graduated in mm, shows the position of the ion source.

5. High Voltage Supply

The high voltage supply consists of a voltage doubler circuit. Vacuum diodes are used as rectifiers. The 100 cycles/sec ripple voltage is smoothed to less than 0.2 volts at normal load. The output impedance of the source is ≈ 2 MΩ at DC and ≈ 50 kΩ at a frequency above 20 cycles/sec.

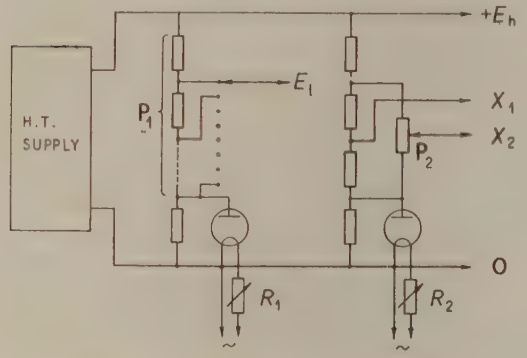

Fig. 5. Simplified circuit diagram of the lens voltage controls.

Fig. 5 shows the lens voltage supply and the voltage supply for the x-plates. Potentiometer P_1 can be operated from the control desk by means of an insulating rod. The two adjustable resistors R_1 and R_2 for accurate adjustment of the voltages, and potentiometer P_2 for adjustment of the position of the beam in axial direction are all placed at the control desk (see fig. 3).

6. Ion Source and Ion Source Supply

During recent years, only magnetic ion sources with end extraction have been used. The results of a systematic investigation of the plasma discharge and of the extracted beam are given in ref. [3]) and the construction of different types of ion sources is described in ref. [4]).

The present ion source consists of a housing with the magnet coil outside, and the discharge chamber placed inside as a separate unit. The requirements on the discharge chamber vary with the different elements to be separated. Therefore, it is important that the discharge chamber can be easily replaced by other types [4]).

All the power needed for the ion source is transmitted to high voltage level by means of insulating transformers (see fig. 3). Seven different supplies are available, five of which are provided with rectifiers and filters. The different supplies are adjusted by means of variacs placed at the control desk.

The following table (see also fig. 3) shows the capacity of the different supplies, which are all fed from the regulated AC unit (see section 4.2).

		Max. voltage	Max. current
F.	Filament supply	25 V	40 A DC
A.	Anode supply	300 V	1 A DC
M.	Ion source magnet coil supply	25 V	15 A DC
H⎓.	Ion source heating supply	25 V	40 A DC
S.	Sputtering supply	1000 V	0.5 A DC
H~.	Furnace heating supply	25 V	40 A AC
N.	Fixed on 220 volts		1 A AC

In order to avoid intensity modulation of the ion beam it is of special importance that the filament heating current I_h and the current to the ion source magnet are well filtered. The ripple is below 0.2 percent for these supplies.

The supply H⎓ is used for heating the discharge chamber (see ref. [4]) fig. 10). The tungsten wire placed around the cylindrical anode is bifilarly wound in order to reduce the magnetic field caused by the heating current. However, as the remaining field is not negligible, it is necessary also to use a rectified and well smoothed current for this filament.

The supply S can be used for a sputtering ion source of the same type as described by Druaux and Bernas [7]). A few investigations have been carried out with molybdenum and tungsten.

7. Accelerating System and Beam Focusing

The ion beam emerging from the ion source is accelerated in one step, whereafter it enters the magnet where the separation takes place.

[7]) I. Druaux and R. Bernas, Proc. 1955, Harwell Isotope Conf. (1956) Ch. 4.

The sector magnet operates like a cylindrical lens, and the image of a point source is a line. It is the normal practice to deposite the separated material on a backing in such a way that the sample can be used directly without chemical recovery. It is therefore of extreme importance that the ion beam be concentrated at the collector on an area so small that the largest possible fraction of the collected material can be utilized.

Both the distance from the ion source to the entrance of the magnet, and the distance from the exit of the magnet to the collector, are approximately equal to the radius of the central orbit in the analyzing magnet. Therefore, if the space charge effect were negligible, the focusing condition would be approximately fulfilled (Cartan's construction, see fig. 6a).

From calculations and experiments[8,9,10]) it appears that the space charge repulsion is appreciable at the ion currents normally used.

To compensate for the influence of the space charge two approaches have been attempted:

(a) The space charge has been neutralized by electrons produced in collisions between high speed ions and gas molecules[10,11]).

(b) The tendency of the space charge to spread the beam has been compensated by a convergent lens.

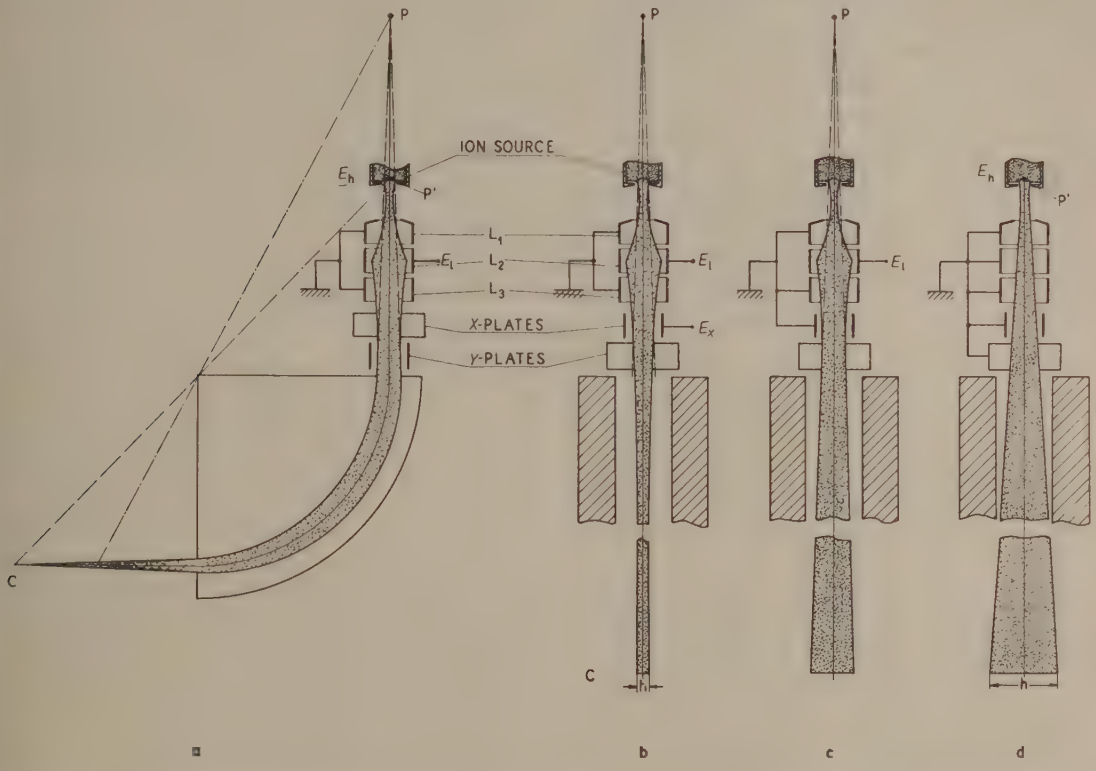

Fig. 6. (a) shows the focusing in the radial direction. The focusing in the axial direction is shown in the following cases: (b) $E_x > 0$ (c) $E_x = 0$ (d). With complete space charge neutralization by electrons and with all lens-electrodes grounded.

[8]) L. P. Smith, W. E. Parkins and A. T. Forrester, Phys. Rev. **72** (1947) 989.

[9]) E. W. Becker and W. Walcher, Cric. U.S. Nat. Bur. Stand. No. 522 (Washington, 1953) p. 225.

[10]) R. K. Wakerling and A. Guthrie, U.S.A.E.C. TID-5217.

[11]) C. J. Zilverschoon, Thesis (Amsterdam, 1954).

7.1. NEUTRALIZATION OF THE SPACE CHARGE

Experiments have been carried out with neutralization by electrons. Collisions between high speed ions and residual gas molecules gave a sufficient number of electrons. To keep electrons in the beam, it is necessary to avoid external electric fields by grounding all electrodes[11]) (see fig. 6d). Furthermore, an electron mirror of the type described by R. Bernas[12]) was introduced.

Good focusing was obtained for a krypton current of the order of 300 μA.

The length h of the mass spectrum image at the collector for an isotope separator with sector magnet and circular aperture in the ion source is determined by the divergence and the cross section of the beam at the entrance of the magnet. In this experiment the marginal trajectories are straight lines, and h will therefore be $(2 + \frac{1}{2}\pi)$ times the diameter of the beam at the entrance (see fig. 6d). h was found to be of the order of 50–60 mm. Since external electric fields could not be allowed, it was concluded that a reduction of h would be difficult†.

Since, however, an appreciable reduction of h is highly desirable, this method was abandoned and replaced by the use of a convergent lens system, as described in the following section.

7.2. LENS SYSTEM AND BEAM FOCUSING

The ion optical system is shown in figs. 6 and 7. Three cylindrical electrodes L_1, L_2 and L_3 constitute a symmetrical convergent lens; L_1 and L_3 are at ground potential while L_2 has the potential E_1 which can be adjusted from the control desk (see fig. 5).

By introducing electrodes with different potentials along the beam, electrical fields are set up, which pull away electrons out of the beam, thus strongly reducing the neutralization effect. Experiments (see section 9.1) indicate, however, that some neutralization by electrons still remains.

† Some reduction of h can be obtained by oblique entry and exit[13]); this seems to have the disadvantage of reducing radial focusing (private communications from the isotope separator group in Stockholm).

An exact calculation of the electrode shape is difficult because of the complexity of the ion paths near the ion source outlet and also because of the partial neutralization by electrons. Although it is impossible to give equations resulting in exact relations, the nature and the order of magnitude of the effects encountered can be indicated.

Since the boundary of the plasma in the ion source is an equipotential surface, the ions tend to leave it at right angles in the direction of the cross-over point P_1 (see fig. 7). The influence of

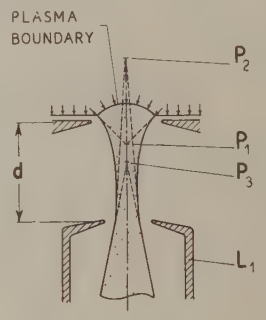

Fig. 7. Acceleration gap.

the space charge is strong as long as the ionic velocity is small. Furthermore, there is no appreciable neutralization of the space charge by electrons which here have a high velocity. The beam therefore diverges quickly, and the virtual object is formed at P_2 (constructed by drawing the tangents to the trajectories at the entrance of L_1).

The beam then passes through the convergent three-component lens consisting of L_1, L_2 and L_3. This convergent lens moves the virtual object upwards, while the space charge on the path length from L_1 to the magnet causes the virtual object to move downwards. The resulting virtual object constructed by drawing tangents to the beam at the entrance of the magnet is P (see fig. 6a). By adjusting the focusing system it is possible to move P up and down along the centre line.

[12]) R. Bernas, L. Kaluszyner et J. Druaux, J. Phys. Rad. 15 (1954) 273.

[13]) F. K. Herzog, Circ. U.S. Nat. Bur. Stand. No. 522 (Washington, 1953) p. 85.

If the space charge repulsion on the path length from the entrance of the magnet to the collector were negligible, the resulting virtual object would be in point P'.

During the passage through the magnet the beams due to the different isotopes separate, and at the same time their cross-sections are drawn out into strips. As a result of the strip-like shape of the cross-section, the major effect of the space charge is to widen the beam in the radial direction. To compensate for this radial spreading it is necessary to adjust the focusing system so that the resulting virtual object falls in point P above point P' (see fig. 6a). Since the beam spread due to space charge is smaller in axial direction than in radial direction, this change in position of the virtual object results in a considerable reduction in the length h of the beam image (comp. figs. 6c and 6d).

A further and adjustable reduction of h is obtained by means of the convergent cylindrical lens consisting of the x-plates. The potential of the x-plates E_x can be varied from zero to about $\frac{1}{20}$ E_h (see fig. 5). For small beam currents, it is actually possible to obtain a circular image with a diameter of about 2 mm.

The shape of the image at the collector can be adjusted by the following four parameters:

(1) *The shape and size* A_p of the plasma boundary at the ion source outlet can be adjusted by changing the values of the ion source parameters (I_h, E_a, B, p). This influences strongly the convergence of the beam near the ion source outlet; (see ref. [3]) section 4.2).

(2) *The distance d.*

(3) *The lens potential* E_1.

(4) *The cylindrical lens potential* E_x.

These four adjustments can be carried out while the separator is at work (see fig. 3).

When the ion source parameters and the lens potential are adjusted until maximum resolving power is obtained, the current I_i^m is represented by the expression

$$I_i^m = C(\theta) \cdot \frac{A_0 \cdot E_h^{3/2}}{d^2 \cdot M^{1/2}} \mu A \ , \qquad (1)$$

where A_0 is the area of the outlet opening in cm², M is the mass number of the ions, E_h the accelerating voltage in volts, d the distance in cm, and $C(\theta)$ a constant depending on the outlet angle θ (see ref. [3]) section 3.2); for $\theta \neq 80°$, we have $C(\theta) \approx 0.5 \times 10^{-2}$. Putting $E_h \approx 70$ kV, and taking the lower limit of 1.5 cm for d, we get a maximum current density of

$$i_i^m \approx \frac{400}{M^{1/2}} \mu A/mm^2 \ . \qquad (2a)$$

If, in addition to the high resolving power, we require a small value for h, it is necessary to increase d. The current density is then reduced to

$$i_i^m \approx \frac{100}{M^{1/2}} \mu A/mm^2 \ . \qquad (2b)$$

From published figures for other isotope separators and calutrons we find current densities out of the ion source of the same order. Thus, for a calutron ion source, the value 15 μA/mm² is given for uranium[14]). $M = 238$ in eqs. (2a) and 2(b) gives ≈ 25 μA/mm² and ≈ 6 μA/mm², respectively.

8. Beam Position Regulation

The full width at half maximum of the beam at the collecting plate is c. 0.7 mm at maximum resolving power (see section 10). Therefore, the position of the beam should be kept well defined to within about 0.2 mm during the separation in order to avoid serious decrease in the effective resolving power. This would require a constancy of 1 part in 10 000 for the magnetic field, and 1 part in 5 000 for the accelerating voltage. As these requirements are not met during an extended period of time, a position regulation based on a feed-back is introduced[11,15]).

Fig. 3 shows the principle of the feed-back system. One of the ion beams, in the following to be referred to as the reference beam, passes between two pins (sniffers) which are mounted

[14]) A. H. Barnes, S. M. MacNeille and C. Starr, U.S.A.E.C. Tid-5219.

[15]) S. Thulin, Ark. Fys. **9**, (1955) 107.

on the collecting plate. Each pin is grounded through resistances of equal value. The difference in ion current to the two pins and, hence, the voltage difference between them is a measure of the position of the beam relative to the pins. The voltage difference is amplified and fed to the y-plates. The amplifier used is DC coupled and able to give $\pm$ 500 volt output, which for $E_h = 60$ kV corresponds to a position change of the beam of $\pm$ 12 mm at the collector.

The total loop gain A will be proportional to the reference beam current and also greatly depend on the shape of the beam. The amplifier has therefore been provided with an attenuator which makes it possible to choose the most suitable loop gain.

The resulting error in position Δy will be $\Delta y = \Delta y'/(1 + A)$, where $\Delta y'$ is the error which would occur without any regulation.

The maximum deviation $\Delta y'$ for which the amplifier is able to compensate without being saturated is $\pm$ 12 mm at $E_h = 60$ kV. The total loop gain will usually be set to about 200. As long as the reference beam is still intercepted by the pins, the maximum resulting error will therefore be 0.06 mm.

When the beam is fixed by means of the regulator, the mass dispersion will be partly dependent upon the error $\Delta y'$. The maximum deviation in mass dispersion that can occur is 1.5% at $E_h = 60$ kV, as far as the reference beam is intercepted by the pins. This deviation must be taken into account if the mass number to be collected is far from the reference mass number.

9. Beam Observation Equipment

In order to obtain maximum resolving power it is important to have reliable information on the shape of the mass spectrum image at the collector[16]).

The image can be observed by means of a fluorescent screen. However, this method has been replaced by the following scanning systems which provide more accurate and exact information.

[16]) J. Schutten, C. J. Zilverschoon and J. Kistemaker, Appl. Sci. Res. B IV (1955) 217.

9.1. ELECTRICAL SCANNING OF THE BEAM

By adding an AC voltage to the accelerating voltage (by means of a transformer inserted between ground and the negative terminal of the last filter condenser of the high voltage supply) the ion beams are swept over a narrow slit in the collector plate. The ions passing through the slit will strike an electrode connected to the vertical deflecting amplifier of an oscilloscope. Voltage from the same source as used for the AC modulation of the high voltage is fed to the horizontal deflecting plates of the oscilloscope. In this way, an oscilloscope display of the mass spectrum is obtained. Since a large number of mass lines can be observed simultaneously on the screen, the electrical scanning system is very well suited for mass identification and for investigations on sidebands. In this connection, it is also advantageous that the focusing conditions for all mass lines seen on the screen are nearly the same because they are all observed at the same position of the collector. However, if this scanning system is used for checking the working conditions before separation takes place, it has to be taken into account that the focusing conditions are different at different positions on the collecting plate.

By means of a fluorescent screen and the mechanical beam scanning device described in the following section, we have found that the focusing conditions are not the same when the beam has a fixed position as when it is swept at 50 c/s. This effect probably occurs because the beam, when swept at this frequency, shifts position so fast in the magnetic field that the space charge neutralization due to the final value of the relaxation time is more incomplete than it is when the beam is fixed.

9.2. MECHANICAL SYSTEM FOR CONTINUOUS BEAM SCANNING

In order to be able to check the focusing conditions and the positions of the ion beams during the course of the entire separation, a mechanical beam scanning device has been developed[5]). The stationary ion beams are

scanned by moving a thin needle (the scanning needle) periodically through them. The position of the needle is translated into an electrical signal and fed to the horizontal deflecting plates of the oscilloscope. The vertical deflection is proportional to the ion current to the needle and, in a similar way as by electrical scanning, an oscilloscope trace of the mass spectrum is obtained.

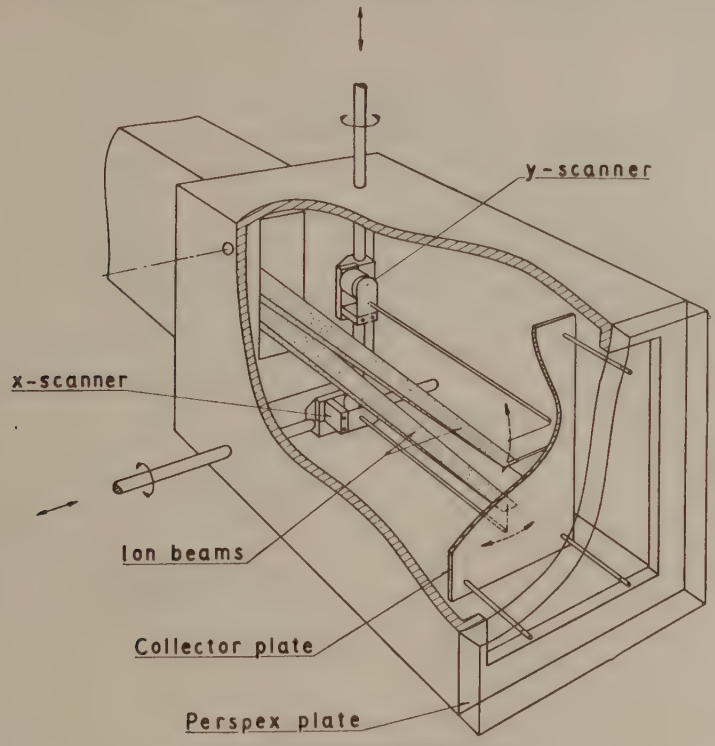

Fig. 8. Collecting chamber.

In fig. 9 is shown a schematic drawing of a scanner. The Rochelle salt crystals used earlier (see ref. [5]), section 2.1) have now been replaced by crystals of bariumtitanate, which are very stable and mechanically resistant. By mounting these crystals in the way shown in fig. 9, signals of the same size as obtained with the Rochelle salt crystals are achieved.

As shown in fig. 8, the collecting chamber has been provided with two scanners. Their positions can easily be changed both in vertical and in horizontal direction. The y-scanner gives the mass spectrum while the x-scanner gives the distribution of the ion current in the axial (horizontal) direction. Both scanners which are of similar construction can be set to cover any distance in the region 20 to 90 mm between the extreme positions of the scanning needle. The large amplitude is especially useful for the y-scanner, when used for mass identification, as

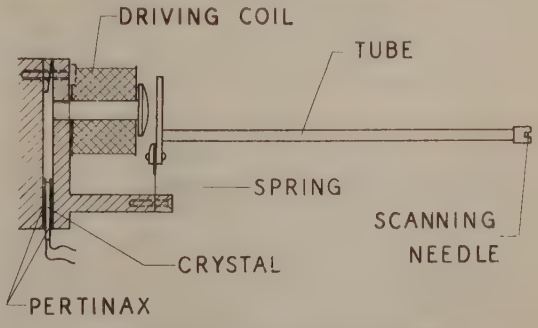

Fig. 9. Schematic drawing of a scanner.

the mass spectra of all elements heavier than lithium can be covered simultaneously. When the scanner is used for monitoring the separation, the amplitude and the position of the scanning needle are often adjusted so that only the reference beam is scanned.

The length of travel of the x-scanning needle is in general set to 50 mm. A more complete description of the mechanical and electronic equipment is given by K. O. Nielsen and O. Skilbreid[5]).

When separating isotopes in the heavy mass region where the mass dispersion is small, it may be difficult to verify which mass beam is intercepted by the pins used for position stabilization. The following, very simple circuit gives the wanted information.

The scanning needle will cast a "shadow" into the ion beam. When this shadow falls on the position regulation pins during the oscillation

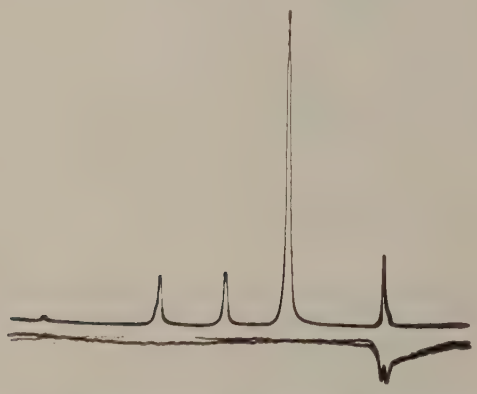

Fig. 10a. Double exposure of the oscilloscope screen showing the mass spectrum of Kr, and the positions of the "pins" relative to the mass spectrum (neg. pict.).

of the needle, negative signals occur in the latter. These signals are supplied to the vertical deflection circuit of the oscilloscope. The two negative pulses which occur on the oscilloscope screen then reveal which beam is being intercepted by the pins. In fig. 10a is shown the mass spectrum of krypton. The two negative pulses on the lower trace indicate the position of the "pins" relative to the position of the mass spectrum. Fig. 10b shows the corresponding distribution of the ion current in the horizontal direction.

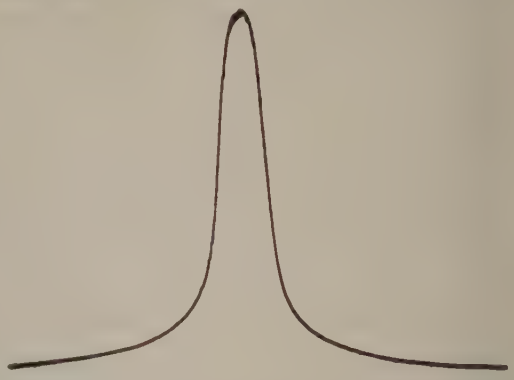

Fig. 10b. Distribution of the krypton beam in the axial direction. The distance between the extreme positions of the scanning needle is 50 mm (neg. pict.).

10. Collector

For an isotope separator of medium size the collected amount of material very seldom exceeds 1 mg. Therefore, the pocket technique with chemical recovery of the separated material is usually not applied, but either the direct deposition method or the sputtering method is used.

10.1. DIRECT DEPOSITION METHOD

Here, the ion beams impinge directly on a metal foil. The energetic ions penetrate into the surfaces, where they are gradually slowed down; at energies about 25 eV they are finally stopped and remain in the metal lattice. The penetration depth of the incoming ions depends on the energy and on the ratio A_1/A_2, where A_1 and A_2 are the mass numbers of the incoming particles and the target material, respectively. For 50 keV ions, the range lies in the region 5 $\mu g/cm^2$ to 100 $\mu g/cm^2$, see ref. [17]), fig. 5.

When sputtering occurs, the impinging ions remove some target material and, with this, also a part of the collected material already deposited. Depending on the degree of sputtering, the elements fall into two groups, those which build up a layer on the metal surface, and those for which the collected amount of material

[17]) K. O. Nielsen, Proc. 1955 Harwell Isotope Conf. (1956) Ch. 9.

reaches a saturation value. According to Dawton and Smith[18]), boron, silicon, titanium, tin, and tungsten belong to the first group, while the great majority of other elements belong to the second group. Only a few investigations have been carried out on this subject. S. Thulin[15]) has studied how krypton and xenon are collected on different target materials. Some measurements on the range, distribution and saturation effects of Mg, Xe, and Gd in aluminium are in progress at this Institute[19]).

Although, for most elements, the amount that can be collected by direct deposition has an upper limit lying in the region 5 $\mu g/cm^2$ to 100 $\mu g/cm^2$ [19,15]), the method has proved to be useful in the following cases:

(1) Preparation of radioactive sources for β- and γ-spectroscopy[15]). Here, the collected amount of material is so small that saturation is never reached. Stable isomers and isobars originating from impurities in the charging material however, can here cause some trouble.

(2) Frequently, the amount of material corresponding to the saturation value is sufficient for nuclear reaction studies in high voltage accelerators. In such studies the direct deposition method has been used with good results[20,21,22]).

(3) In collecting gases, the direct deposition method is the most practical one hitherto known, and has been extensively used by the Scandinavian isotope separator groups[23]).

10.2. SPUTTERING METHOD

When stable isotopes are to be collected, the limitation of the deposited amount of material due to the saturation effect often makes the direct deposition method unapplicable. A further inconvenience is the necessity of a thick backing in order to avoid destruction of the target by the ion beam. For collecting stable isotopes the sputtering method illustrated in fig. 11 is therefore useful in many cases. The

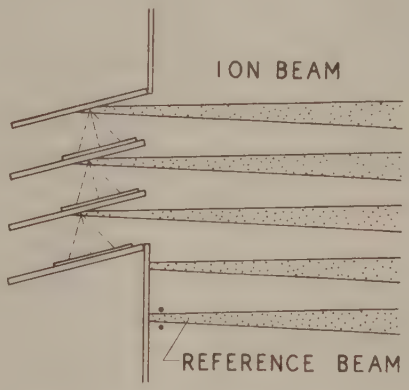

Fig. 11. Collection by the sputtering method.

ion beams impinge under an oblique angle on a metal target plate. Both the target material and the collected material will sputter from the surface and most of it will be caught on a plate placed in such a way that it is protected from the direct beam (see fig. 11). Since the sputtered atoms have low energies, it is possible to collect the separated material on a very thin formvar foil[22]). Furthermore, the collected amount seems not to be limited by any saturation effect. For rare earths on aluminium, preliminary measurements indicate that about 5 Al-atoms are deposited for each atom of the rare earth. Detailed investigations of this method of target preparation are under way[19]).

10.3. COLLECTOR ARRANGEMENT

The collector setup varies with the element to be separated and with the purpose for which the collected material is intended. We have therefore tried to build the collector unit in such a way that a great number of different collector arrangements, built according to a simple standard, can be easily mounted.

For accurate measurements of the ion current a small electromagnetic device is used; the magnetic field prevents the secondary electrons

[18]) R. H. V. M. Dawton and M. L. Smith, Quarterly Reviews (1955) Vol. IX, No. 1.

[19]) B. Elbek, K. O. Nielsen and M. C. Olesen, to be published.

[20]) K. J. Brostrøm, T. Huus and J. Koch, Nature **160** (1948) 498.

[21]) B. Elbek, B. S. Madsen and O. Nathan, Phil Mag. **46** (1955) 663.

[22]) B. Elbek, K. O. Nielsen and M. C. Olesen, Phys. Rev. **108** (1957) 406.

[23]) J. Koch, Nature **161** (1948) 566.

from leaving the collector[3]). This device can be mounted on the movable frame. The method for accurate measurements of the ion current has been checked both calorimetrically and with a Faraday cage. The same results were obtained with the different methods.

The movable frame can be replaced by a smaller frame which can be moved in the vertical direction. The same rack and pinion is used as before. This frame can be used when the collected material is to be deposited on a greater area than corresponding to the beam image. The ion beam to be collected passes through a fixed resolving slit and hits the collector plate which can be moved during the separation. In this way a rather uniform deposition can be obtained.

When the mass dispersion is sufficiently

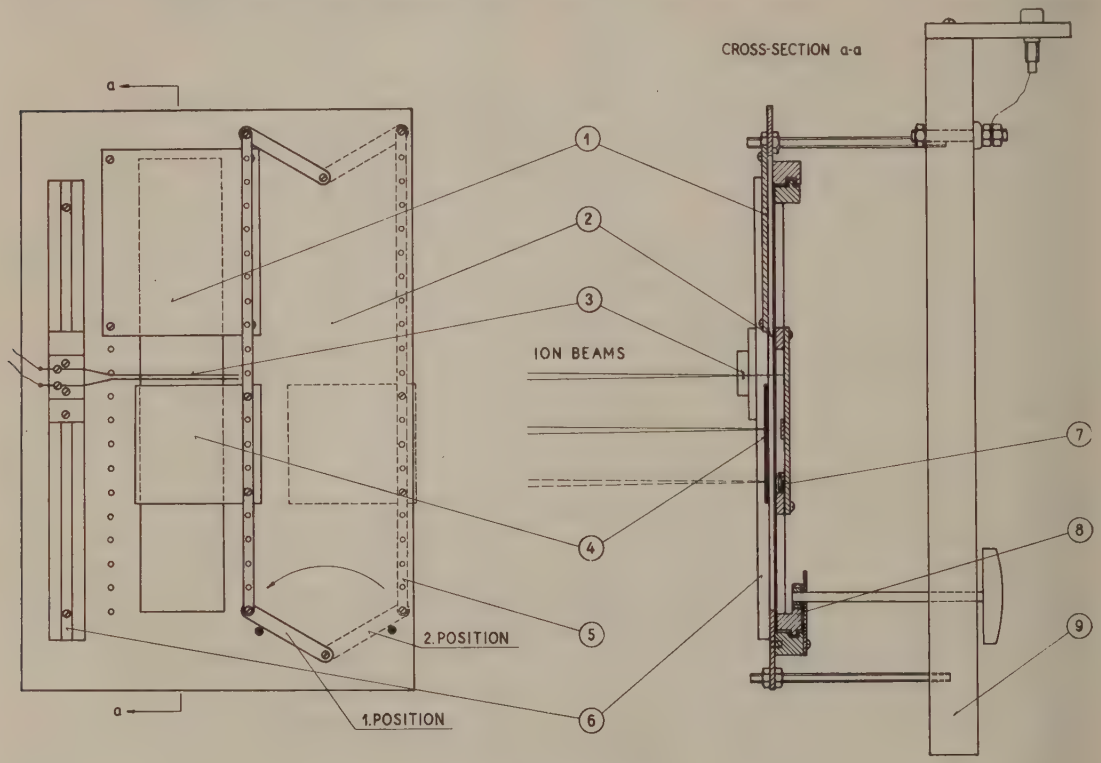

Fig. 12. Collector unit.

Fig. 12 shows the collector. The base plate (2) is mounted on a perspex plate (9). The two plates constitute a unit that can be mounted in the collecting chamber by four rods. The perspex plate is the end cover of the chamber (see fig. 1); it carries all electrical connections for the collector. The different collector arrangements are mounted on the base plate (screw holes and dimensions are standardized).

The movable shield (4) protects the collector against contamination during the initial stages of a separation and also in cases of high tension breakdown. Shields of different sizes and shapes can be mounted on the rod (5) which is provided with a row of screw holes.

On the front side of the base plate (the side facing the magnet), we also have a rod (6) provided with a dove-tail formed grove. A slider which fits this grove and can be locked in any wanted position carries the pins (3) for position regulation of the beam.

The rear side of the base plate carries a large frame (8). By means of a rack and pinion this frame can be moved in the horizontal direction. Smaller frames and special collector arrangements can be mounted on the movable frame. If several samples are to be made of the same isotope, a number of collectors (foils or sputter arrangements) are mounted side by side on the movable frame. 5 to 10 targets can be deposited in this way without breaking the vacuum in the collecting chamber.

great, such an extension of the deposited area can also be achieved by sweeping the beam electrically over the wanted area.

11. Operating Characteristics

In this section a short summary will be given of the operating data characterizing the separating process.

Fig. 13 shows the ion current distribution at the collector. The curve consists of the lines

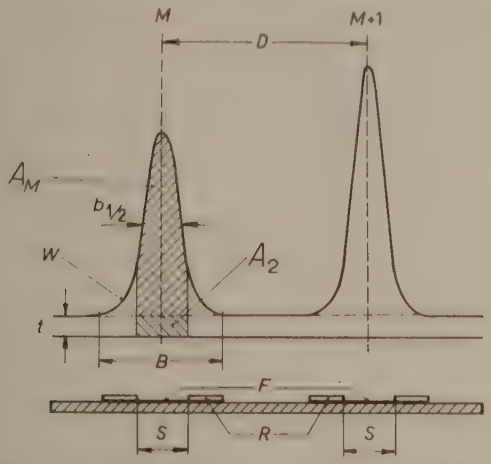

Fig. 13. Distribution of the ion currents to the collector in the direction of the mass spectrum.

representing the isotopes of the element, and a background t. According to a few measurements carried out with radioactive elements, we presume that this background has a nearly constant density in the extension of a mass spectrum, and that the amount of different isotopes in the background are proportional to their relative abundances in the element.

Fast ions interact with residual gas atoms by the following processes:

(a) Capture of electrons.

(b) Loss of electrons.

(c) Ionization.

(d) Elastic scattering.

Ions for which the processes (a) and (b) take place in the magnetic will contribute to the background. We therefore expect the background to decrease with decreasing pressure.

For processes (c) and (d) the ions suffer small angular deflections. Therefore, these processes increase the wings (w in fig. 13) and the width at half maximum $b_{\frac{1}{2}}$. At a pressure below 10^{-5} mm Hg the contribution to $b_{\frac{1}{2}}$ due to scattering seems to be negligible. Upon increasing the pressure above this value the first effect noticed is an enlargement of the wings.

Other contributions to the width $b_{\frac{1}{2}}$ have been discussed by S. Thullin[15]).

Usually $b_{\frac{1}{2}}$ lies in the region 0.7–2 mm, depending on the working conditions.

11.1. DISPERSION D

The distance between the collector plate and the exit of the magnet is equal to the radius R of the central orbit in the analyzing magnet. For isotopes with ionic mass $M \gg 1$, the dispersion at the collector is

$$D = 2 \cdot \frac{1}{2} \cdot R \cdot \frac{\Delta M}{M} = 800 \cdot \frac{\Delta M}{M} \text{ mm} \qquad (3a)$$

or for

$$\Delta M = 1 \qquad D = \frac{800}{M} \text{ mm} . \qquad (3b)$$

11.2. RESOLVING POWER R.P.

From the oscilloscope picture of the mass spectrum the resolving power can be determined by the equation

$$\text{RP} = \frac{D}{b_{\frac{1}{2}}} \cdot M = \frac{800}{b_{\frac{1}{2}}} . \qquad (4)$$

Corresponding to the values of $b_{\frac{1}{2}}$ mentioned above, RP lies in the region 400–1100...

11.3. ION CURRENT

When the ion source parameters and the lens voltage are adjusted to yield maximum RP, the ion current is given by eq. (1). From this equation it follows that I_i^m can be changed by changing either E_h, d, or the area A_0 of the outlet opening. E_h and d can easily be varied during the separation, while A_0 can only be altered by changing the bottom plate in the ion source.

The results of an investigation of I_i^m and RP during different running conditions are

given in ref. [3]), section 3. At the resolving power usually required, the total ion current is of the order

$$I_1^{\mathrm{m}} \approx \frac{1000}{M^{1/2}}\,\mu\mathrm{A}\ . \tag{5}$$

At the collector it is very often not the total beam current, but rather the area into which this current can be concentrated that is important. A deposited area of the order 1.5×5 mm^2 can easily be obtained (the boundary being taken where the intensity is half the maximum). For an isotope with the relative abundance a_M the current density at the collector will therefore be

$$i_{\mathrm{c}} \approx a_M \frac{150}{M^{1/2}}\,\mu\mathrm{A/mm^2}\ . \tag{6}$$

11.4. EFFICIENCY

The overall efficiency obtained $\eta_{\mathrm{t}} = g/G$, where g is the deposited amount of material and G is the amount of material fed to the ion source, usually is difficult to measure accurately. However, by using radioactive isotopes, reliable measurements of η_{t} can often be obtained by comparing the collected activity with the activity fed to the ion source[3]). Instead of η_{t} we mostly use the efficiency η_{s} found by integration of the total ion current to the collector. If the loss of ions in the region between the ion source and the collector is negligible, η_{s} is equal to the efficiency of the ion source given in ref. [8]) eq. (24). Consequently we have

$$\eta_{\mathrm{s}} = \frac{k}{p}\cdot\frac{E_h^{3/2}}{d^2}\ , \tag{7}$$

where p is the pressure in the discharge chamber and k is a constant depending on the ionization cross section of the element and on the geometry of the discharge chamber. For krypton and argon, efficiency η_{s} of the order up to 20% has been measured. Because of the formation of side bands an appreciable reduction of η_{s} often occurs when using chemical compounds as charging material. Usually η_{s} lies in the region 1–10%.

11.5. CONTAMINATION

In fig. 13 are shown the frames R which hold the foils F and serve as defining slits. Due to the background t a complete separation is never obtainable, even if $D \gg B$. In this case, the contamination q of an isotope sample at mass number M is

$$q = \frac{A_2(1-a_M)}{A_M + A_2} = \frac{S\cdot t(1-a_M)}{A_M + S\cdot t}\ , \tag{8}$$

where A_M and A_2 are the areas shown in fig. 13, S the width of the slit in the frame, and a_M the relative abundance of the isotope.

Taking t proportional to the total ion current I_{c}, we have:

$$t = \alpha\cdot I_{\mathrm{c}}\ . \tag{9}$$

At normal working pressure α is of the order 0.002 pr. mm. By means of eq. (9) we find

$$A_M = a_M\cdot\frac{t}{\alpha}\cdot\frac{S}{b_{\frac{1}{2}}}\cdot C\ . \tag{10}$$

Here, C is a constant which depends on the ratio $S/b_{\frac{1}{2}}$ and on the shape of the mass line.

$$S \ll b_{\frac{1}{2}}\ , \qquad C \approx 1$$

$$S \approx B\ , \qquad C \approx \tfrac{1}{2}$$

$$S \gg B\ , \qquad C \approx B/2S\ .$$

By introducing eq. (10) into eq. (8) we obtain

$$q = \frac{1-a_M}{C\dfrac{a_M}{\alpha\cdot b_{\frac{1}{2}}} + 1} = \frac{\alpha b_{\frac{1}{2}}(1-a_M)}{C\cdot a_M + \alpha b_{\frac{1}{2}}} \tag{11a}$$

or

$$q = \frac{\alpha\cdot b_{\frac{1}{2}}\cdot(1-a_M)}{C\cdot a_M} \tag{11b}$$

For RP constant, the smallest value of q is obtained when $S \ll b_{\frac{1}{2}}$, at the expense of η_{t}. In this case, we have $C = 1$ and for $b_{\frac{1}{2}} \approx 1$ mm, $C\cdot a_M \gg \alpha b_{\frac{1}{2}}$ and $\alpha \approx 0.002$ pr. mm we have

$$q \approx 0.002\,\frac{1-a_M}{a_M}\ . \tag{11c}$$

11.6. ENRICHMENT

For our purpose it is practical to define the enrichment as

$$n = f_2/f_1 \,, \tag{12}$$

where $f_2 = (1 - q)/q$ and $f_1 = a_M/(1 - a_M)$. Introducing eq. (11a) into eq. (12) we get, for $a_M \neq 1$,

$$n \quad \frac{C}{\alpha \cdot b_{\frac{1}{2}}} \; ; \; 1 \,, \tag{13a}$$

or

$$n = \frac{C}{\alpha \cdot b_{\frac{1}{2}}} \quad \text{for} \quad n \gg 1 \,. \tag{13b}$$

As seen from eqs. (13a) and (13b), the enrichment n is independent of the relative abundances of the isotopes and is therefore very convenient for the evaluation of the operating conditions. The enrichment will be independent of the relative abundance of the collected isotope even in the case where the assumption that the different isotopes contribute to the background relative to their relative abundances is not valid.

$C \approx 1$, $\alpha \approx 0.002$ pr. mm and $b_{\frac{1}{2}} \approx 1$ mm in eq. (13b) gives

$$n \approx 500 \,.$$

Under normal operating conditions the enrichment lies in the interval 200–500.

By introducing $f_2 = (1 - q)/q$ into eq. (12) we get

$$q = 1/(nf_1 + 1) \,. \tag{14}$$

In those cases where $q \ll 1$, eq. (14) can be used in the form

$$n \cdot q = 1/f_1 \,. \tag{15}$$

As already mentioned, the calculations above are carried out on the condition that $D \gg B$. In those cases where $D \approx B$, the contamination q of an isotope sample increases rapidly with decreasing D due to the wings on neighbouring mass lines. Furthermore, under this condition, the enrichment n will also depend on the relative abundance of the neighbouring mass lines.

12. Applications

A survey of the investigations in which the isotope separator has been used during recent years is given below. These fall into three groups: (a) sources for beta-gamma spectroscopy; (b) targets for nuclear reaction studies in high voltage accelerators; and (c) samples for hyperfine structure measurements.

12.1. SOURCES FOR β- and γ-SPECTROSCOPY

The direct deposition method has always been used, and the activity has usually been collected on 150 μg/cm^2 aluminium foils. The main advantages of this technique are discussed in refs. [24,25,26]).

A list of separated radioactive sources produced by means of the isotope separator is given in table 1.

A short description of some typical separations of radioactive isotopes follows below.

Re^{186} *and* Re^{188}

Natural Re has two isotopes, Re^{185} and Re^{187}. By irradiating natural Re in a reactor, the unstable isotopes Re^{186} and Re^{188} are produced with half-lives of 90 hours and 18 hours, respectively. Because of its longer half-life, Re^{186} can be studied without using separated sources, while in order to investigate Re^{188}, separated sources are necessary. The charge material, Re_2O_7, in a tight aluminium container (Re_2O_7 is very hygroscopic) was sent to a reactor. After irradiation, the container was opened and placed directly in the evaporation furnace which was immediately introduced into the ion source through the vacuum lock (see fig. 1). The separation was started 15 min after the arrival of the activity at the Institute. The result of the beta-gamma spectroscopic investigations is given in ref. [32]).

[24]) G. Andersson, Proc. 1955 Harwell Isotope Conf. (1956) Ch. 29.

[25]) R. Bernas, Proc. 1955 Harwell Isotope Conf. (1956) Ch. 30.

[26]) K. O. Nielsen, ot be published.

TABLE 1

Element	Collected isotopes	Half-Life	Production reaction	References
Phosphorus	P^{33}	25 d	$S^{33}(n,p)P^{33}$	27)
Krypton	Kr^{87}	78 m	Fission product	28)
Krypton	Kr^{88}	2.8 h	Fission product	28)
Krypton	Kr^{89}	3.2 m	Fission product	29)
Krypton	Kr^{90}	33 s	Fission product	29)
Krypton	Kr^{91}	10 s	Fission product	29)
Antimony	Sb^{115}	ca. 15 m	$Sn^{114}(d,n)Sb^{115}$	30)
Antimony	Sb^{116}	ca. 1 h	$Sn^{115}(d,n)Sb^{116}$	30)
Antimony	Sb^{116}	ca. 1 h	$In^{113}(\alpha,n)Sb^{116}$	30)
Antimony	Sb^{118}	5.1 h	$Sn^{117}(d,n)Sb^{118}$	30)
Antimony	Sb^{120}	5.2 d	$Sn^{118}(d,n)Sb^{120}$	30)
Gadolinium	Gd^{159}	18 h	$Gd^{158}(n,\gamma)Gd^{159}$	31)
Rhenium	Re^{186}	90 h	$Re^{185}(n,\gamma)Re^{186}$	32)
Rhenium	Re^{188}	17 h	$Re^{187}(n,\gamma)Re^{188}$	32)
Radon	Em^{222}	3.8 d	Emanation	33, 34)

27) B. Elbek, K. O. Nielsen and O. B. Nielsen, Phys. Rev. **95** (1954) 96.

28) J. Koch, O. Kofoed-Hansen, P. Kristensen and W. Drost-Hansen, Phys. Rev. **76** (1949) 279.

29) O. Kofoed-Hansen and K. O. Nielsen, Mat. Fys. Medd. Dan. Vid. Selsk. **26** (1951) no. 7.

30) B. Skytte Jensen, K. O. Nielsen, O. B. Nielsen and R. Sheline, to be published.

31) O. B. Nielsen and K. O. Nielsen, to be published.

32) K. O. Nielsen and O. B. Nielsen, to be published in Nuclear Physics.

33) K. O. Nielsen, O. B. Nielsen and M. A. Waggoner, Nuclear Physics **2** (1956) 476.

34) O. B. Nielsen and K. O. Nielsen, to be published.

RaB *and* RaC

The only suitable method of preparing β-ray sources of inert gases is the direct deposition method which is easily carried out in an isotope separator.

In the case of radon, it is not the β-decay of the radon itself, but the decay of its short-lived daughters, RaB and RaC, that is of interest. Although these isotopes have been studied for many years, it has not been possible to carry out accurate β-ray measurements owing to their short half-lives. By the deposition of radon, sources of 3.8 days half-life of high quality were available and, for the first time, it was possible to measure the conversion line intensities accurately[33,34]).

One of the needle valves connected to the ion source gas inlet is used for normal argon and the other for a mixture of argon and radon. Bismuth evaporated from the sublimation furnace inside the ion source is used as the reference beam. At the collector the distance between Bi^{209} and Em^{222} is about 5 cm.

The separation was started with a mixture of bismuth and argon. When the separator was working at optimum conditions, the needle valve for normal argon was closed and that for the mixture of argon and radon was opened, maintaining a constant pressure. A total efficiency of 22% was obtained in the most favourable case.

Antimony

Natural tin was bombarded in the cyclotron, and the radioactive antimony isotopes were formed by (d,n) reactions.

Antimony was then chemically separated from tin, and a suitable amount of stable antimony was added to the purified sample. The sample was introduced into the ion source, and the separation was started immediately.

Since some of the antimony isotopes have half-lives shorter than 15 min, the added amount of carrier should be small, so that the separation time is of the order of the half-life. However, it is always difficult to find stable operating

conditions when the amount of charge material is smaller than 5 mg (see ref. [4]), section 4.1). For a beam current equal to 50 μA and at an efficiency of the order of 1 percent, this amount of charge material corresponds to a separation time of about 10 min.

Another difficulty originates from the background of Sb^{117} which has a half-life of 2.7 h. The relative abundances of Sn^{114} and Sn^{115} are 0.65% and 0.34%, respectively. After bombardment with deuterons in the cyclotron we therefore expect, at an enrichment of about 200, the contamination from Sb^{117} to be of the order of 10 percent in Sb^{115} and in Sb^{116} (see eq. (16)). Some of these difficulties could be avoided by producing the radioactive isotopes with α-bombardment of indium. The remaining difficulties can probably be solved by using enriched tin and indium.

12.2. PREPARATIONS OF STABLE TARGETS FOR HIGH VOLTAGE ACCELERATORS

For this purpose the collector arrangement shown in fig. 11 is used. Two targets of each isotope are obtained at the same time, one produced by the direct deposition method on a thick backing and one by the sputtering method on a thin formvar foil.

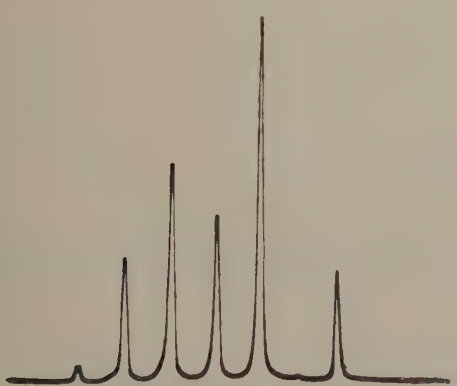

Fig. 14. Mass spectrum of Yb (neg. pict.).

Table 2 gives a list of separated targets produced during recent years. The mass spectrum of ytterbium is shown in fig. 14.

Table 2

Element	Collected isotopes	References
Mg	24, 25, 26	[21])
Ce	140, 142	
Gd	154, 155, 156, 157, 158, 160	
Dy	160, 161, 162, 163, 164	[22])
Er	166, 167, 168, 170	
Yb	171, 172, 173, 174, 176	[22])
Lu	175, 176	[35])

[35]) B. Elbek, M. C. Olesen and O. Skilbreid, to be published.

12.3. SEPARATED SAMPLES FOR OPTICAL HYPERFINE STRUCTURE MEASUREMENTS

For this purpose samples of almost all inert gas isotopes have been produced by means of the isotope separator[2,23]), and most of these separations were carried out at a time when the low voltage capillary ion source was used. After the introduction of the new ion source, samples of Kr^{84} and Kr^{85} have been made for the same purpose[36,37]). Although an ion source with high temperature is not necessary when separating gases, it proved to be very useful, because the formation of hydrides decreases faster at higher temperatures (see ref. [4]) section 4.1).

13. Acknowledgements

We wish to express our gratitude to Professor Niels Bohr for the excellent working conditions at the Institute for Theoretical Physics.

We are indebted to Professor J. Koch, who built the isotope separator at the Institute and initiated the reconstruction in the new laboratory, for his continuous interest in our work.

We also want to thank Mr. Gudbjerg-Hansen and the workshop personnel for very valuable assistance.

Furthermore, we like to emphasize that the extremely good contact with the three separator groups in Sweden has been of invaluable importance for the development of the isotope separator in Copenhagen.

[36]) E. Rasmussen and V. Middelboe, Mat. Fys. Medd. Dan. Vid. Selsk. **30** (1955) no. 13.

[37]) E. Rasmussen and V. Middelboe, Z. f. Phys. Bd. **141** (1955) 160.

NUCLEAR INSTRUMENTS 2 (1958) 34–38; NORTH-HOLLAND PUBLISHING CO. – AMSTERDAM

STUDY OF SOME CHARACTERISTICS OF THE GM-DISCHARGE

J. KOCH

Central Research Institute for Physics, Budapest

Received 5 November 1957

The GM-pulse was investigated in the case of a small working resis ance such as is commonly used in a quenching circuit. The experimental results are in terpreted on hand of a new model of the GM-discharge.

1. Introduction

It is well known from the literature that two periods may be distinguished during a discharge in a GM-tube.

The first period starts when an electron is released in the GM-tube. This, under the influence of the applied electric field, moves towards the wire and initiates an avalanche in the close vicinity of the wire, where the field strength is great enough for collision ionization. The electrons originating in the avalanche travel to the wire, while the photons start new avalanches by ionization or photoelectric effect, till the wire is completely covered by the space charge of the slowly moving positive ions.

In the second period the positive space charge moves towards the cathode under the influence of the applied electric field.

The investigations of Stever[1]) and others, made with beaded wire GM-counters, revealed the fact, that in self-quenching counters the discharge spreads in the close vicinity of the wire. The velocity of the spread has been measured by many authors[2–12]).

If, shortly after the beginning of the discharge, the voltage on a GM-counter is reduced to a value under the starting voltage, the spread of the discharge stops and a great part of the tube remains sensitive. Thus the relatively slow spread of the discharge may be used to increase the resolving power of GM-counters.

Simpson[13]) and Hodson[14]) were the first to use circuits which were suitable for stopping the discharge. Such quenching circuits have been frequently studied since, among others by Fenyves and Haiman[15]).

As for quenching circuits of short dead time working resistance has to be low, we investigated the characteristics of the GM-pulse at similar low working resistances.

2. The GM-Pulse

The current in a GM-counter is carried by electrons and positive ions. Accordingly, the current pulse has also two components: electron and ion current pulse. The duration of the electron pulse is essentially the duration of the spread of the discharge, which is of the order of microseconds. The duration of the ion current pulse is the time of travel of the ion sheath,

[1]) H. G. Stever, Phys. Rev. **61** (1942) 38.
[2]) A. G. M. van Gemert, Physica **9** (1942) 556; 658.
[3]) J. M. Hill and J. V. Dunworth, Nature **158** (1946) 833.
[4]) P. Huber *et al.*, Helv. Phys. Acta **19** (1946) 204.
[5]) F. Alder *et al.*, Helv. Phys. Acta **20** (1947) 73.
[6]) E. Wantuch, Phys. Rev. **71** (1947) 646.
[7]) D. H. Wilkinson, Phys. Rev. **74** (1948) 1417.
[8]) A. J. Knowles, Phys. Rev. **74** (1948) 627.
[9]) C. B. Balakrishnan and J. D. Craggs, Proc. Phys. Soc. A **63** (1950) 358.
[10]) H. Saltzmann and C. G. Montgomery, Rev. Sci. Instr. **21** (1950) 548.
[11]) A. R. Laufer, Rev. Sci. Instr. **21** (1950) 244.
[12]) A. C. Mortin and J. F. Roose, Proc. Phys. Soc. B **67** (1954) 161.
[13]) J. A. Simpson, Phys. Rev. **66** (1944) 39.
[14]) A. L. Hodson, J. Sci. Instr. **25** (1948) 11.
[15]) E. Fenyves and O. Haiman, Proc. IIIrd Class of the Hung. Acad. Sci. **2** (1952) 351 (in Hungarian).

being of the order of milliseconds. As will be seen, the character of the GM-pulse is highly dependent on the value of the working resistance.

In order to design a quenching circuit, the characteristics i.e. rise time and amplitude of the GM-pulse, have to be known. For their investigation we used the arrangement shown in fig. 1. R is the working resistance and C is

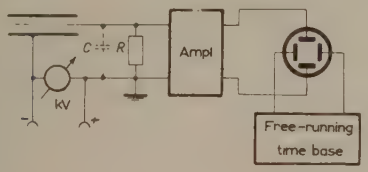

Fig. 1. Experimental arrangement.

the sum of capacity of the GM-tube, stray capacities and input capacity of the circuit using the GM-pulse. If $\tau = RC$ is much greater than the time of spread of the discharge, the counter is a source of charge and the amplitude of the output is then $V = QC^{-1}$, where Q is the charge liberated in one discharge. If τ is much less than the time of spread of the discharge, the momentary value of voltage on the working resistance is proportional to the momentary value of current flowing in the tube.

When a small working resistance is used, the current originating from the motion of electrons is on the whole much greater than the current originating from the motion of positive ions, for the positive and negative charges liberated in one discharge are equal and the mobility of electrons is much greater than that of positive ions.

The question arises as to the value of the working resistance which is to be regarded as small. It is known from the literature, that the velocity of the spread is of the order of 10 cm/μsec. The time of spread is in our case about 10 μsec. The working resistance can be regarded as small when τ is smaller than 1/100 of the time of spread, i.e. 0.1 μsec. As in our case $C = 20$ pF, R must be smaller than 5 000 ohms.

One cannot find data on the electron current in the literature. Only papers of Huber and of Alder *et al.*[4, 5]) contain data on GM-pulses studied at a low working resistance, but in the author's opinion their theoretical basis is somewhat doubtful. In the present investigations it was attempted to introduce a new model in the hope of a better understanding of the GM-discharge. In this way, among other questions, the very much disputed problem as to the magnitude of the electron pulse was solved.

3. Experimental Arrangement

The block diagram of the experimental arrangement is shown in fig. 1. Individual GM-pulses appearing on the load resistance were photographed from the screen of the cathode-ray tube. A free-running time base was used to avoid the difficulties of the distortion-free delaying of pulses. The photographs were taken at random times with suitable time of exposition and counting rate of the tube, so that nearly all photographs show GM-pulses. The amplifier had a rise time of 0.15 μsec. The accelerating potential of the cathode-ray tube was 6 kV. The estimated accuracy of time and amplitude measurement was about 10%.

The cathode of the GM-tube was a copper cylinder of 38 mm internal diameter and the anode a tungsten wire of 0.1 mm diameter. The end pieces were soft soldered and fixed with Araldite[16]). The wire wore a glass bead near each end, their distance being 121 cm. The filling was argon and alcohol at a pressure of 90 mm and 10 mm Hg, respectively. The starting voltage was 982 V. The supply voltage of the GM-tube was measured with an absolute error of 1% and reproducibility of 3 V.

4. Results and their Interpretation

Two typical photographs of current pulses may be seen in figs. 2a and 3a. They were taken at 51 V overvoltage. When comparison is made between figs. 2a and 3a and figs. 2b and 3b, it is seen that the shape of pulses may well be approximated by a single or double rectangle. This fact may be easily explained on the basis

[16]) A. Somogyi, Reports of Cent. Res. Inst. Phys., Budapest 2 (1954) 38 (in Hungarian).

of some wellknown properties of the discharge.

So as to interpret the behaviour of the GM-counters in the case of low working resistance, we attempt to visualize the discharge in the following way. One may suppose that collision ionization is possible only at the edge of the ion sheath. The discharge is "burning" at the ends of the ion sheath in the form of two rings around the wire, their width being of the order of the mean free path of the photons. The rings travel on the wire to where there is not yet any space charge. The absorption mean free path of the photons in the filling gas of a self-quenching GM-tube is of the order of 1 mm[1]). Thus the width of the ring can be assumed to be constant and as the rate of avalanches is also constant, it follows that the electron current of the discharge is constant (disregarding the time of development and dying off of the ring).

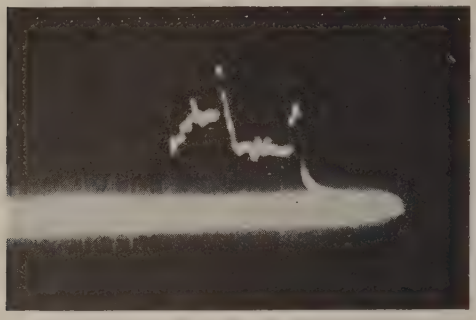

Fig. 2a

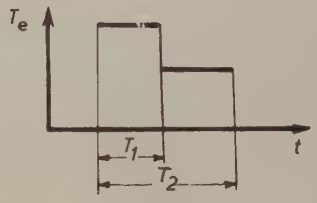

Fig. 2b

Fig. 2. Individual G.M.-pulse. (a) Actual photograph. (b) First Approximation of its shape.

The burning rings are travelling on the wire in opposite directions from the starting point until the one which had the shorter way to travel, reaches the end of the tube and dies off. The remaining ring travels until in its turn it reaches the other end of the tube. This model is supported by the fact that on some of the oscillograms the current is seen to decrease in two steps: first, corresponding to the extinction of the first ring, the current drops to half its value and at a later time, corresponding to the extinction of the second ring, it ceases altogether (figs. 2a and b).

It may happen that the discharge starts from one end of the tube. In such a case (see fig. 3) one ring only travels over the whole length of the wire, the duration of the current pulse being longer and the current intensity equalling half the initial current intensity of the former case.

One can easily calculate the velocity of the spread when the duration of the components of the pulse described above are known. In the case of the pulse of fig. 3 the velocity v is obtained by $v = L/T$, where L is the sensitive length of the wire. For pulses of the type shown in fig. 3, T is equal to the duration of the pulse, while for pulses containing two sections, as

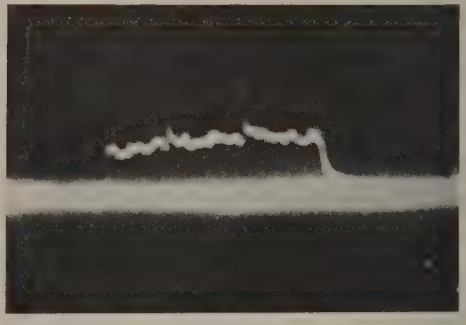

Fig. 3a

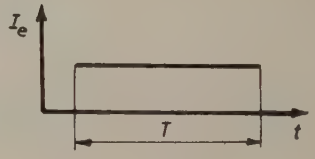

Fig. 3b

Fig. 3. Individual G.M.-pulse. (a) Acutal photograph. (b) First approximation of its shape.

shown in fig. 2, $T = T_1 + T_2$, where T_1 is the time after which the first part of the discharge goes out, and T_2 the duration of the whole pulse.

One can see from the photographs, that the pulses are not exactly rectangular, but that their tops show a rising or falling tendency. This phenomenon is easily explained when considering the effects of the current originating from the motion of positive ions. The current of the pulse of fig. 3a has two components (fig. 4) : the electron current I_e, which is constant,

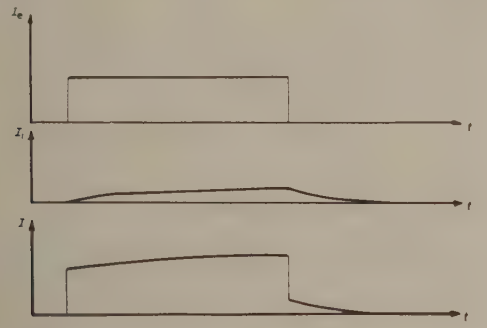

Fig. 4. Second approximation of shape of pulse from fig. 3a.

and the ion current I_i which increases during the time of spread, when the number of moving ions increases, and then decreases when the ions reach the region of lower field strength.

The case of the pulse of fig. 2 is a little more complicated. Here owing to the bidirectional spread, one must take into account four components of current.

The formation of the pulse is shown in fig. 5. The discharge spreads in both directions for the time T_1, during this time electron currents I_{e1} and I_{i2} are flowing. As the first ring reaches the end of the tube, I_{e1} ceases and I_{i2} begins to decrease. The total current I is the sum of the components.

As can be seen from the photographs, the top of the pulses is wavy, and also peaks are visible. This fact may be explained by the exponential character of the absorption law of photons. A fraction of the photons can travel for a length many times the mean free path without being absorbed and when absorbed, these photons start a new pair of burning rings thus momentarily increasing the value of the current. After some time the original ring reaches one ring of the pair started by some of the above-mentioned photons, they die off and the current decreases to its former value.

We remark that the time of development of the space charge is very short in comparison with the time of spread of the discharge and may in first approximation be neglected. Considering namely a small section of the tube, where the discharge starts, it is known that the time required for the avalanche to develop is of the order of 10^{-10} sec [17]).

If the above explanation of the differences between pulses is correct, different shapes of pulses must be obtained when starting the discharges at different places. That this is indeed so, was experimentally proved by means

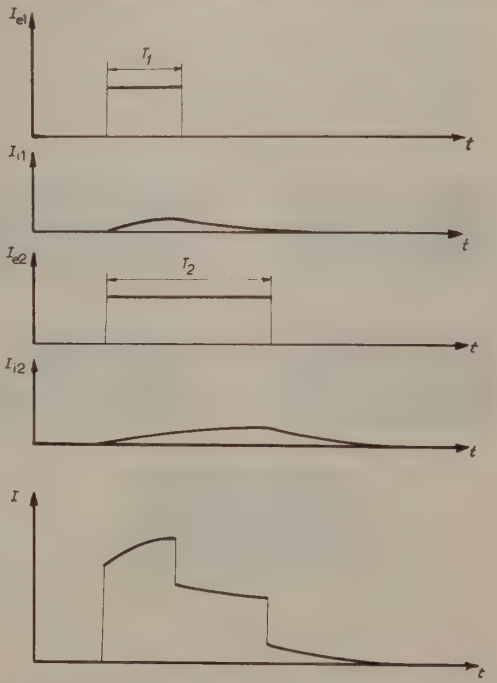

Fig. 5. Second approximation of shape of pulse from fig. 2a.

of an investigation carried out with an arrangement similar to that of Huber[4]) and Alder[5]), shown in fig. 6. A γ-ray source placed in one of

[17]) S. C. Curran and J. D. Craggs, Counting Tubes (Acad. Press New York, 1949).

the channels in the lead block increases the counting rate of the GM-tube to twenty times

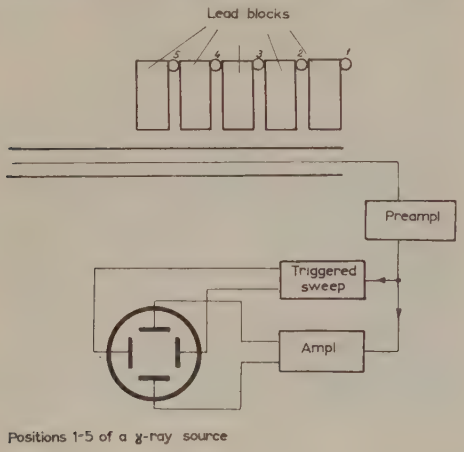

Fig. 6. Arrangement for control measurement.

its background rate and in consequence of this most of the discharges start from a well-defined place in the tube. The sweep of the oscilloscope was triggered by the GM-pulses.

The average of many pulses was photographed

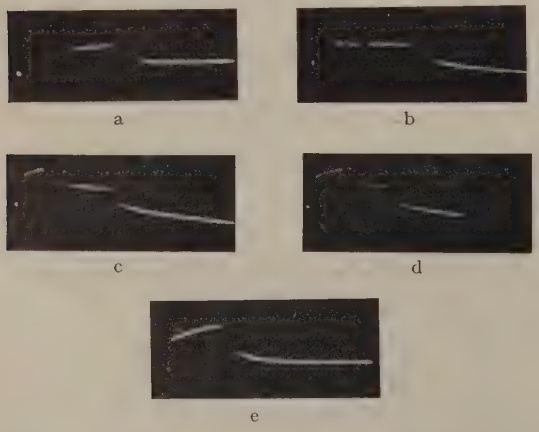

Fig. 7. Photographs obtained with the arrangement shown in fig. 6.

from the screen of the cathode-ray tube. The pulse shapes obtained when the γ-ray source was in positions 1–5 (fig. 6) are shown in figs. 7a–e, respectively.

The dependence of the velocity and current of the spread on the voltage was studied by evaluating the individual pulse photographs. Fig. 8 shows the dependence of the velocity of spread on the voltage. The velocity is nearly linearly proportional to overvoltage.

The dependence on the voltage of the electron

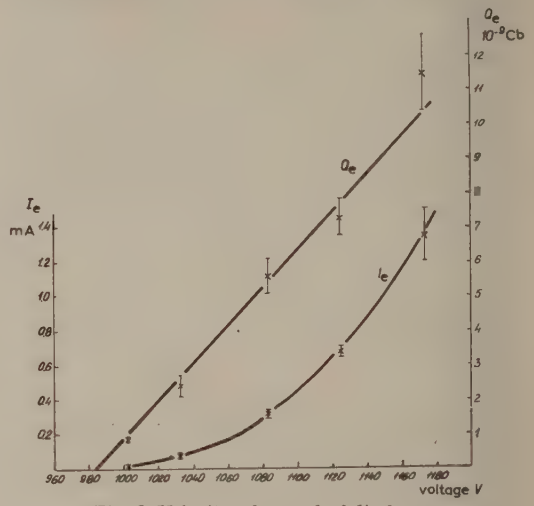

Fig. 8. Velocity of spread of discharge.

current I_e and the charge Q liberated in one discharge is given in fig. 9. The dependence of the charge on voltage serves as a check for the

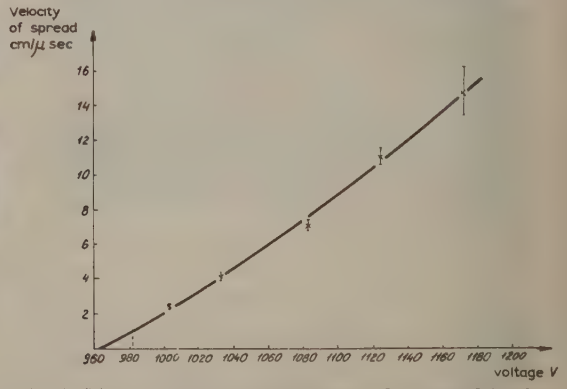

Fig. 9. Electron current I_2 and charge Q liberated in the discharge.

measurement, for it is well known, that the liberated charge is linearly proportional to overvoltage. Fig. 9 shows this condition to be fulfilled. The deviations here as wel las those in fig. 8 are standard errors.

The author is indebted to Prof. L. Jánossy and Mr. Zs. Náray for their valuable advice.

NUCLEAR INSTRUMENTS 2 (1958) 39–43; NORTH-HOLLAND PUBLISHING CO. – AMSTERDAM

CHEMICAL TECHNIQUES USED IN CONNECTION WITH β-SPECTROSCOPIC WORK ON RARE EARTH ELEMENTS

P. GREGERS HANSEN† AND R. K. SHELINE††

Institute for Theoretical Physics, University of Copenhagen

Received 12 October 1957

Cyclotron target preparation, chemical separation by ion exchange chromatography, and source preparation are described.

1. Introduction

Individually, the specific methods described in this paper have been used previously. It is therefore intended here to describe their collective application in beta spectroscopy with emphasis on the range of their applicability and usefulness rather than the specific details of the individual methods.

In general, procedures for the preparation of sources for β-ray spectroscopy should fulfill two conditions, viz.:

(1) The resulting source must be sufficiently thin for the energy region to be studied.

(2) The period of time needed for the preparation of the source must not be long as compared with the half-life involved.

Since these two conditions, in the case of short half-lives, will have a tendency to counteract each other, the appropriate method will often have to be a compromise.

A sequence of procedures that has been found applicable for work on rare earth activities with half-lives greater than two hours follows.

2. Experimental Procedure

Most of the spectroscopic work was carried out on cyclotron produced activities. The chemistry involved in this problem, can be considered under the following headings illustrated by Tb-activity produced from separated Eu-isotopes by (α, n) reactions:

(A) Preparation of a cyclotron target of Eu_2O_3.

(B) Separation of Tb from Eu by ion exchange chromatography.

(C) Source preparation by microcolumn method.

A relatively small column was used for the chromatographic separation since the time required for the separation decreases with the size of the ion exchange column. This, in turn, limited the amount of material that could be bombarded.

A general requirement in the preparation of sources is the necessity of high purity. Therefore all reagents used were made up from double distilled cation exchanged water. Ammonia and hydrochloric acid were prepared by bringing their respective gases into contact with water. Stock solutions of lactic acid or α-hydroxy-isobutyric acid were purified by passing the solution through a Dowex 50 column on the hydrogen form. All reagents were stored in polyethylene bottles.

2.1. TARGET PREPARATION

In order to obtain as high a specific activity as possible, it was desirable not to bombard more than the 5 mg of Eu which could be

† Permanent address: Danish Atomic Energy Commission, Risø, Roskilde, Denmark.

†† Guggenheim and Fulbright research scholar on leave of absence from Florida State University. Fla.

tolerated in the ion exchange step (see § 2.2). Furthermore, the targets had to be heat resistant and to some extent shock resistant so that bombardments could be carried out in the internal beam of the Copenhagen cyclotron without any covering of the target.

The method used for this purpose was a modification of that originally used by Glover and Borrell [1]) for the preparation of thin films of plutonium and uranium. 5 mg Eu_2O_3 were dissolved in conc. HNO_3 and heated under an infrared lamp to form $Eu(NO_3)_3$. The $Eu(NO_3)_3$ was dissolved in approx. 2 cc of acetone, and a small amount of Zapon lacquer was added. A gold plate, $30 \times 15 \times 1$ mm^3, was used as target backing. The solution was transferred to the gold plate first by means of a brush to define the target area, subsequently dropwise from a small separatory funnel.

After each 1–3 drops, the acetone was allowed time to evaporate and the gold plate was then heated slowly in the small flame of a Bunsen burner until only Eu_2O_3 was left. The layer of Eu_2O_3 finally obtained in this way adhered well to the target and was rather uniform. Bombardments were carried out with the gold plate held to the cyclotron target holder by means of screws.

2.2. The ion exchange columns used were of the type described by Thompson, Harvey, Choppin and Seaborg [2]). The Dowex 50 resin had a settling rate in water of 2–4 mm/min. Spherical and colloidal types of resin were applied. They give about the same separation characteristics, the latter, however, seems less convenient since the dropping rate is more difficult to control. The resin bed was 2 mm in diameter and approximately 7 cm long. The free column volume was 5 drops. A glass jacket through which trichloroethylene vapor was passed maintained the temperature at 87°C. α-hydroxy isobutyric acid [3]) was used as the eluant, except for a few cases where it was replaced by lactic acid. The columns were usually operated with a water head, 0.5 to 3 m, obtained by means of a mercury pressure system.

Prior to use, a column was conditioned with the eluant for a few hours in order to bring it to the ammonia form. Liquid above the resin was then removed and a few drops of water were added and pushed down into the column. Subsequently the irradiated europium dissolved in a small excess of hydrochloric acid was added and pushed down. After another few drops of water, the elution could start.

Experiments were carried out in order to determine the amount of material that could be handled on this type of column.

Previous work by Nervik [4]) had stated that a carrier-free rare earth could be separated from massive amounts of rare earth of lower atomic number as long as there were no excessive massive amounts of a rare earth of higher atomic number present. Pile irradiated europium and terbium were used as tracers—about 1 μg of each being applied in each run together with varying amounts of stable europium. The elution curves are shown in fig. 1. It is seen that good separations of Tb are obtained with up to 5 mg of Eu_2O_3. If neighboring rare earths were to be separated, this limit should be somewhat lower. For separations where the desired activity comes out after the bulk amount, 400 μg will probably be the upper limit. These results are seen to be in accordance with the general rule given by Nervik.

The flow rate used (1.1 cm/min) was selected in accordance with ref. [3]). An increase in flow rate to 2.7 cm/min almost doubled the band widths.

From fig. 1 it is evident that a high degree of separation is obtained in all cases. When, however, it is the purpose to prepare sources for β-ray spectroscopy, rather severe demands are imposed upon the procedure. Assuming a source area of 0.03 cm^2, the fraction of the 5 mg target material that can be tolerated in the

[1]) K. M. Glover and P. Borrell, J. Nuclear Energy **1** (1955) 214.

[2]) S. G. Thompson, B. G. Harvey, G. R. Choppin and G. T. Seaborg, J. Am. Chem. Soc. **76** (1954) 6229.

[3]) G. R. Choppin and R. I. Silva, J. Inorg. and Nucl. Chem. **3** (1956) 153.

[4]) W. E. Nervik, J. Phys. Chem. **59** (1955) 690.

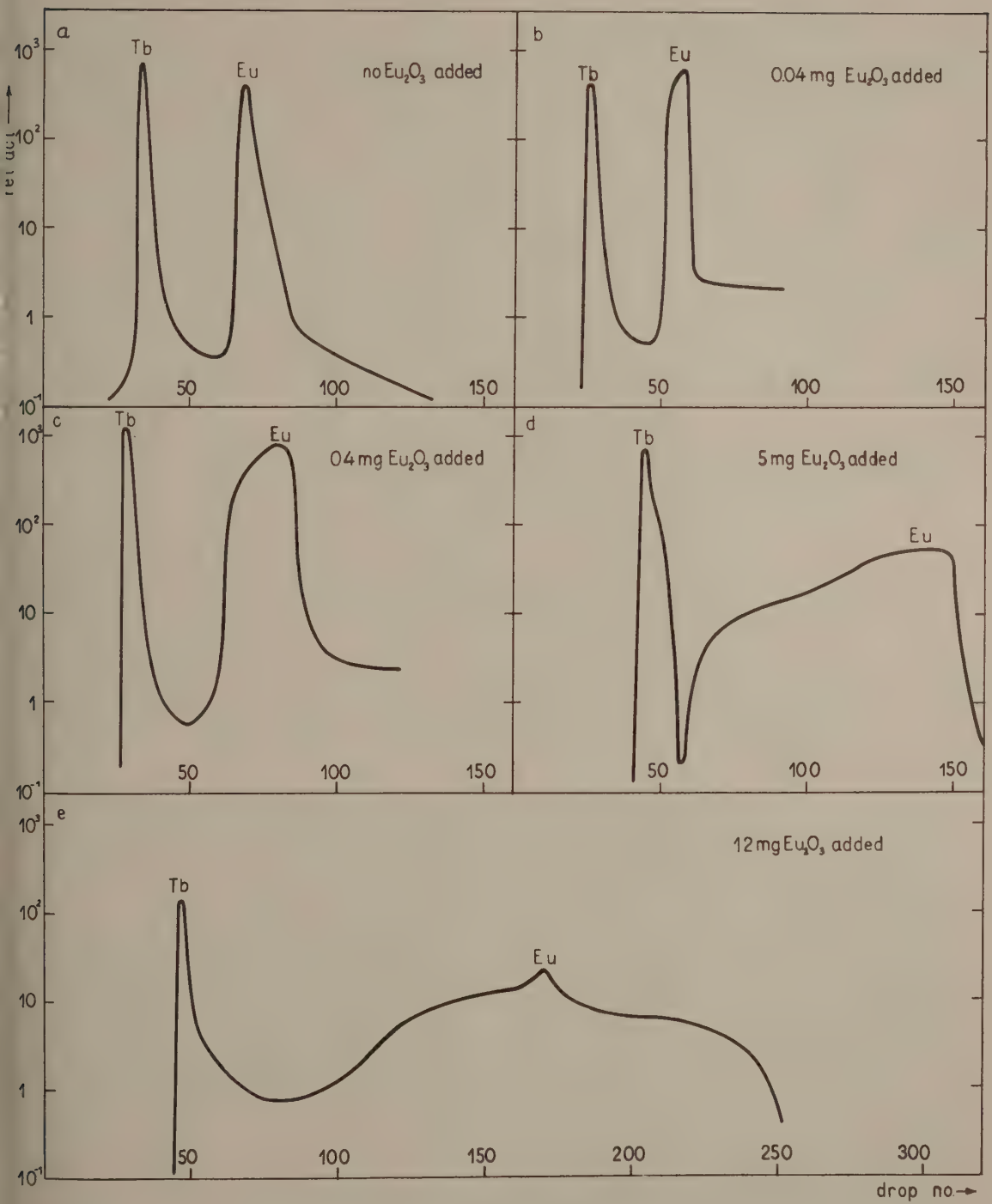

Fig. 1. Separation of Eu and Tb.
Flow rate: 1.1 cm/min. Eluant: 0.20 *M* ammonium α-hydroxy isobutyrate; 0.11 *M* α-hydroxy isobutyric acid.

product must be less than 5×10^{-5}, if a β-source better than 10 $\mu g/cm^2$ is desired. Therefore, under circumstances where a satisfactory separation is likely to be difficult to obtain, it is generally safer and less time-consuming to perform two successive separations than to improve the conditions for a separation in one step.

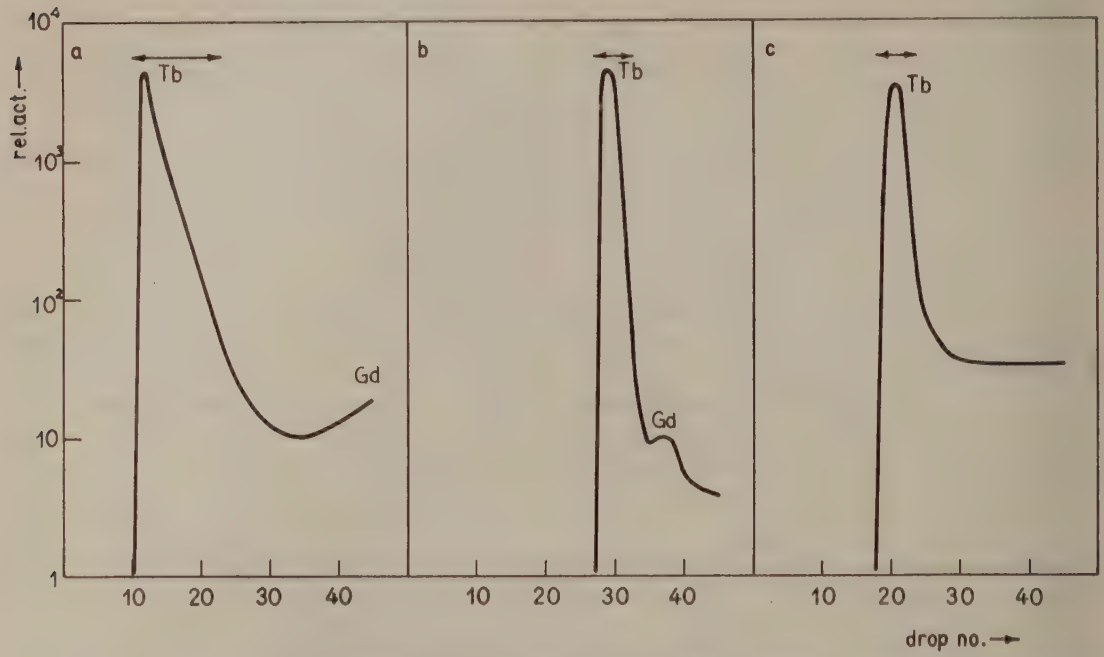

Fig. 2. Separation of Tb^{161} from Gd. Flow rate: 0.7 cm/min.
Eluant: (a) 0.25 *M* ammonium α-hydroxy isobutyrate; 0.11 *M* α-hydroxy isobutyric acid. (b) and (c) 0.30 *M* ammonium lactate; 0.15 *M* lactic acid. ◂ ▸ drops taken out for next step in the procedure.

This was demonstrated in the preparation of a Tb^{161} source produced from a 14 days pile irradiation of 2 mg of Gd^{160} (isotope separated, but containing some Gd^{158}). The first separation was carried out with α-hydroxy isobutyric acid as the eluant (fig. 2a). The elution curve showed a strong overlap between the Tb and Gd peaks. Two successive separations with lactic acid as the eluant were then performed (figs. 2b and 2c). The first one of these gave a small and well defined peak of Gd activity. The final separation showed no trace of Gd activity. Furthermore, a very pronounced tailing due to adsorption of activity on the glass on top of the column indicated that the activity was essentially carrier-free at the end of run two. The final source had a thickness of about 10 $\mu g/cm^2$.

Fig. 3 shows the three L-lines of the 25.6 keV transition in Tb^{161}, as measured from this source with two gaps of an orange spectrometer[5]) (max. resolution 0.8%).

2.3. SOURCE PREPARATION

The sources were prepared by a microcolumn technique[6]).The drops were made slightly acid and pushed through a Dowex 50 column with a 1–3 μl resin bed. After washing with water the activity was taken out with 1 M ammonia lactate and 1 μl fractions collected on 150 $\mu g/cm^2$ aluminium foil. After drying and igniting the foil, the sources were ready for mounting.

[5]) O. B. Nielsen and O. Kofoed-Hansen, Mat. Fys. Medd. Dan. Vid. Selsk **29** (1955) no. 6.

[6]) S. Bjørnholm, O. B. Nielsen and R. K. Sheline, Nature **178** (1956) 1110.

3. Conclusion

Using the procedures mentioned above, sources suited for most β-spectroscopic work have been prepared. The time elapsed from the end of the bombardment to the beginning of the source mounting has usually been 6–8 hours. However, this time probably can be much reduced in cases where time is a decisive factor. The ultimate choice of conditions under different circumstances will depend on parameters such as half-life, amount of activity available, and desired source quality. Any quantitative guide can hardly be given. On the basis of work done at this Institute, the procedure recommended is to rely on a single separation in case of rare earth activities produced by (α, n) reactions, but to perform two separations where an activity is produced by a (d, n) reaction.

Work has so far been done on the elements Tb–Eu, Lu–Tm and on the neighboring Tb–Gd and Ho–Dy.

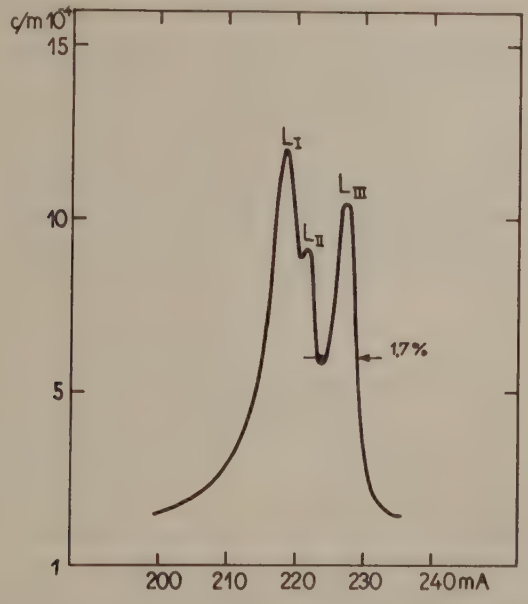

Fig. 3. L_I (16.5 keV), L_{II} (17.0 keV) and L_{III} (17.6 keV) conversion lines of the 25.6 keV E1 transition in Tb^{161} measured in a β-ray spectrometer.

4. Acknowledgements

The hospitality and ideal working conditions at Professor Niels Bohr's Institute are gratefully acknowledged. P. G. H. wishes to express his gratitude to the Danish Atomic Energy Commission, and especially to Dr. C. F. Jacobsen, for having given him the opportunity to participate in this work. The authors also wish to acknowledge the assistance of Mr. G Sørensen and of the cyclotron group. Thanks are due Mr. O. B. Nielsen and Mr. S. Bjørnholm for their interest and helpful suggestions.

NUCLEAR INSTRUMENTS 2 (1958) 44–48; NORTH-HOLLAND PUBLISHING CO. – AMSTERDAM

GAIN-SCANNED SINGLE CHANNEL KICKSORTER USING PRECISION CASCADE ATTENUATORS

C. F. COLEMAN

Atomic Energy Research Establishment, Harwell, Didcot, Berksh.

Received 11 November 1957

The paper begins by discussing the characteristics and advantages of a single channel kicksorter in which the voltage channel is fixed, and the pulse spectrum is scanned by changing the gain of the preceding amplifier. Attenuators which can be operated in cascade and have a precision $\approx 0.2\%$ have been developed for use in such an instrument. Examples of spectra obtained with an automatically scanned digital recording kicksorter of this kind are presented. They involve pulse height and counting rate ranges of up to 30:1 and up to 3 000:1 respectively.

1. Introduction

Åström [1]) has recently described a mechanically scanned single channel kicksorter arranged to have a constant percentage channel width. Such a characteristic is obtained automatically if one uses a fixed kicksorter channel and sweeps the pulse spectrum across it by varying the gain of the preceding amplifier. Peirson and Iredale [2]) have built such a device, with characteristics similar to Åström's, by using a potentiometer type attenuator for gain sweeping. In the instrument described below this is achieved by using a set of precision cascade attenuators.

2. Characteristics of Gain-Scanned Kicksorters

All pulses triggering a gain-scanned kicksorter encounter identical amplifier and discriminator conditions beyond the attenuators. Thus the variations in effective channel width and mean triggering delay through the spectrum which occur when conventional kicksorters are used to sort pulses of non-ideal shape are largely eliminated. If the attenuators are placed before the high level amplifier stages, which are the usual source of non-linear distortion, this too will not affect the observed pulse spectrum. The system lends itself to scanning wide ranges of input pulse height in one operation, and the practical limitation arises from overloading of the amplifiers at the bottom of the spectrum. If the output counting rate is plotted linearly against the attenuation on a logarithmic scale, the total counting rate in any portion of the spectrum is proportional to the area under the corresponding portion of the curve so obtained. Whatever attenuation scale is used, gain shifts have no effect on the heights of lines in the spectrum.

3. Details of a Gain-Scanned Kicksorter System

Fig. 1 shows the block diagram of a gain-scanned kicksorter built in this laboratory. The circuit is conventional except for the attenuators. These are arranged in cascaded pairs to give a maximum attenuation of about 1 000, variable in steps of 0.5%. Since small steps in the total attenuation may require 5 db to be interchanged between two attenuator chains, an overall precision $\approx 0.1\%$ was required on the coarse steps. The special attenuators developed to meet this requirement are described below. An additional difficulty was that transferring 5 db from the output to the input of a ring-of-three produced an increase of 5 db in the hum level, and slightly altered the ringing characteristics of the amplifier. To stabilise the channel width

[1]) B. Åström, Nuclear Instruments 1 (1957) 143.

[2]) D. P. Peirson and P. Iredale, Brit. Journal of Applied Physics (to be published).

a cut-off amplifier with a gain of seven, biased at about 85 volts, was used. This accentuated overload problems in the main amplifier when small pulses were being analysed, and restricted the pulse height range scanned in a single sweep to about 30:1. This range could be considerably increased by working at a lower bias voltage, and using a kicksorter based on the very stable discriminator circuits described by Kandiah[3]).

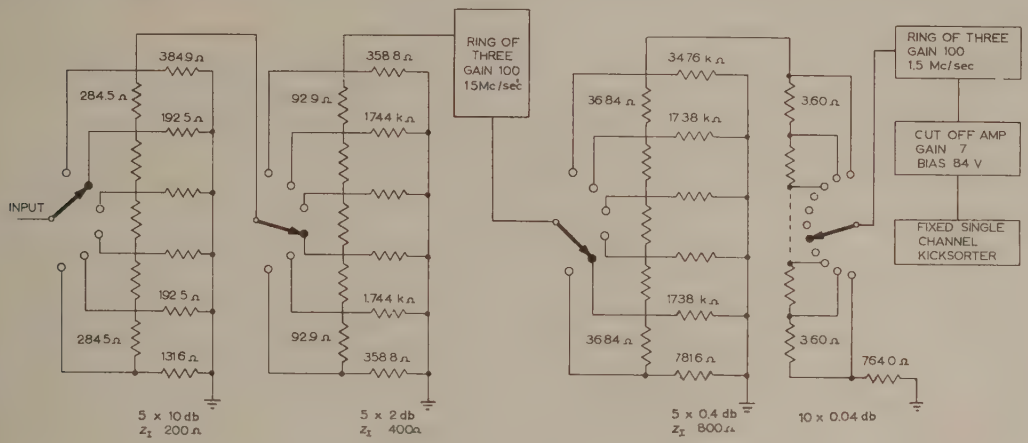

Fig. 1. Block diagram of attenuation-scanned single channel kicksorter.

4. Design and Construction of Attenuators

To obtain in reasonably compact form a total of 60 db attenuation variable in 0.04 db steps it was found necessary to use a cascaded system of coarse, medium, and fine attenuators. The need for buffer amplifiers between each set was avoided by devising a system which allowed the attenuators to be used directly in cascade. A chain of identical symmetrical π sections terminated at each end by its iterative impedance z_I presents at each junction point the input impedance $z_I/2$. Thus a source of pulses which can be switched from junction to junction will see a constant load impedance, while the output at either termination will be attenuated stepwise as the input junction is altered. A switched-input attenuator of this kind can serve as part or whole of the terminating impedance of another similar attenuator, allowing a number of such attenuators to be used in cascade. Each additional attenuator will have a minimum insertion loss of 6 db if its iterative impedance is equal to that of its predecessor, or 0 db if its iterative impedance is twice that of its predecessor. The attenuators were required to operate at a band width of 1 Mc/sec, and component tolerances were as small as 1/10%. The more critical resistors were wound from enamelled 0.02″ diameter Karma resistance wire supplied by the British Driver-Harris Co. Ltd., using a standard low capacitance low inductance winding. Since this wire is hard to solder the resistances were made low, and were brought up to the design value with a few turns of heavier gauge manganin. To retain the calibration it was found essential to bind the wires in position, which was done by dipping the resistors in coldsetting araldite. To minimise stray capacitances the attenuators were assembled between two Yaxley wafers with the rotors electrically linked, and the contacts were arranged so that in successive switch positions the variable connection was made by the back and front rotors in turn. The resistors could then be wired straight from the back to the front wafers without any return leads. The individual resistors were shielded from one another by earthed radial vanes and the completed assemblies were enclosed in aluminium cans. The

[3]) K. Kandiah, Proc. Inst. Elec. Eng. **101** (2), (1954) 239.

precision of the units was such that with a source of 1 microsecond pulses nominally identical combinations with attenuations of up to 10 db gave the same output pulse height to within a few parts in a thousand.

5. Performance

The kicksorter was set up for automatic operation by mounting the attenuators on Ledex electromechanical switches. The counting system was arranged to count for a preset time, print the count on a tape, step the attenuators on by a preset amount, and repeat the cycle. The preset attenuation step changed twice during the course of a 39 db scan to follow the variation in scintillation spectrometer resolution over such an energy range. The printing and resetting time fluctuated about 6 seconds. Counts of up to 100 000 could be recorded, while significant details were seen in spectra yielding about 100 cts per point over counting times of ten minutes.

The equipment has been used mainly in looking for weak high energy gamma rays, including those produced by impurities in nominally pure activities. Fig. 2 shows an In^{114} spectrum run in about 1½ hours. Even with the high energy enhancement produced by gain-scanning it requires a range of counting rates of 1000:1. The 1.30 MeV. Sn^{114} line is clearly visible with individual points containing ≈ 25 counts. Fig. 3 shows the spectrum of V^{48} produced by spallation of iron with 150 MeV protons, including the 2% abundant 2.23 MeV gamma-ray line. Fig. 4 shows two spectra of iron activities taken consecutively to compare the decay of the various lines. The low energy line is a previously unreported transition following the decay of Fe^{52}. The change in shape of the low energy region between the two runs is due in part to rate dependent overloading effects in the kicksorter amplifier. The annihilation peak shows a gain shift of ≈ 3% between successive runs. Fig. 5 is a spectrum of Nb^{92} prepared by a reactor induced (n, p) reaction on molybdenum. The Zr^{92} 1.83 MeV transition and Co^{60} contamination peaks can be seen. The latter, arising from cobalt impurity in the molybdenum, account for a few percent only of the total source activity. Changes in the attenuation steps can be seen at 5 and 15 db. The performance of the attenuators is shown by the absence of jumps in the spectra at multiples of 5 db, when 5 db is transferred from

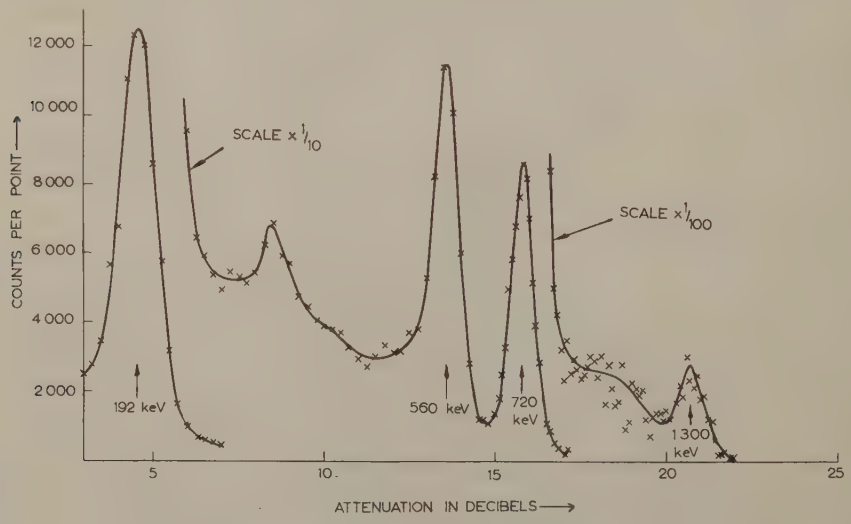

Fig. 2. Scintillation spectrum of In^{114} (24 sec points).

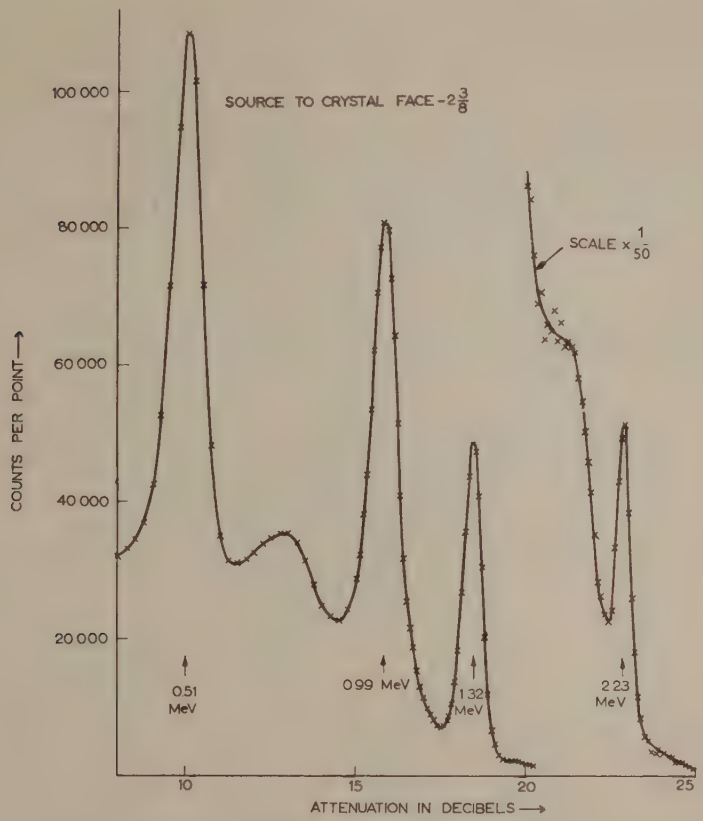

Fig. 3. Scintillation spectrum of V^{48} produced by spallation of iron. (5 min points).

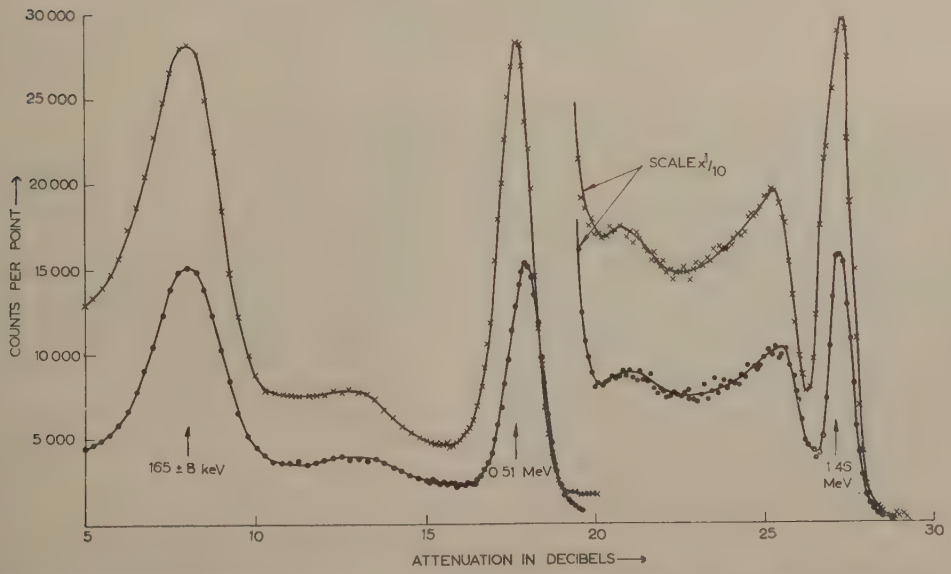

Fig. 4. Scintillation spectrum of iron activities produced spallation by of iron, showing relative decay of lines (2 min points).

the output to the input of the first ring-of-three amplifier.

6. Summary

The use of gain-scanned single channel kicksorters eliminates many of the factors, such as pulse rise time effects and amplifier non-linearities, which can distort spectra obtained with conventional kicksorters. In a gain-scanned spectrum the height of a given line is unaffected by amplifier gain-shifts, and there is a useful enhancement of the high energy region. Such kicksorters are however more susceptible to rate-dependent over-loading effects, and require the use of exceptionally precise attenuation systems. A suitable system, based on an attenuator design which can be used in cascade, has been developed. An automatically scanned kicksorter of this type, arranged for digital recording, has proved very useful for seeking low intensity high-energy gamma ray transitions.

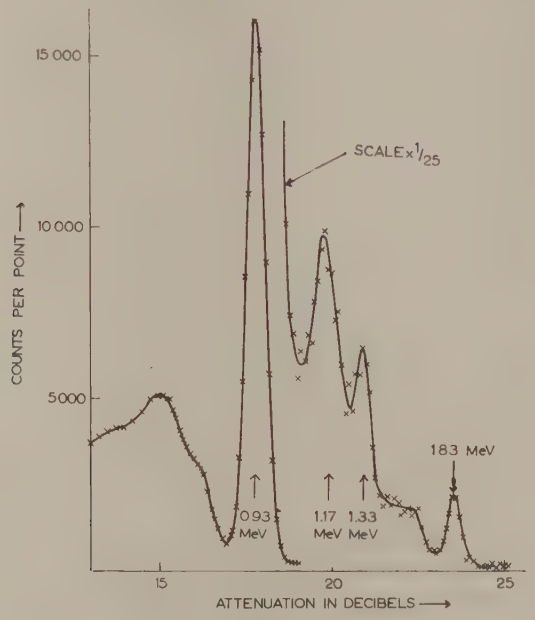

Fig. 5. Scintillation spectrum of Nb^{92} produced by the pile induced Mo^{92} (n,p) Nb^{92} reaction, with Co^{60} contamination (5 min points).

7. Acknowledgements

I am grateful to Dr. P. E. Cavanagh for his interest in and support for this project, to Mr. C. Scott-Kestin for his skilful work in building the kicksorter proper, including the attenuators and precision resistors, and to the members of the Automatics Group, especially Mr. R. L. Elliot, who designed and built the automatics.

NUCLEAR INSTRUMENTS 2 (1958) 49–52; NORTH-HOLLAND PUBLISHING CO. – AMSTERDAM

AUTOMATIC COUNTING-RATE RECORDER†

M. A. POMERANTZ and A. E. SMITH

Bartol Research Foundation of The Franklin Institute, Swarthmore, Pennsylvania

Received 6 May 1957

A counting-rate recorder, originally designed for a cosmic-ray neutron monitor station, incorporates a scale-shifting arrangement which automatically changes the sensitivity as required in accordance with the input counting rate.

1. Introduction

A neutron monitor[1]) which measures the intensity of the nucleonic component of the cosmic radiation must operate continuously and reliably for protracted periods during which it is ordinarily unattended. It is therefore necessary to incorporate provisions for automatic recording of the various data both in digital and graphical form. One essential mission of such a station is to observe the cosmic-ray intensity as a function of time on occasions when the counting rate suddenly increases above the base value, and subsequently slowly decays to normal. In such cases it is important to relate the detailed features of the cosmic-ray variation with time to observations of solar and geophysical phenomena, such as H-α flares, sudden ionospheric disturbances, etc.

To accomplish this, an automatic counting-rate recorder has been developed and installed in a shipboard cosmic-ray observatory currently operating aboard a Swedish merchant ship as part of a collaborative program among Upsala University, the National Research Council of Canada, and the Bartol Research Foundation. Inasmuch as, in addition to fulfilling the requirements for which it was designed, the device is readily adaptable to other applications in the field of nuclear physics, it is described in some detail herewith.

† Assisted by the U. S. National Committee for the International Geophysical Year and the joint program of the Office of Naval Research and the U. S. Atomic Energy Commission.

2. Principles of Operation

The instrument in its present form comprises a counting-rate computer circuit which drives a direct-inking pen recorder, and a scaleshifting circuit which automatically changes the sensitivity as required in accordance with the input counting rate.

Fig. 1 is a block diagram of the system. $B^{10}F_3$ counter pulses from two individual linear amplifiers are fed into the pulse-height discriminator. For each pulse which exceeds the threshold setting, regardless of wave form, an equalized pulse is transmitted to the integrator circuit. The reading of the voltmeter represents the average counting rate, and the scale-shifter is actuated by the voltmeter whenever the latter attains full-scale deflection.

3. Counting-Rate Meter

The counting-rate meter and pulse-height discriminator circuits are rather conventional, and are shown in fig. 2. Positive pulses (minimum amplitude 0.5 V, minimum width 1 μsec) exceeding the discriminator bias setting are accepted. These trigger the univibrator stage V_2 and consequently V_3, which then delivers to the integrator (and to an aural monitor) corresponding pulses which are identical whithin rather close limits. The resolving time of the ratemeter, as determined by this pulse width, is approximately 125 μsec in the present case.

Integration occurs in the circuit consisting of

[1]) M. A. Pomerantz, Jour. Frank. Inst. 263 (1957) 153.

the rectifier V_4 and associated *RC* network. The potential developed across GH is directly proportional to the average number of counts per unit time, and is measured by a standard vacuum-tube voltmeter circuit, V_5.

For varying the full-scale range of the counting-rate meter, the capacitor EF and resistor GH are changed to yield the desired sensitivity and time-constant respectively.

and also interrupts RY 1 and the meter-relay coils. When this occurs, the contacts of the latter are forced apart by spring action, and the meter pointer returns to zero. Two other sets of contacts on RY 2 simultaneously change the input capacitor EF and the resistor GH, thereby increasing the full-scale range of the counting-rate meter by a factor of 10. The contacts of RY 4 also control the scale-indicating panel

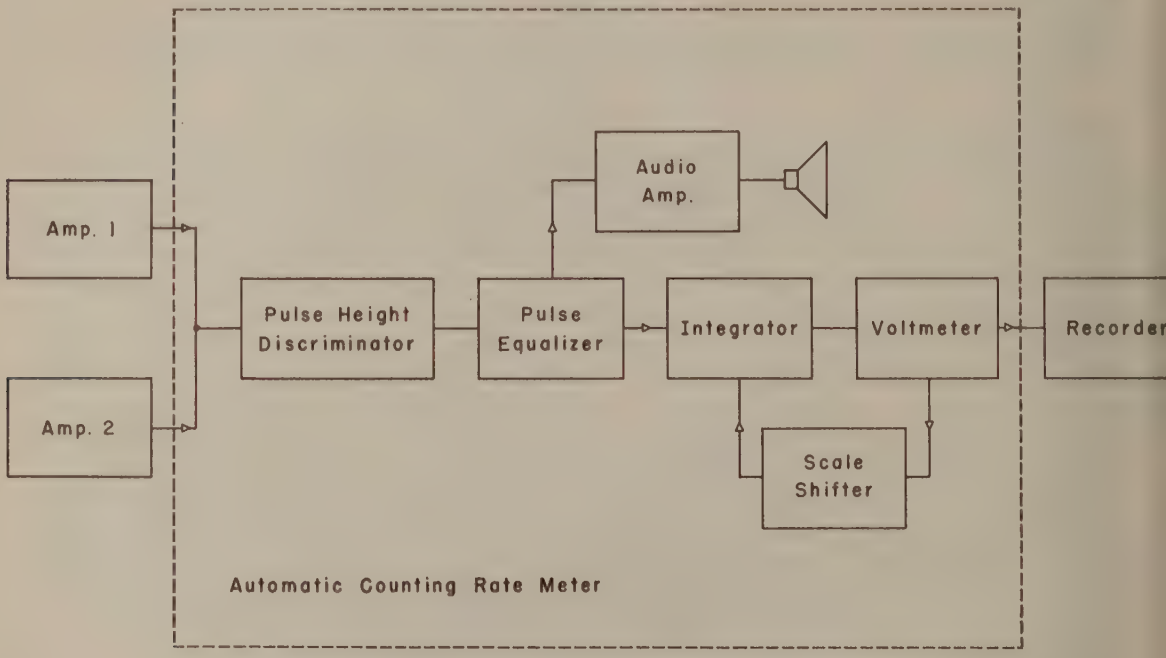

Fig. 1. Block diagram of automatic counting-rate recorder.

4. Scale-Shifting Circuit

Fig. 3 shows the scale-shifting circuit. The locking-type meter relay[2]) not only provides a direct reading of the counting rate, but also closes a contact when the deflection is full scale. This actuates RY 1[3]), thereby discharging the storage capacitors GH, and also closing RY 2 and RY 4. One set of contacts of RY 2 now completes a holding circuit for itself and RY 4, lights, and energize two time-delay relays. The first, NO 3, after a delay of 3 sec, completes the circuit to the RY 1 coil which has been interrupted through the contacts of RY 2. This permits an additional shift of sensitivity if the meter again deflects full scale. The second, NO 10, starts a timing motor which, after 6 minutes, releases all of the relays, thus resetting the sensitivity to the X1 scale. If, upon this interruption, the counting rate is still off scale, the shift to X10 occurs immediately and the timing cycle repeats.

If the meter deflection attains full scale while

[2]) Meter-Relay Model 261-6 (Assembly Products, Inc., Chesterland, Ohio).

[3]) Hermetically-sealed relay Model SK 18014 (C. P. Clare and Co., Chicago, Ill.).

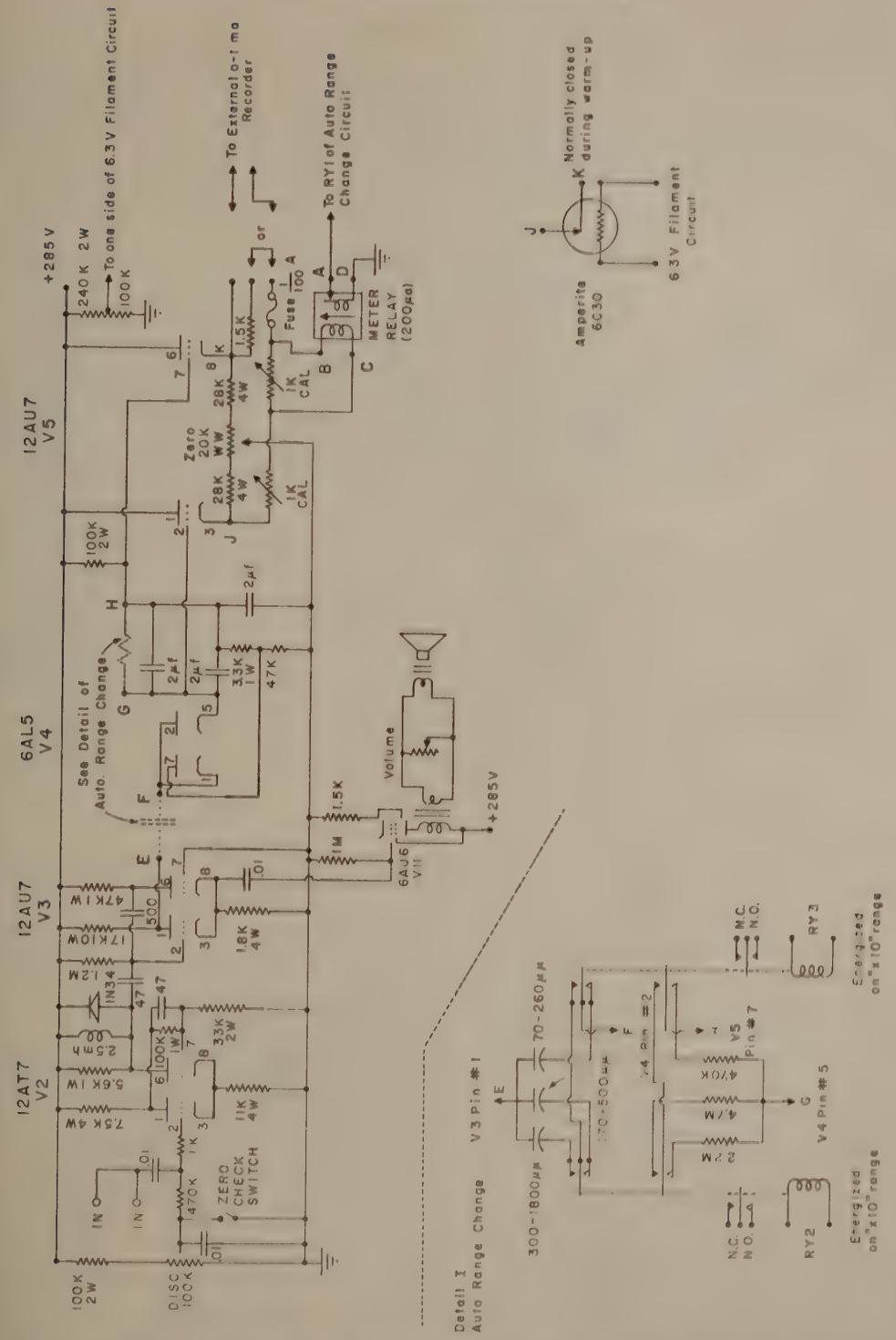

Fig. 2. Counting-rate meter and range-change circuits. The conventional regulated power supply is not shown.

the sensitivity is X10, RY 1 again closes. This energizes RY 3 which has self-holding contacts, thereby causing another change in capacitor EF and resistor GH, and interrupting RY 1 as previously. The sensitivity will remain on the X100 scale for the remainder of the 6-minute period.

For test purposes, a change-reset switch on the front panel permits manual operation of the scale-shifting circuit and reset of the sensitivity to X1. To call the observer's attention to an increase in the counting rate which has occurred while the monitor was unattended, a red lamp marked "EVENT" lights whenever any scale shift occurs, and remains on until it is cleared by depressing the reset switch.

5. Conclusion

The indicated components provide full-scale ranges of 0–200, 0–2000, and 0–20 000 cpm with an accuracy of 2%. A chart speed of 6 inches per hour is satisfactory for the cosmic-ray observations. This instrument has been in continuous operation without interruption a-

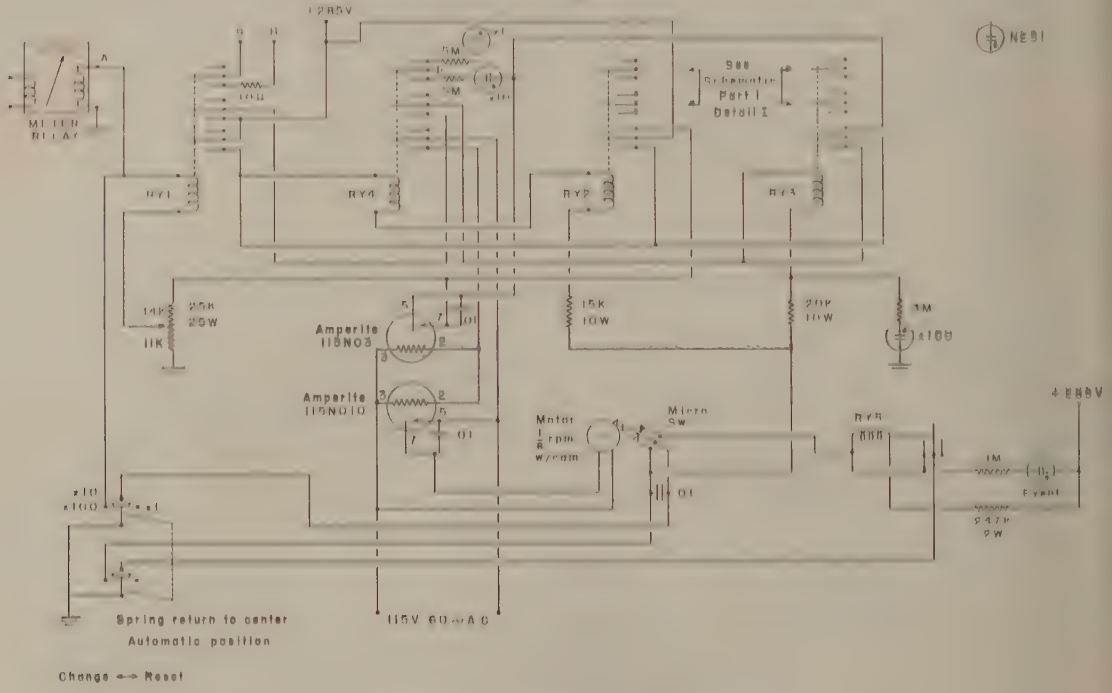

Fig. 3. Automatic scale-shifting circuit.

board the M/S Lommaren for more than 6 months.

Modifications of the automatic counting-rate recorder for other applications, such as measurements of radioactive decay, tracer experiments, etc. are straightforward, and the various possibilities need not be discussed in detail.

NUCLEAR INSTRUMENTS 2 (1958) 53-60; NORTH-HOLLAND PUBLISHING CO. — AMSTERDAM

CORRECTION DE DIFFUSION LORS DES MESURES DE SECTIONS EFFICACES TOTALES POUR NEUTRONS RAPIDES

J. P. VERVIER

Centre de Physique Nucléaire de l'Université de Louvain, Louvain (Belgique)

Received 25 October 1957

A general formula is given for the calculation of the in-scattering correction which is to be applied to the total cross section for fast neutrons as measured by transmission experiments. It is shown that inelastic scattering and (n, 2n) reactions are negligible for this evaluation; only elastic scattering is to be taken into account. This influence can be estimated by comparison with some experimental results or by application of the diffraction theory of neutron scattering using, as nuclear radius, $R = r_0 A^{1/3}$ where $r_0 = 1.25 \times 10^{-13}$ cm; the maximum error involved in this evaluation is $\pm 20\%$.

1. Introduction

On mesure, en général, les sections efficaces totales pour neutrons rapides par des expériences de transmission[1]. Les neutrons diffusés élastiquement et inélastiquement dans l'échantillon, ou ceux qui y sont produits par réaction (n, 2n), sont émis dans toutes les directions, et une partie d'entre eux atteint le détecteur, ce qui augmente la transmission et diminue la section efficace; pour tenir compte de cet effet, on doit appliquer une correction de diffusion ("in-scattering") à la section efficace totale que l'on a mesurée. Elle a été calculée à plusieurs reprises[2-7]), mais les formules et les hypothèses utilisées diffèrent assez bien d'un auteur à l'autre, ce qui produit parfois des divergences entre les sections efficaces totales mesurées par des expérimentateurs différents pour une même énergie de neutrons (par exemple[8, 9, 10]) et [11, 12])).

Nous donnons une formule générale pour calculer la correction de diffusion à appliquer aux sections efficaces totales pour neutrons rapides mesurées par des expériences de transmission; nous étudions l'ordre de grandeur et l'importance relative des différents termes. Nous proposons également une méthode pour estimer, avec une précision suffisante, les facteurs inconnus de la correction de diffusion.

2. Calcul de la Correction

La géométrie utilisée est représentée à la figure 1; nous généralisons ici les calculs de Ricamo et Zünti[4]). Désignons par σ, $\sigma_{\text{él}}$, $\sigma_{\text{inél}}$ et $\sigma_{\text{n, 2n}}$ les sections efficaces totales, de diffusion élastique et inélastique, et de réaction (n, 2n) et par λ, $\lambda_{\text{él}}$, $\lambda_{\text{inél}}$ et $\lambda_{\text{n, 2n}}$, les libres parcours moyens correspondants. Soient également $\sigma_{\text{él}}(\theta)$, $\sigma_{\text{inél}}(\theta)$ et $\sigma_{\text{n, 2n}}(\theta)$ les sections efficaces différentielles de diffusion élastique et inélastique, et de réaction (n, 2n), normalisées à

$$\frac{1}{4\pi}\int \sigma_{\text{él, inél, (n, 2n)}}(\theta)\, d\omega = 1$$

[1]) H. H. Barschall, Revs. Mod. Phys. **24** (1952) 120.
[2]) Amaldi, Bocciarelli, Cacciapuotti et Trabacchi, Nuovo Cimento **3** (1946) 203.
[3]) J. L. Lamph et D. Lester et J. H. Williams, Phys. Rev. **80** (1950) 854.
[4]) R. Ricamo et W. Zünti, Helv. Phys. Acta **24** (1951) 419.
[5]) H. L. Foss, E. O. Salant, G. A. Snow et L. C. Yuan, Phys. Rev. **87** (1952) 11.
[6]) E. M. Hafner, W. F. Hornyak, C. F. Falk, G. Snow et T. Coo, Phys. Rev. **89** (1954) 204.
[7]) R. B. Day et R. L. Heckel, Phys. Rev. **92** (1953) 1508.
[8]) D. W. Miller, R. K. Adair, C. K. Bockelman et S. E. Darden, Phys. Rev. **88** (1952) 83.
[9]) M. Walt, R. L. Becker, A. Okazaki et R. E. Fields, Phys. Rev. **89** (1953) 1271.
[10]) A. Okazaki, S. E. Darden et R. B. Walton, Phys. Rev. **93** (1954) 461.
[11]) N. Nereson et S. Darden, Phys. Rev. **89** (1953) 775.
[12]) N. Nereson et S. Darden, Phys. Rev. **94** (1954) 1678.

et liées aux sections efficaces différentielles

$$\frac{\mathrm{d}\,\sigma_{\text{él, inél, (n, 2n)}}(\theta)}{\mathrm{d}\Omega}$$

exprimées en barn/stéradian par les relations

$$\sigma_{\text{él, inél, (n, 2n)}}(\theta)\cdot\sigma_{\text{él, inél, (n, 2n)}} = \frac{\mathrm{d}\,\sigma_{\text{él, inél, (n 2n)}}(\theta)}{\mathrm{d}\Omega}\,.$$

Nous supposons enfin que le détecteur a une sensibilité ε_1, pour les neutrons incidents et les neutrons diffusés élastiquement, ε_2, pour les neutrons diffusés inélastiquement, et ε_3, pour les neutrons produits par réaction (n, 2n). Nous négligeons les diffusions multiples et les réactions (n, 3n)...

$\omega_2\,\varepsilon_3 \exp[-(l-x)/\lambda]$, pour la réaction (n, 2n) seront comptées par le détecteur. Celui-ci reçoit donc, par seconde, de la tranche dx, le nombre de neutrons utiles (c'est-à-dire qui sont effectivement comptés):

$$Q\omega_1 \mathrm{e}^{-x/\lambda}\,\mathrm{d}x\left[\sigma_{\text{él}}(0)\frac{\varepsilon_1}{\lambda_{\text{él}}} + \sigma_{\text{inél}}(0)\frac{\varepsilon_2}{\lambda_{\text{inél}}} + 2\,\sigma_{\text{n, 2n}}(0)\frac{\varepsilon_3}{\lambda_{\text{n, 2n}}}\right]\omega_2\,\mathrm{e}^{-(l-x)/\lambda}.$$

Le flux de neutrons mesuré par le compteur s'obtient en intégrant l'expression précédente entre $x = 0$ et $x = l$, et en tenant compte des neutrons transmis; il vaut:

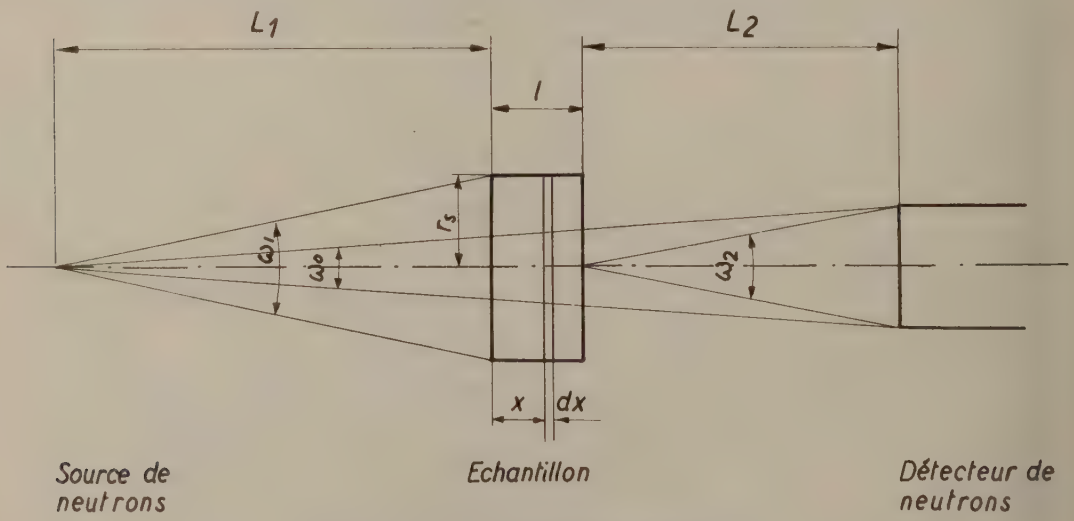

Fig. 1. Géométrie de l'expérience de transmission.

La source, supposée ponctuelle, émet Q neutrons par unité d'angle solide et par seconde.

Considérons une tranche dx de l'échantillon, située à une distance x de la face avant (la plus proche de la source, fig. 1): elle est soumise à un flux de neutrons $Q\omega_1 \exp(-x/\lambda)$. Le nombre de neutrons qui y subissent, par seconde, une diffusion élastique est $Q\omega_1 \cdot \exp(-x/\lambda)\cdot \mathrm{d}x/\lambda_{\text{él}}$, une diffusion inélastique, $Q\omega_1\cdot\exp(-x/\lambda)\cdot \mathrm{d}x/\lambda_{\text{inél}}$, et une réaction (n,2n), $Q\omega_1\cdot\exp(-x/\lambda)\mathrm{d}x/\lambda_{\text{n, 2n}}$; parmi eux, les fractions $\sigma_{\text{él}}(0)\,\omega_2\,\varepsilon_1 \exp[-(l-x)/\lambda]$, pour la diffusion élastique, $\sigma_{\text{inél}}(0)\,\omega_2\,\varepsilon_2 \exp[-(l-x)/\lambda]$, pour la diffusion inélastique, et $2\sigma_{\text{n, 2n}}(0)$

$$Q\omega_0 \mathrm{e}^{-l/\lambda}\,\varepsilon_1 + Q\omega_1\omega_2\left[\sigma_{\text{él}}(0)\frac{\varepsilon_1}{\lambda_{\text{él}}} + \sigma_{\text{inél}}(0)\frac{\varepsilon_2}{\lambda_{\text{inél}}} + 2\,\sigma_{\text{n, 2n}}(0)\frac{\varepsilon_3}{\lambda_{\text{n, 2n}}}\right]\mathrm{e}^{-l/\lambda}\cdot l\,.$$

La transmission mesurée T est donc liée à la transmission réelle $T_0 = \mathrm{e}^{-l/\lambda}$ par la relation

$$\Delta T = T - T_0 = \frac{\omega_1\omega_2}{\omega_0}\,T_0 \ln\frac{1}{T_0}\left[\sigma_{\text{él}}(0)\frac{\sigma_{\text{él}}}{\sigma} + \sigma_{\text{inél}}(0)\frac{\sigma_{\text{inél}}}{\sigma}\frac{\varepsilon_2}{\varepsilon_1} + 2\,\sigma_{\text{n, 2n}}(0)\frac{\sigma_{\text{n, 2n}}}{\sigma}\cdot\frac{\varepsilon_3}{\varepsilon_1}\right]. \quad (1)$$

La courbe $T_0 \ln(1/T_0)$ a été calculée par Ricamo et Zünti[4].

Comme nous le montrerons plus loin, en

général, les termes de diffusion inélastique et de réaction (n, 2n) sont négligeables dans l'éq. (1). D'autre part, si on suppose que la diffusion élastique est isotrope ($\sigma_{\text{él}}(0) = 1/4\pi$), hypothèse peu justifiée[14]), et qu'elle constitue l'interaction principale des neutrons avec la substance étudiée ($\sigma_{\text{él}}/\sigma \approx 1$), on retrouve la formule de Ricamo et Zünti (éq. (8) de [4])), équivalente à celle de Lampi *et al.* (éq. (5) de [3])) mais seulement pour $T_0 \approx 1$ comme l'ont montré Ricamo et Zünti[4]).

Pour calculer la correction de diffusion $\Delta\sigma$ à appliquer à la section efficace totale mesurée σ_{m}, on suppose ΔT petit, et on obtient:

$$\frac{\Delta\sigma}{\sigma_{\text{m}}} = \frac{\Delta(\ln T)}{\ln T} \simeq \frac{\Delta T}{T_0 \ln 1/T_0}$$

soit donc, d'après: l'éq. (1):

$$\frac{\Delta\sigma}{\sigma_{\text{m}}} = \frac{\omega_1\omega_2}{\omega_0}\left[\sigma_{\text{él}}(0)\frac{\sigma_{\text{él}}}{\sigma} + \sigma_{\text{inél}}(0)\frac{\sigma_{\text{inél}}}{\sigma}\cdot\frac{\varepsilon_2}{\varepsilon_1} + 2\,\sigma_{\text{n, 2n}}(0)\frac{\sigma_{\text{n, 2n}}}{\sigma}\cdot\frac{\varepsilon_3}{\varepsilon_1}\right]. \quad (2)$$

Si on néglige les termes de diffusion inélastique et de réaction (n, 2n), on retrouve les formules de Hafner *et al.* (éqs. (1) et (2) de [6]) et de Day *et al.* (page 361 de [7])), à un facteur 4π près.

3. Calcul des Différents Termes de la Correction

Etudions l'importance relative des trois termes du crochet, dans l'éq. (2).

3.1. NEUTRONS INCIDENTS DE QUELQUES MeV (en dessous d'une dizaine de MeV)

Le seuil des réactions (n, 2n) se trouve, en général, aux environs de 10 MeV et même au delà, et donc, dans le cas présent, $\sigma_{\text{n, 2n}} = 0$: le 3e terme du crochet n'intervient pas.

Les niveaux du noyau cible qui peuvent être excités par diffusion inélastique de neutrons de quelques MeV sont peu nombreux et assez espacés, c'est-à-dire que $\sigma_{\text{inél}}/\sigma$ est petit, et qu'on peut, avec un détecteur approprié, discriminer les neutrons diffusés inélastiquement de ceux du faisceau direct, donc faire en sorte que $\varepsilon_2/\varepsilon_1$ soit petit. D'autre part, la distribution angulaire des neutrons diffusés inélastiquement n'est que faiblement anisotrope[13]) et donc $\sigma_{\text{inél}}(0) \approx 1/4\pi = 0.08$: le 2e terme du crochet est négligeable.

La principale interaction des neutrons de quelques MeV avec les noyaux est la diffusion élastique, et donc $\sigma_{\text{él}}/\sigma$ est de l'ordre de 1; la distribution angulaire des neutrons diffusés élastiquement est anisotrope, avec un pic vers l'avant[14]), c'est-à-dire que $\sigma_{\text{él}}(0)$ est, en général, très supérieur à $1/4\pi$. Le terme de diffusion élastique est donc le plus important dans le crochet, les autres étant, en général, négligeables devant lui.

Etudions le cas du fer, avec des neutrons incidents de 2.45 MeV; d'après les résultats de Cranberg[13]), on peut calculer que:

$$\sigma_{\text{él}}/\sigma = 0.74 \quad \sigma_{\text{inél}}/\sigma = 0.26 \quad \sigma_{\text{n, 2n}} = 0$$
$$\sigma_{\text{él}}(0) = 0.445 \quad \sigma_{\text{inél}}(0) = 0.083 \quad \sigma_{\text{n, 2n}}(0) = 0.$$

Dans le cas le plus défavorable où le détecteur ne discrimine pas les neutrons diffusés inélastiquement de ceux du faisceau direct ($\varepsilon_2/\varepsilon_1 \simeq 1$), on a:

$$\sigma_{\text{él}}(0)\frac{\sigma_{\text{él}}}{\sigma} + \sigma_{\text{inél}}(0)\frac{\sigma_{\text{inél}}}{\sigma}\cdot\frac{\varepsilon_2}{\varepsilon_1} + 2\,\sigma_{\text{n, 2n}}(0)\frac{\sigma_{\text{n, 2n}}}{\sigma}\cdot\frac{\varepsilon_3}{\varepsilon_1} = 0.330 + 0.022 = 0.352\,.$$

On voit que le terme de diffusion inélastique est beaucoup moins important que celui de diffusion élastique; il l'est moins encore si on réalise la discrimination, c'est-à-dire si $\varepsilon_2/\varepsilon_1$ est petit. D'autre part, si, comme la plupart des expérimentateurs le font pour des neutrons de cette énergie, on avait supposé que $\sigma_{\text{él}}/\sigma = 1$, $\sigma_{\text{él}}(0) = 1/4\pi$ (distribution angulaire isotrope pour les neutrons diffusés élastiquement) et $\sigma_{\text{inél}}(0) = 0$, on aurait obtenu, comme crochet, 0.08 au lieu de 0.352: l'erreur ainsi commise est donc importante; elle provient surtout de ce que la distribution angulaire des neutrons diffusés élastiquement est anisotrope et présente un pic marqué vers l'avant.

[13]) L. Cranberg et J. S. Levin, Phys. Rev. **103** (1956) 343.
[14]) D. J. Hughes et J. A. Harvey, Neutron Cross Sections BNL 325 (1955).

3.2. NEUTRONS INCIDENTS D'ÉNERGIE SUPÉRIEURE À UNE DIZAINE DE MeV

La section efficace de réaction (n, 2n) augmente rapidement au-dessus du seuil[14]) et $\sigma_{n,2n}/\sigma$ peut devenir proche de 1: pour le Cu^{63}, par exemple $\sigma_{n,2n}/\sigma = 0.4$ à 19.5 MeV[14]). Cependant la distribution angulaire des neutrons émis par réaction (n, 2n) est isotrope, et leur énergie moyenne est très différente de celle des neutrons incidents (1 MeV devant 10 MeV), car la réaction (n, 2n) est une "évaporation"[15]); on a donc $\sigma_{n,2n}(0) \approx 1/4\pi$ et le détecteur peut discriminer aisément les neutrons émis par réaction (n, 2n) de ceux du faisceau direct, c'est-à-dire que $\varepsilon_3/\varepsilon_1$ est petit: l'influence des réactions (n, 2n) sur la correction de diffusion est donc négligeable, même pour des neutrons incidents de plus de 10 MeV.

Les niveaux excités par diffusion inélastique de neutrons d'énergie supérieure à 10 MeV sont nombreux et rapprochés, et donc $\sigma_{inél}/\sigma$ est proche de 1. Le spectre d'énergie des neutrons diffusés inélastiquement se divise en deux parties[16-17]): la 1e, entre 0.5 et 5 MeV environ, la plus intense, a une distribution angulaire isotrope; on peut donc discriminer aisément ces neutrons de ceux du faisceau direct, c'est-à-dire que $\varepsilon_2/\varepsilon_1$ est petit, et $\sigma_{inél}(0) \approx 1/4\pi$. La 2e partie, au-dessus de 5 MeV, la moins intense, a une distribution angulaire anisotrope, avec un pic marqué vers l'avant; $\varepsilon_2/\varepsilon_1$ n'est donc pas négligeable, et $\sigma_{inél}(0)$ est grand. Cependant, l'intensité de cette 2e partie est faible devant celle de la 1e et, au total, l'influence de la diffusion inélastique sur la correction de diffusion est, elle aussi, négligeable.

Le facteur $\sigma_{él}/\sigma$ est plus petit que pour des neutrons de quelques MeV, car la diffusion inélastique et d'autres réactions ont pris plus d'importance; cependant $\sigma_{él}(0)$ est très grand, car la distribution angulaire des neutrons diffusés élastiquement est fortement anisotrope, avec un pic marqué vers l'avant. Le terme de diffusion élastique est donc, ici encore, prépondérant dans le calcul de la correction de diffusion.

Etudions le cas du bismuth, avec des neutrons incidents de 14 MeV; d'après les résultats d'Elliott[18]) pour la diffusion élastique, et de Rosen[16]) pour la diffusion inélastique, on peut calculer que:

$$\sigma_{él}/\sigma = 0.49 \qquad \sigma_{inél}/\sigma = 0.475 \text{ (1e partie)}$$
$$\sigma_{inél}/\sigma = 0.037 \text{ (2e partie)}$$

$$\sigma_{él}0 = 2.85 \qquad \sigma_{inél}(0) = 0.08 \text{ (1e partie)}$$
$$\sigma_{inél}(0) = 0.61 \text{ (2e partie)}.$$

Aucune donnée n'existe, jusqu'à présent, sur une réaction (n, 2n) avec le bismuth, et nous l'avons négligée. Dans le cas le plus défavorable où $\varepsilon_2/\varepsilon_1 \simeq 1$, on a:

$$\sigma_{él}(0)\frac{\sigma_{él}}{\sigma} + \sigma_{inél}(0)\frac{\sigma_{inél}}{\sigma}\cdot\frac{\varepsilon_2}{\varepsilon_1} =$$
$$= 1.395 + 0.038 + 0.023 = 1.456 .$$

De nouveau, le terme de diffusion inélastique est beaucoup moins important que celui de diffusion élastique. Notons que la correction de diffusion est plus importante à 14 MeV qu'à 2.45 MeV à cause du maximum plus prononcé vers l'avant que présente la distribution angulaire des neutrons diffusés élastiquement.

3.3. CONCLUSION

Dans le crochet de l'éq. (2), les termes de diffusion inélastique et de réaction (n, 2n) peuvent être négligés devant celui de diffusion élastique, c'est-à-dire que

$$\frac{\Delta\sigma}{\sigma_m} = \frac{\omega_1\omega_2}{\omega_0}\cdot\frac{1}{\sigma}\cdot\left(\frac{d\sigma_{él}(\theta)}{d\omega}\right)_{\theta=0} \qquad (3)$$

où $(d\sigma(\theta)/d\omega)_{\theta=0}$ est exprimé en barns/stéradian, et σ_m, en barns. D'autre part, l'hypothèse d'une distribution angulaire isotrope pour les neutrons diffusés élastiquement donne des erreurs importantes dans la détermination de

$$f(0) = \frac{1}{\sigma}\left(\frac{d\sigma_{él}(\theta)}{d\omega}\right)_{\theta=0} . \qquad (4)$$

[15]) B. T. Feld, H. Feshbach, M. L. Goldberger, H. Goldstein et V. F. Weisskopf, Final Report on the fast neutron data project NYO – 636 (1951).

[16]) L. Rosen et L. Stewart, Phys. Rev. **99** (1955) 1052.

[17]) A. H. Armstrong, L. Rosen et L. Stewart, Bull. Am. Phys. Soc. Series II, vol. **1** (1956) 296.

[18]) J. O. Elliot, Phys. Rev. **701** (1956) 684.

Une autre méthode doit donc être employée pour calculer ce facteur avec une plus grande précision.

4. Calcul de f(0)

4.1. VALEURS THÉORIQUES

La section efficace différentielle de diffusion proximativement, pour de grandes valeurs de $x = k\,R$ ($x > 3$ ou 4)[19]:

$$\sigma = 2\,\pi\,(R + \lambda)^2 \qquad (6)$$

On a donc finalement[7]:

$$f(0) = \frac{1}{2}\,\frac{(kR + 1)^2}{4\pi} \cdot 0.04\,(0.22\,r_0 A^{1/3} E^{1/3} + 1)^2 \qquad (7)$$

où r_0 est exprimé en 10^{-13} cm.

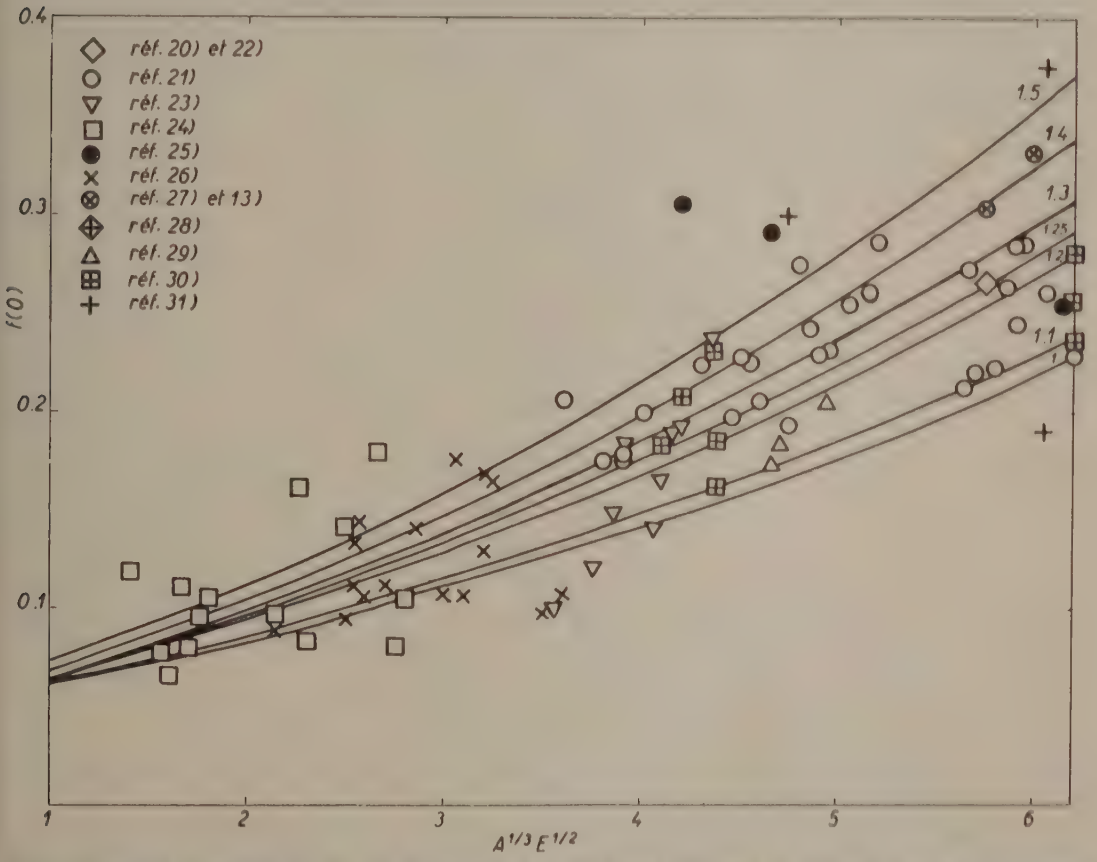

Fig. 2. Facteur de correction $f(0)$ (éq. (4)) en fonction de $A^{1/3}E^{1/2}$ entre $A^{1/3}E^{1/2} = 1$ et 6.2. Les points expérimentaux sont obtenus d'après les résultats des références indiquées. Les courbes en trait plein ont été calculées d'après la théorie de la diffraction (éq. (7)), pour les valeurs indiquées de r_0 (en 10^{-13} cm).

élastique pour $\theta = 0$ est donnée, d'après la théorie de la diffraction[15]) par:

$$\left(\frac{d\sigma_{el}(\theta)}{d\omega}\right)_{\theta=0} = \frac{(R + \lambda)^2}{4}\,(kR + 1)^2 \qquad (5)$$

où $k = 2.2 \times 10^{12}\sqrt{E} = 1/\lambda$ est le nombre d'onde (en cm^{-1}) d'un neutron d'énergie E (en MeV) et $R = r_0 A^{1/3}$ est le rayon du noyau (en cm). La section efficace totale vaut ap-

4.2. VALEURS EXPÉRIMENTALES

Les figs. 2 à 5 donnent les valeurs de $f(0)$ en fonction de $A^{1/3}E^{1/3}$ pour différents noyaux et diverses énergies; elles ont été calculées d'après les sections efficaces différentielles de diffusion élastique de neutrons données dans

[19]) H. Feshbach et V. F. Weisskopf, Phys. Rev. 76 (1949) 1550.

la littérature[13,14,18]) et [20-31]). Les points expérimentaux des figs. 2 à 4 sont obtenus d'après les résultats des références indiquées à la fig. 2; les courbes en trait plein sont les courbes théoriques (éq. (7)) pour plusieurs valeurs de r_0 indiquées dans les figures. A la fig. 5, $f(0)$ est représenté en fonction de $A^{1/3}E^{1/2}$ pour le carbone, le fer et l'azote; les courbes en trait plein donnent la forme générale de la variation de $f(0)$ d'après les points expérimentaux, mais pas les valeurs théoriques.

Quelques conclusions générales peuvent être tirées de ces figures:

(a) Dans les figs. 2 à 4, les valeurs expérimentales de $f(0)$ sont en majeure partie contenues entre les courbes théoriques $r_0 = 1.5$ et $r_0 = 1$ pour $1 < A^{1/3}E^{1/2} < 22$.

La variation moyenne de $f(0)$ avec $A^{1/3}E^{1/2}$

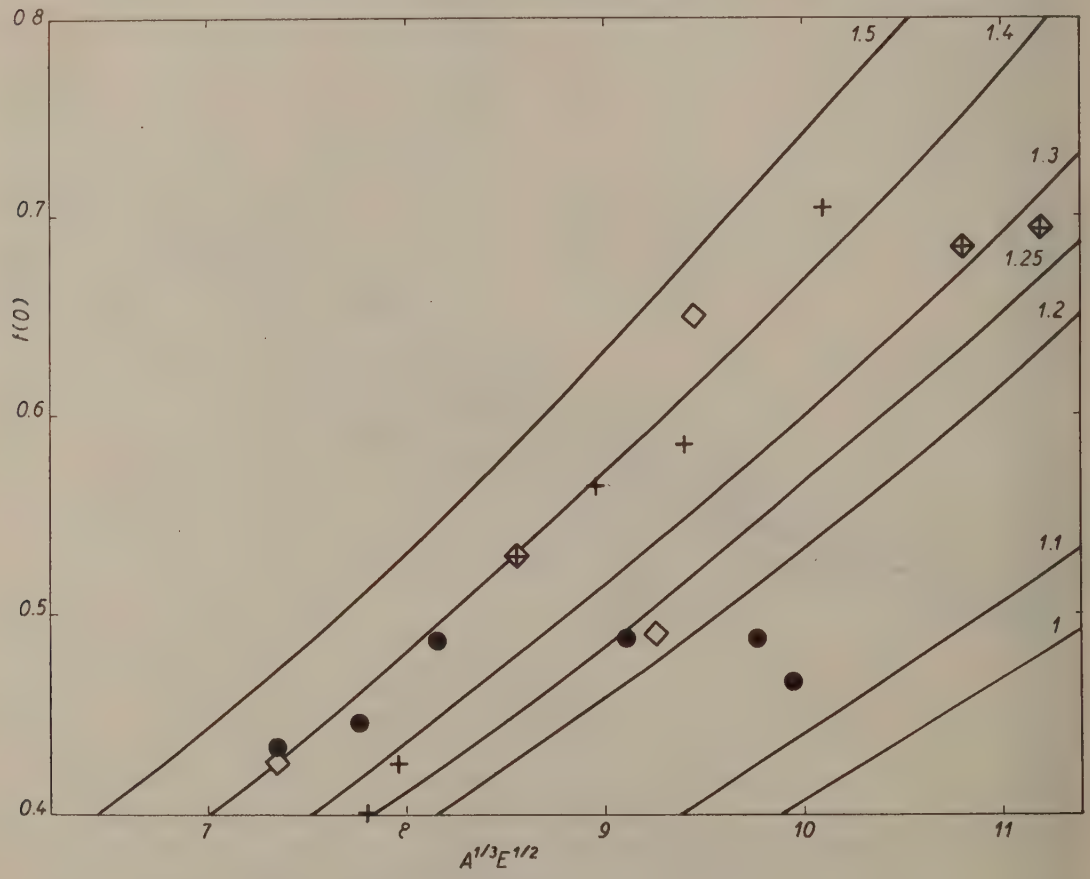

Fig. 3. Facteur de correction $f(0)$ en fonction de $A^{1/3}E^{1/2}$ entre $A^{1/3}E^{1/2} = 6.2$ et 11.4.

[20]) W. D. Whitehead et S. C. Snowdon, Phys. Rev. **92** (1953) 114.
[21]) M. Walt et H. H. Barschall, Phys. Rev. **93** (1954) 1062.
[22]) S. C. Snowdon et W. D. Whitehead, Phys. Rev. **94** (1954) 1267.
[23]) R. W. Meier, P. Scherrer et G. Trumpy, Helv. Phys. Acta **27** (1954) 577.
[24]) H. B. Willard, J. K. Bair et J. D. Kington, Phys. Rev. **98** (1955) 669.
[25]) M. Walt et J. R. Beyster, Phys. Rev. **98** (1955) 677.
[26]) J. L. Fowler et C. H. Johnson, Phys. Rev. **98** (1955) 728.
[27]) W. J. Rhein, Phys. Rev. **98** (1955) 1300.
[28]) G. Culler, S. Fernbach et N. Sherman, Phys. Rev. **101** (1956) 1047.
[29]) C. O. Muehlause, S. D. Bloom, H. E. Wegner et G. N. Glasoe, Phys. Rev. **103** (1956) 720.
[30]) R. C. Allen, R. B. Walton, R. B. Perkins, R. A. Olson et R. F. Taschek, Phys. Rev. **104** (1956) 731.
[31]) J. R. Beyster, M. Walt et E. W. Salmi, Phys. Rev. **104** (1956) 1319.

est assez bien représentée par la courbe théorique $r_0 = 1.25$ pour $1 < A^{1/3}E^{1/3} < 6.2$; au delà de $A^{1/3}E^{1/3} = 6.2$, les points expérimentaux sont moins nombreux et ne permettent pas de déterminer une courbe moyenne. Dans certains cas particuliers, les valeurs de $f(0)$ pour des noyaux et des énergies de neutrons différents concordent de façon remarquable (par exemple pour $A^{1/3}E^{1/3} = 2.15$, 3.9, 4.35, 7.35 et 11.4). (b) Dans la fig. 5, les valeurs expérimentales de $f(0)$ pour un même noyau mais des énergies de neutrons différentes se placent plus ou moins sur des courbes régulières qui ne sont d'ailleurs pas les courbes théoriques (cas du Fe et, dans une certaine mesure, du C). Par contre, pour N, on obtient une variation irrégulière dont les maxima correspondent à des résonances dans la section efficace totale[26]); la courbe expérimentale de $f(0)$ pour C présente d'ailleurs un pic pour $A^{1/3}E^{1/3} = 3.9$, qui provient, lui aussi, d'une résonance.

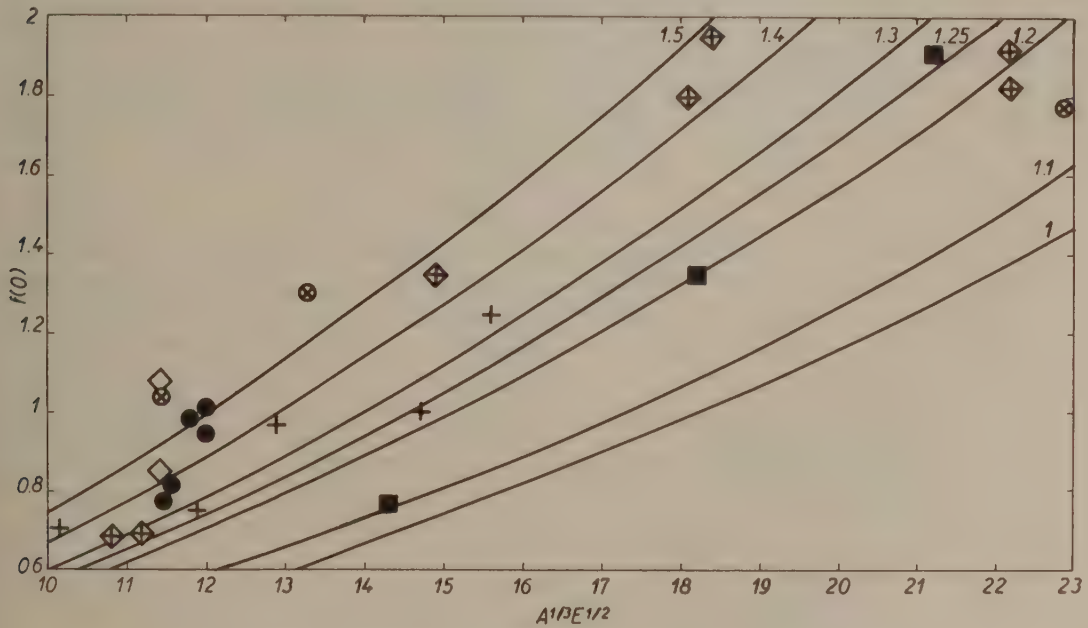

Fig. 4. Facteur de correction $f(0)$ en fonction de $A^{1/3}E^{1/3}$ entre $A^{1/3}E^{1/3} = 10$ et 23.

4.3. APPLICATION

On peut donc déterminer $f(0)$ pour A et E donnés par comparaison avec les valeurs expérimentales voisines, d'après les figs. 2 à 4, ou par l'éq. (7), avec $r_0 = 1.25$; l'incertitude sur la valeur de $f(0)$ ainsi obtenue est au maximum de $\pm$ 20%. On peut tenter d'avoir une meilleure précision en utilisant des courbes comme celles de la fig. 5, tracées d'après les valeurs expérimentales déjà mesurées de $f(0)$, pour le noyau étudié mais pour des énergies différentes; cette méthode ne donne des renseignements utiles qu'en dehors des résonances dans la section efficace totale. Notons que l'erreur maximum de $\pm$ 20% est beaucoup moindre que celle que l'on commet en utilisant l'hypothèse de l'isotropie dans la distribution angulaire des neutrons diffusés élastiquement (§ 3.1); comme d'autre part $\Delta\sigma/\sigma_m$ est en général de l'ordre de quelques %, l'erreur sur la section efficace totale σ_m, due à l'incertitude sur $f(0)$ est inférieure à 1 %, ce qui est, en général, plus petit que les erreurs statistiques sur σ_m. Remarquons également que $f(0)$, donc la correction de diffusion $\Delta\sigma/\sigma_m$, varie avec le noyau étudié et l'énergie des neutrons, contrairement à ce qu'on suppose généralement.

5. Calcul de $\omega_1\,\omega_2/\omega_0$

Dans l'éq. (3),

$$\omega_1\omega_2/\omega_0 = \frac{A_s}{4\pi}\left(\frac{L_1 + L_2}{L_1 L_2}\right)^2.$$

La correction de diffusion est proportionnelle à la surface A_s de l'échantillon; pour une distance $L_1 + L_2$ donnée, elle est minimum pour $L_1 = L_2 = L$, auquel cas $\omega_1\,\omega_2/\omega_0 = (r_s/L)^2$. On a donc avantage, pour la diminuer, à placer l'échantillon à mi-distance entre la source et le détecteur, et à choisir son diamètre petit devant la distance source-détecteur, résultats bien connus[1]).

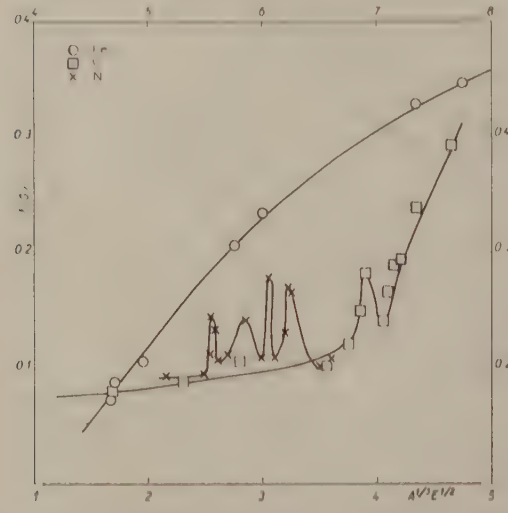

Fig. 5. Facteur de correction $f(0)$ en fonction de $A^{1/3}E^{1/2}$ pour Fe, C et N. Les courbes en trait plain donnent la forme générale de la variation de $f(0)$ d'après les points expérimentaux, mais pas les valeurs théoriques.

6. Détermination Expérimentale de la Correction

On peut déterminer expérimentalement la correction de diffusion de la manière suivante[3]) et [9]). Supposant ΔT petit devant T_0, on a:

$$\sigma_m \simeq \sigma - \frac{1}{lN_{cm^3}}\frac{\Delta T}{T_0} \qquad (8)$$

où N_{cm^3} est le nombre d'atomes par cm³ dans l'échantillon. Comme ΔT est proportionnel à la surface A_s de l'échantillon, la section efficace mesurée σ_m est une fonction linéaire de A_s, avec, comme terme constant, la section efficace réelle σ; on peut donc déterminer σ en extrapolant la droite (σ_m, A_s) pour $A_s = 0$. De même σ_m est une fonction linéaire de $1/L_1^2$, et peut être obtenu en extrapolant la droite $(\sigma_m, 1/L_1^2)$ pour $1/L_1^2 = 0$; cette dernière mesure peut se faire en même temps que la détermination du bruit de fond dû aux neutrons diffusés par les murs du laboratoire[1]): on mesure le taux de comptage sans échantillon pour différentes valeurs de L_1, et on trouve une loi en $1/L_1^2$ avec, comme terme constant, le bruit de fond recherché.

7. Conclusion

La correction de diffusion est difficile à calculer avec précision, et on doit s'efforcer de la réduire le plus possible en choisissant une géométrie appropriée (§ 5). Elle est surtout déterminée par la diffusion élastique des neutrons dans l'échantillon, la diffusion inélastique et les réactions (n, 2n) n'intervenant que peu (§ 3); on peut estimer sa valeur avec une erreur maximum de $\pm$ 20% par comparaison avec divers résultats expérimentaux, ou par application de la théorie de la diffraction avec, comme rayon du noyau, $R = 1.25 \cdot A^{1/3} \times 10^{-13}$ cm (§ 4). Enfin on peut également la déterminer expérimentalement, (§ 6).

Les corrections de diffusions multiples sont difficiles à calculer car elles nécessitent une intégration numérique sur le volume de l'échantillon; Poss *et al.*[5]) ainsi que Day *et al.*[7]) ont montré qu'elles sont inférieures d'un ordre de grandeur aux corrections de diffusion simple: elles sont donc, en général, tout à fait négligeables.

Nous remercions MM les Professeurs M. de Hemptinne et J. M. Delfosse pour leurs encouragements au cours de ce travail.

NUCLEAR INSTRUMENTS 2 (1958) 61-68; NORTH-HOLLAND PUBLISHING CO. - AMSTERDAM

25-CHANNEL TIME ANALYZER FOR THE mμs-RANGE AND A SIMPLE TIME TO PULSE-HEIGHT CONVERTER

BERTIL JOHANSSON

Nobel Institute of Physics, Stockholm 50

Received 7 December 1957

A multi-channel system is described which consists of 25 equal coincidence circuits. The time separation is carried out by a lumped delay-line. Because the delay-line can easily be exchanged, the arrangement can be used in a wide time-range.

A simple time-to-pulse-height converter is described which is a variant of the above 25-channel analyzer.

1. Introduction

In the study of nuclear level schemes one is often faced with the problem of measuring the half-life of an isomeric state which is an energy-level in a short-lived isotope. In such a case it is always difficult to obtain reliable results if one has to take up the coincidence curve by gradually changing a delay by hand. A better method is to go through the coincidence curve automatically several times and in such a way that an automatic correction is made for the decay of the mother isotope. With this method there is still a disadvantage, namely the fact that when the delay is set at a certain position, events with delays different from this are lost. This disadvantage can be avoided by using a multichannel system which takes up the whole coincidence curve at the same time. The arrangement described in this paper is such a system.

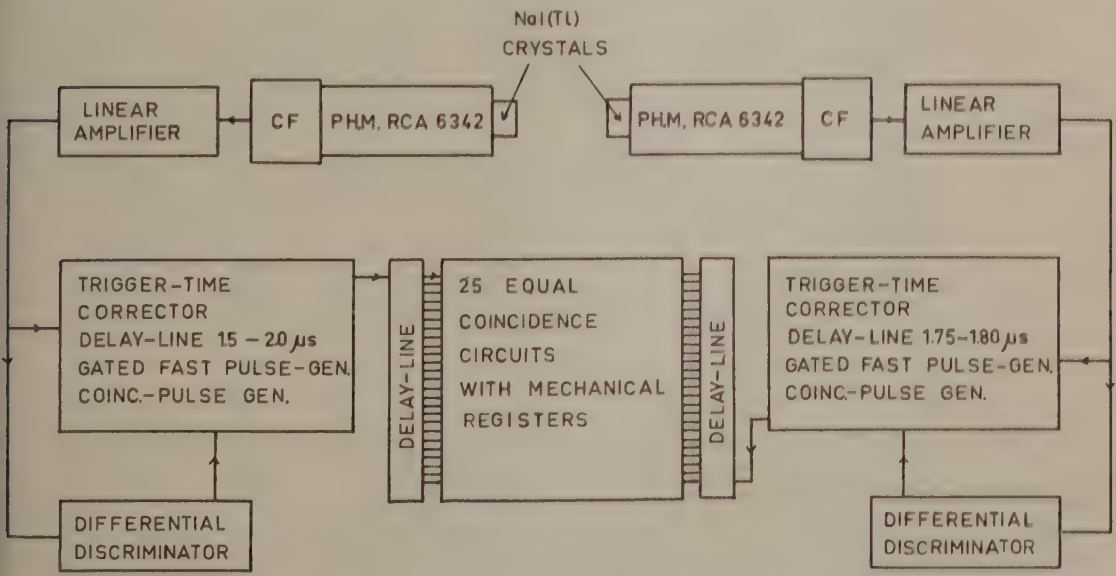

Fig. 1. Block diagram of the 25-channel analyzer.

2. The 25-channel System

Fig. 1 shows a block-diagram of the arrangement. The amplifiers, the differential discriminators and the pulse-forming circuits have been used in another arrangement and have been described earlier[1,2,3]). It can be mentioned that the amplifiers used consist of common, *RC*-coupled stages with a rise-time of 0.25 μs. This rise-time has not been found to be an essential disadvantage for the operation of the pulse-forming circuits. In order to exclude undershot of the output-pulses, some changes in the original circuit have been made.

erator. The operation of these circuits has been described in detail in an earlier paper[3]). I have recently been informed by G. F. Pieper at Yale University that G. S. Stanford and G. F. Pieper[4]) had already in 1955 used this Gate-principle[5]) or "Slow-fast" method.

The present circuit differs from the earlier one with respect to the choice of tubes and the way in which the coincidence-pulses are produced. The pulse-height of the fast pulse-generator varies slightly with the height of the trigger-pulse. For this reason a separate coincidence-pulse generator, triggered by the fast

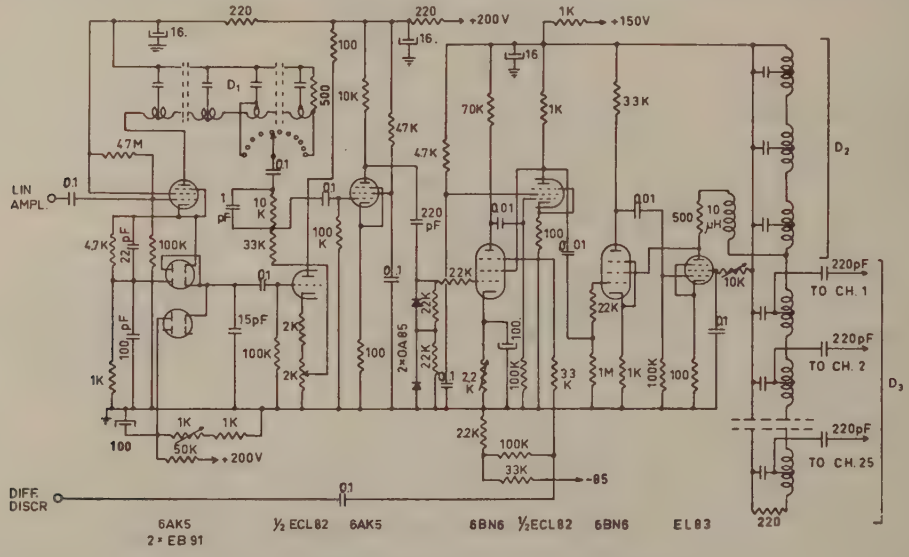

Fig. 2. Complete diagram of the pulse-former circuits.

A discriminator circuit containing a 6BN6 tube has been introduced in the output stage of the differential discriminator in order to obtain constant pulse-height and pulse-length of the output-pulses. These pulses then form gate-pulses for the gate-circuit. Fig. 2 shows a complete diagram of the pulse-forming circuit. The pulse-forming circuit consists of three parts, a trigger-time corrector, a gated fast pulse-generator and a coincidence-pulse generator, was introduced. This delivers a 3.5-volt pulse with triangular shape and a width at half-maximum of 30 mμs. The length of this pulse is determined by the shorted delay-line D_2. This delay is matched to the lumped delay D_3 the sections of which are connected to the control grids of the coincidence-tubes. Each section of the delay D_3 consists of the coil L and the condenser C, which, in the case when

[1]) B. Åström, Ark. f. Fysik **12** (1957) 215.
[2]) B. Åström, Nuclear Instruments **1** (1957) 143.
[3]) B. Johansson, Nuclear Instruments **1** (1957) 274.
[4]) G. S. Stanford and G. F. Pieper, Rev. Sci. Instr. **26** (1955) 847.
[5]) B. Åström, B. Johansson and I. Bergström, Ark. f. Fysik **12** (1957) 205.

the shortest delay is required, is formed by the input capacitor of the coincidence-tube.

from pulse-former II propagate along D_4 in the reverse direction.

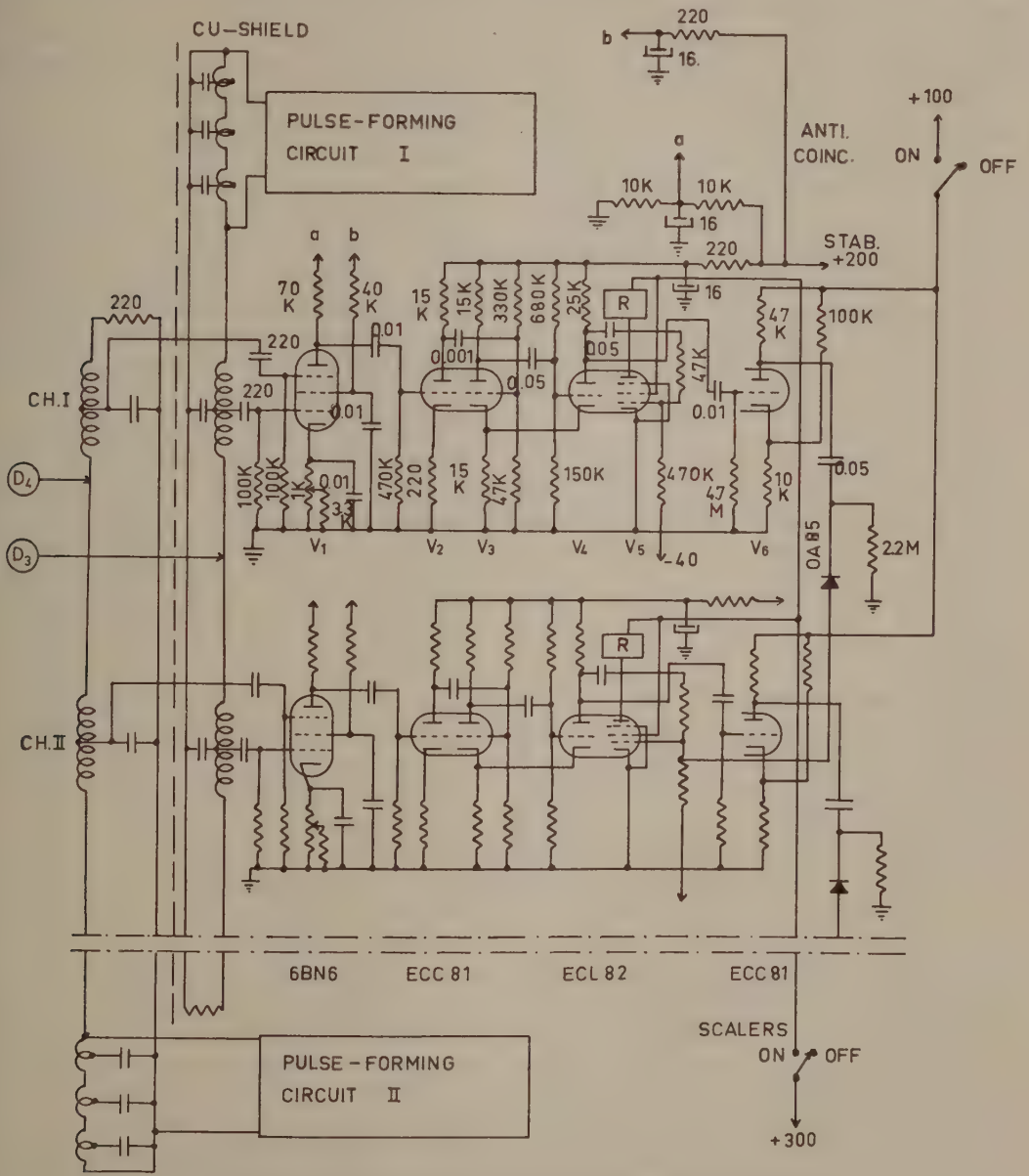

Fig. 3. Wiring diagram of two channels of the coincidence circuits.

The 25-channel system is shown in fig. 3. The pulses from the pulseformer I are fed to the delay D_3 where they propagate in the direction of increasing channel number. The pulses

The time-distance between channel 1 and channel 25 is then twice the total delay of D_3, provided that $D_3 = D_4$. This conditions is fulfilled here in order that the system should

have symmetrical properties. Each coincidence-channel consists of a 6BN6-tube (V_1) with control-grid g_1 connected to D_3 and control-grid g_2 connected to the corresponding section of D_4. The negative output-pulse of the 6BN6-tube is fed to a phase-inverter and amplifier stage (V_2) followed by a discriminator circuit containing the tubes V_3 and V_4. The discriminator-pulses have a width of 5–10 ms and are fed to the tube V_5 the anode-circuit of which contains a mechanical register (R). The tube V_6 delivers an anticoincidence-pulse to the next channel and prevents more than one register from being actuated at the same time. The width of the discriminator pulses increases with increasing channel number in order that the channel with the lowest channel number shall be ready first for recording a new coincidence. The pulse-height of the output-pulses of the coincidence-tube is a function of the overlapping of the input pulses. This feature is treated in the last section where a new time-to-pulse-height converter is described which is based on this fact.

3. The Coincidence-Curve

When the anticoincidence-system is switched off the curve-shape will be as shown in fig. 5. In this case more than one register is actuated at the same time. The number of registers that are actuated is determined by the resolving time 2τ. In the actual case the resolving time was 30 mμs. If the coincidence-curve should be correctly represented the resolving time should be equal for all channels. If the measured half-life is much smaller than the resolving time no difficulties will arise but in the case of Hf^{181} where the half-life is one third of the resolving time some difficulties appear. This is due to the fact that the time-separation between two channels is determined by the displacement of the prompt coincidence-curve for each channel. If the resolving-time in the two channels is unequal the two sides of the coincidence-curves have obtained a different displacement because the position of the centre of the prompt coincidence-curve is fixed by the lumped delay-line and does not change with respect to the resolving time.

In order that the channels be independent of the resolving time and in order to decrease the curve-width the anticoincidence-system was introduced. By this system the curve-width is determined by the measured half life and the actual time-spread. The shape of the coincidence-curve will in this case be a differentiated coincidence-curve; while the curve in fig. 5 and the usual coincidence-curve will be an integrated time-function. This is due to the fact that the analyzer will record the number of events occurring in subsequent time-intervals lying side by side while the usual technique uses overlapping intervals.

Different resolving times will in this case give rise to different channel widths. Because it is difficult to obtain exactly equal channel-widths a method to tranform the differentiated curve into an integrated curve is developed. The difficulties lie in the fact the channel-width is small compared to the resolving-time and that an artificial step-delay-line with 25 equal steps is difficult to construct.

The method is based on the assumption that the coincidence-pulse has an infinite length so that only one edge of the pulse should appear within the channel-range. This means that if a coincidence has been recorded in channel n it has also been present in channel $n + 1$, $n + 2$, ... 25, but excluded here by the anti-coincidence-system. It can also have been present in channel $n - 1$, $n - 2$, ... 1 because the registers can not see in what direction the anticoincidence-pulse has been delivered. Thus one edge of the coincidence-curve will be obtained if one makes the following integration. If a_n is the integrated number then $A_n = a_n + a_{n-1} + \ldots a_1$ or $A_n = a_n + a_{n+1} + \ldots a_{25}$.

If the measured curve is prompt so that it does not extend outside the channel-range then the above integration is valid with corrections for only accidental coincidences. If the curve is a delayed coincidence curve one has to correct for events falling outside the channel-range. This can be seen in the following way. If no

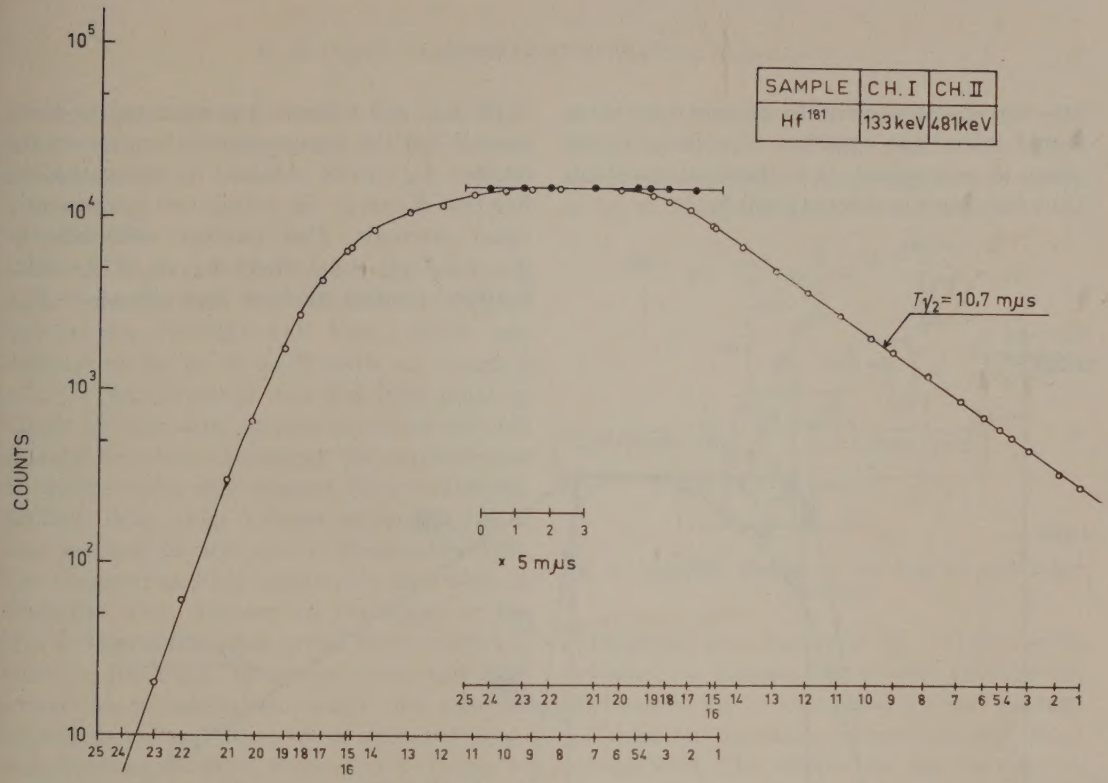

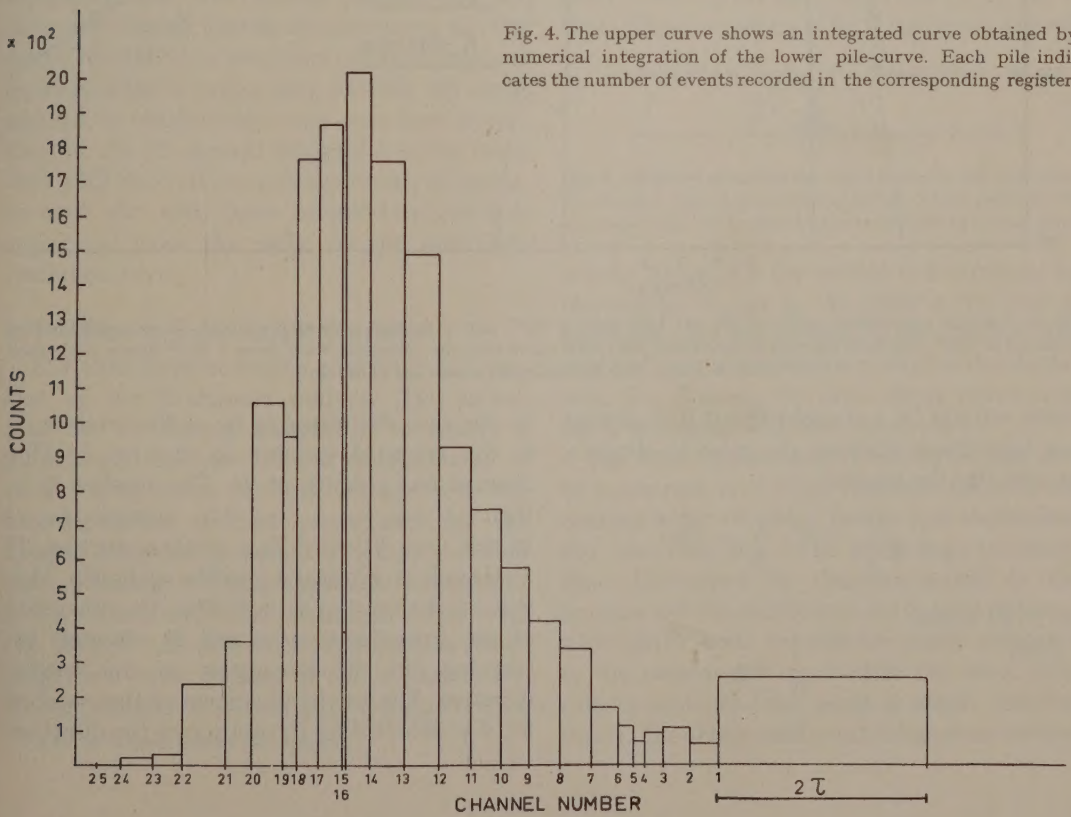

Fig. 4. The upper curve shows an integrated curve obtained by numerical integration of the lower pile-curve. Each pile indicates the number of events recorded in the corresponding register.

time-spread were present the differentiated curve should follow the equation $N = K \exp(-\lambda t)$ where K = constant, λ = the decay-constant. Thus the above number A_n will be

$$A_n = K \int_{t_n}^{t_{25}} e^{-\lambda t} = \frac{K}{\lambda}(e^{-\lambda t_n} - e^{-\lambda t_{25}})$$

Thus, t_n will indicate a position on the time-axis. When the decay-constant is unknown the numbsr A_∞ can be obtained by integrating the function $K \exp(-\lambda t)$ within two subsequently equal intervals. This number will then be $A_\infty = A_2^2/(A_1 - A_2)$ where A_1, A_2 is the total recorded number in these intervals ($A_1 > A_2$).

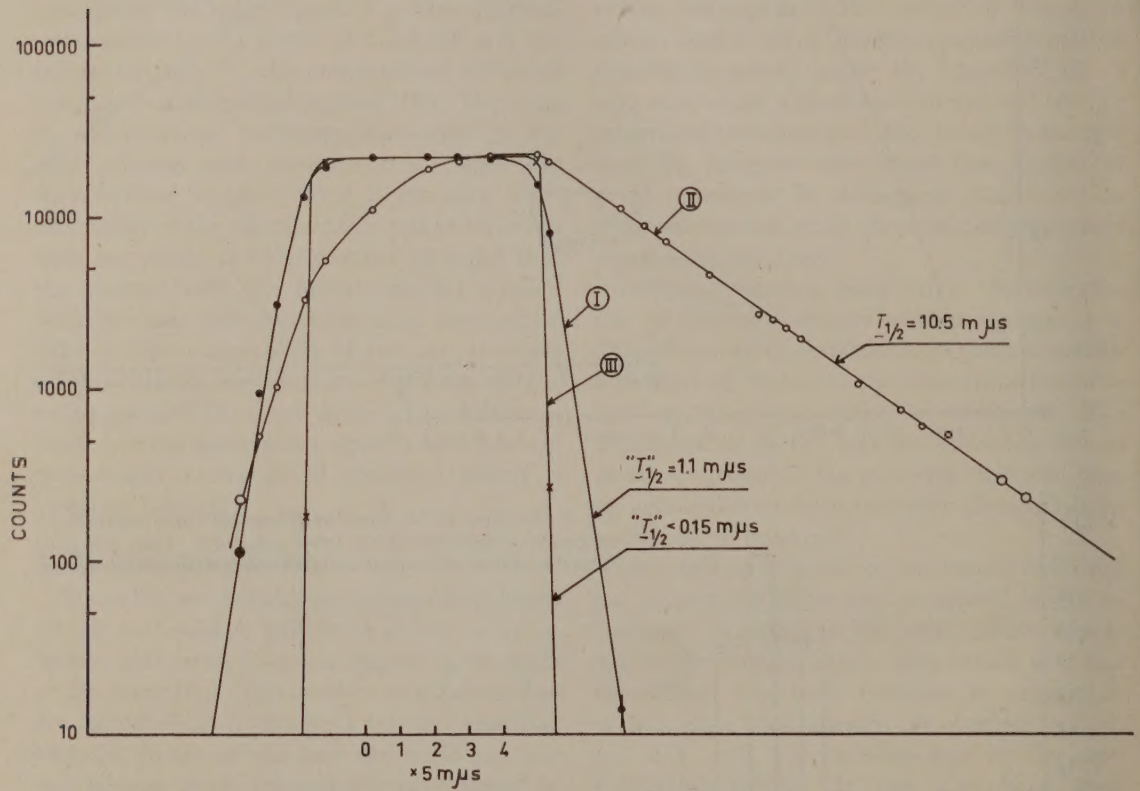

Fig. 5. Delayed coincidence curve of the 481 keV level of Hf^{181} and a prompt coincidence curve of the annihilation radiation of Na^{22}. The third curve is an electronic resolution curve with the pulse-spectrum from a Na^{22} source connected to both channels. The discriminators were set at 511 keV.

which will not be a straight line if it is plotted in a logarithmic diagram. In order to obtain a straight line the number

$$A_\infty = K \int_{t_{25}}^{\infty} e^{-\lambda t} = \frac{K}{\lambda} e^{-\lambda t_{25}}$$

has to be added.

Then

$$A_n + A_\infty = \frac{K}{\lambda} e^{-\lambda t_n}$$

In the case illustrated in fig. 4 the number A_2 is the recorded number in channel 1. This channel has a width of 2τ. The number A_1 is then $a_{10} + a_9 + \ldots + a_2$. The number A_∞ is in this case 30 which is a small correction. If 2τ is made larger then A_∞ will be negligible. This will not change the channelwidth. The other side of the coincidence-curve will be obtained by carrying out the integration in the reverse direction. The left hand portion of the curve in fig. 4 is obtained by integration in the direction

of decreasing channel number and the right hand portion by integration in the reverse direction.

4. Calibration

The calibration is carried out by employing a Hf^{181}-sample with the well-known 10.6 mμs half-life for the 481 keV level, which was determined by de Waard[6]) with an accuracy of 3%. The calibration has also been done by taking up a prompt coincidence-curve for each channel and then measuring the displacement of these curves with respect to a calibrated, artificial delay. Fig. 5 shows an application of this method to the above mentioned Hf^{181}. The obtained half-life agrees very well with de Waard's value. Because of statistical errors, this calibration has not given better accuracy than the above 3%. We intend to use this Hf^{181} source as a calibration source for planned measurements and then, when improved accuracy has been obtained, remeasure it. It can be mentioned that the channel position did not show any change during measurements for one week. This Hf^{181} is a very good calibration source because it has a rather long half-life (45 days) and can be obtained in a very pure form from a reactor. The 25-channel analyzer is so far being used with NaI (Tl) crystals but it can, of course, be used also with faster scintillators which is appearant from the slope of the electronic resolution curve.

5. The Time-to-Pulse-Height Converter

The time-to-pulse-height converter is a variant of the 25-channel analyzer. This means that the 25-channel analyzer is in reality a pulse-height analyzer with a discriminator in each channel set at the same voltage level. The time-separation is then carried out by the lumped delay-line in such a way that a certain time difference will give optimum pulse-height in that coincidence-tube or channel corresponding to this time-difference. The time-to-pulse-height converter consists of one of these coincidence circuits delivering output-pulses with a pulse-height which is a function of the time difference between the two input pulses within the operating range. The arrangement is shown in fig. 6. The pulse-height is a function of the

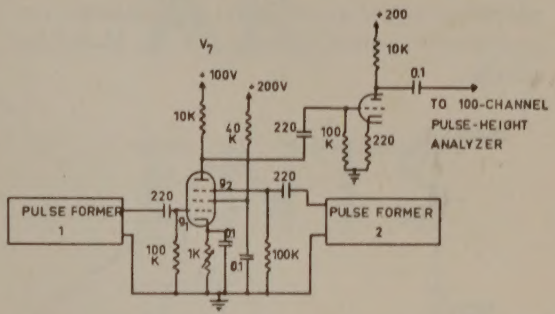

Fig. 6. Simplified diagram of the time to pulse-height converter.

overlapping area shaded in fig. 7. This can be explained as follows. The current through the 6BN6-tube (V_7) is determined by that control-grid which at a certain moment has the lowest voltage-level. The 6BN6-tube has two equivalent control-grids and can be cut off by one of these. Thus, at point a of fig. 7, the anode current

Fig. 7. Idealized shapes of the input pulses to the converter. The shaded area is proportional to the anode pulse of the convertertube. The horizontal line indicates the cut-off-level.

is zero. At point b the current is determined by the voltage V_1 on g_2. At point c the grid g_1 has taken over the control of the current. The shape of the pulse will thus be that of the shaded area. Fig. 8 shows the same decay curve as in fig. 5, measured with this arrangement.

The time-to-pulse-height converter can also be connected to a single-channel analyzer, the channel-width of which in this case determines the resolving-time. The optimum resolving-time determined by the time-spread in the crystals and the multipliers can thus be obtained with rather wide coincidence-pulses compared to the pulse-width required in the usual coincidence-arrangements using a single discriminator. The above mentioned integration-method

[6]) H. de Waard, Thesis (Groningen).

can be used here with advantage because in this case the linearity of the coincidence-pulses is not essential.

This time-to-pulse-height converter will be employed in a pair-spectrometer arrangement connected to the small cyclotron of the Nobel Institute.

6. Acknowledgements

I wish to thank Dr. B. Åström for many valuable discussions and interesting comments. Thanks are also due to Mr. R. Åkerlund for technical assistance and to G. Oelsner, B. Sc. for correcting the English.

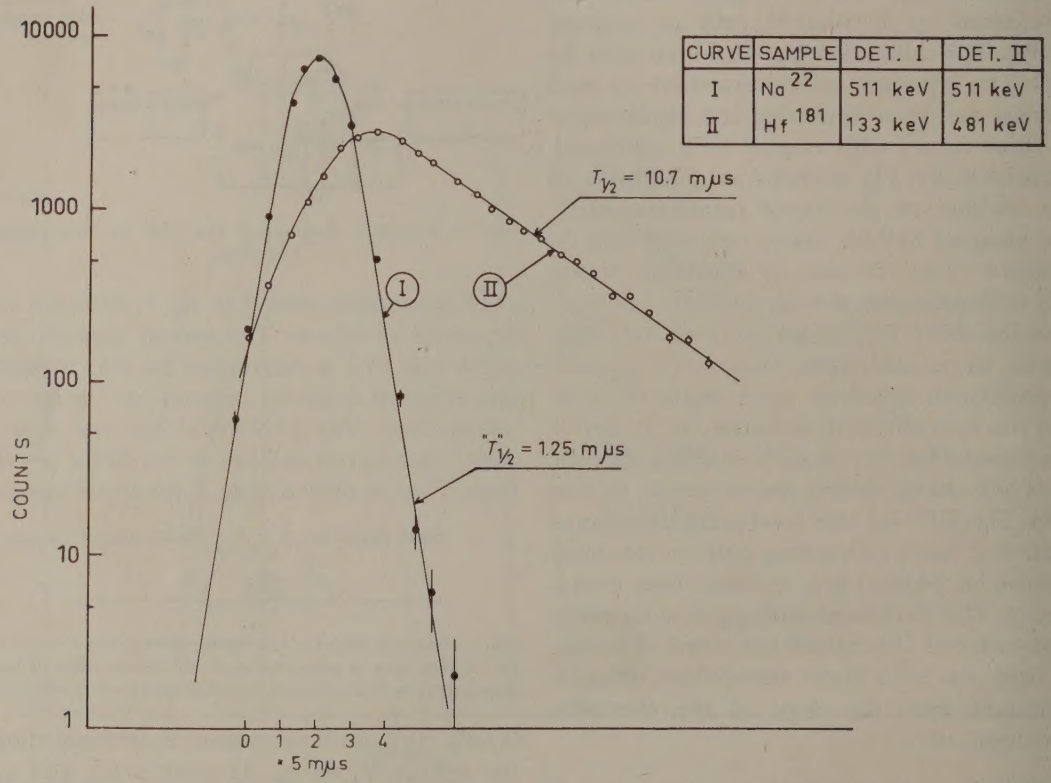

Fig. 8. The same delayed and prompt coincidence curve as in fig. 5 measured with the 100 channel system.